

UC Berkeley

UC Berkeley Electronic Theses and Dissertations

Title

Nanomechanical Testing of Medical Grade Polymeric Materials: Evaluating Nanoindentation as a Characterization Tool

Permalink

<https://escholarship.org/uc/item/0h21263g>

Author

Arevalo, Sofia Ester

Publication Date

2022

Peer reviewed|Thesis/dissertation

Nanomechanical Testing of Medical Grade Polymeric Materials: Evaluating Nanoindentation as
a Characterization Tool

by
Sofia Arevalo

A dissertation submitted in partial satisfaction of the
requirements for the degree of
Doctor of Philosophy
in
Engineering-Mechanical Engineering
in the
Graduate Division
of the
University of California, Berkeley

Committee in charge:

Professor Lisa A. Pruitt, Chair
Professor Grace O'Connell
Professor Ronald Gronsky

Summer 2022

Abstract

by

Sofia Ester Arevalo

Doctor of Philosophy in Engineering – Mechanical Engineering

University of California, Berkeley

In the coming decades, there will be a significant growth in primary and revision total joint replacement (TJR) procedures. The increase in TJR poses stress on the healthcare system and the patients afflicted by the need for joint replacement. An important concern arising in the arthroplasty community is the increase demand for TJR in the younger and more active population. Many of the current designs and material formulations are aimed towards an older and sedentary population. As a result there is a need to understand current clinical failures, material microstructure and implant design to address the changing patient demographics – active lifestyle and longer lifespan. Over the past decades there has been an extensive effort to develop new material formulations to improve ongoing challenges in orthopedic bearings; namely resistance to wear, fatigue and fracture, as well as oxidation or corrosion in metals. The majority of TJR use a metal-on-polymer articulation to restored function to damaged or diseased articular cartilage. The gold standard polymeric material used in orthopedics is ultra-high molecular weight polymer (UHMWPE). While there are a variety of UHMWPE formulations that address challenges such as wear, fracture and fatigue, and oxidative degradation, the optimal UHMWPE formulation does not yet exist. Furthermore, identifying a material formulation that is well suited and assessing its microstructural-property relationship is important for understanding the long-term behavior *in vivo*. A common technique to characterize mechanical properties to understand the mechanical behavior of materials is to perform bulk mechanical testing. However, bulk testing such as tensile and compression are insufficient to capture information related to minute changes in the microstructure. Alternatively, nanoindentation (the focus of my doctoral work) can provide insight into UHMWPE's nano-scale behavior, including the surface property changes of retrieved implants. Surface properties such as of localized modulus and load-displacement behaviors are important to understanding the changes in properties at the articulating surface and provide insight into tribological behavior. Understanding nanomechanical behavior is important for optimizing wear resistance and tailoring UHMWPE microstructures for long-term performance in orthopedic bearings.

In the past few decades, the need for developing bio-inspired materials to address many shortcomings from current medical-grade biomaterials gave rise to PEEK and PEEK composites. As such, there is a need to understand the mechanical behavior to assess suitability for load bearing applications in the body. Thus, equally important to studying the nanomechanical properties of UHMWPE is assessing the nanomechanical properties of Poly-ether-ether-ketone (PEEK) and PEEK composites, a potential alternative to UHMWPE and metallic components. Insight into the nanoscale may offer valuable information about fiber-matrix interactions that may influence long-term integrity of these biomaterials when used in the body.

This dissertation is the first study to use nano in PEEK and to bridge the nano-micro-macro scales in UHMWPE and elucidate a unified methodology for use in polymers biomaterials. This

body of work shows the utility and validity of using nanoindentation as a characterization technique for characterizing medical-grade polymers. This research highlights the structure-property development and the comparison across the microstructural length scales of UHMWPE. Secondly, characterizing the nanomechanical properties of PEEK and PEEK composites provide insight into the relationship between the heat treatment process, microstructure, and tip diameter.

Since nanoindentation is a growing field for characterizing biomaterials, there is a dire need for developing robust nanoindentation protocol that yields reproducible and reliable data. As such, this dissertation develops a framework for (a) addressing challenges and potential errors when performing indentations on soft or hydrated materials and (b) explore best practices for mitigating experimental error. This framework is a primer and an impactful body of work for researchers performing indentations on soft/hydrated biomaterials and polymers.

Lastly, this research aims to validate nano-indentation to study UHMWPE-based orthopedic retrievals' surface properties. The benefit of using nano-indentation is understanding and quantifying the changes in mechanical properties at the articulating surface. Prior research has shown that articulating motion yields a damaged layer on the surface (3-5 μm in-depth), a precursor to wear. Unlike bulk mechanical testing, nanoindentation probes the local surface properties and can measure properties on the damaged layer. By assessing the surface properties, we can learn more about the wear mechanisms and the structure-property evolution owed to *in vivo* conditions. Looking forward, more research studies on the nanomechanical characterization of polymers may allow researchers to optimally tailor the microstructure for long-term structural applications and gain insight into the mechanics of other bio-inspired systems.

I dedicate this to my family.
This accomplishment is yours as much as it is mine.

ACKNOWLEDGEMENTS

After a decade in Berkeley, it is with sweet sorrow that I must depart. Berkeley and the University have a special place in my heart. I knew, the moment I stepped on campus in 2007, that this was the place I needed and wanted to be. It was simply my destiny to be a Cal student. I didn't care about rankings. But it certainly didn't hurt that it was a prestigious University. My time as an undergraduate was not the easiest nor smoothest. It was actually quite traumatic. The following saying became my mantra, "if it doesn't challenge you, then it doesn't change you." It challenged me, it broke me, but I grew stronger and my perspective changed. But most importantly it fostered an intellectual curiosity and built a determination that will not falter. With every obstacle I overcame, I grew confident in my ability to do challenging things and I grew less afraid of failure.

I am forever indebted to the mentors, friends and family that cheered me on and supported me along the way. I would seriously not be here, getting a PhD, without the mentorship and support from Prof. Pruitt. Professor Pruitt and I met when I was a sophomore, a quiet and awkward 18 year-old trying to figure out the world and myself. When I first joined the Medical Polymer Group (MPG), I never imagined that I would go on to pursue a PhD and be part of the lab for almost a decade. I am forever grateful to Lisa, for giving me the opportunity to fall in love with research and let me explore my research passion. My favorite parts of my academic career at UC Berkeley has been engaging in research conversations with Lisa and my lab-mates. And to have had an opportunity to teach alongside the best and most charismatic professors. I am also thankful to Prof. O'Reilly for being a kind professor and showing me that dynamics is fun, and for writing a letter of recommendation for graduate school and NSF GRFP.

During my graduate experience, I had the opportunity to collaborate with many wonderful professors and researchers: Prof. Donna Ebenstein, Prof. O'Connell and Andre Montes. It was such a wonderful experience to work alongside top researchers.

My graduate experience would not have been complete without my old and new friends. One of my first friends in graduate school was Nicole, our love for long distance running bonded us and led us to have many fun runs in SF and Berkeley. I still miss giggling and having long conversations. Then, post-shelter-in-place, I had the opportunity to meet Shiyin, Reece, Andre and Lisa T. I hope we can have more adventures together. Last but not least, I am really happy to have had my best friend and partner in crime, Brian, alongside me. We shared our woes for academia, celebrated each other's successes and made the most out of our graduate school experience. Brian, thank you for being there for me and for instilling a passion to explore the outdoors and try new things. I don't think I could have gotten through the hard times in life without you. Let's have many more adventures and continue chasing our dreams!

To my family – mom, dad, CJ, and Javi: Thank you for always being there, and being the best support system. I really appreciate you guys never letting me forget that I am amazing and deserve all of my accomplishments.

I was always my happiest in lab and always feel grateful to have had such an amazing opportunity to become a lifelong scholar. An opportunity that was beyond my ancestors' reach. I am excited to embark on my next journey and continue to grow.

Table of Contents

ABSTRACT.....	2
ACKNOWLEDGEMENTS.....	ii
TABLE OF CONTENTS.....	iii
CHAPTER 1 – INTRODUCTION TO TOTAL JOINT REPLACEMENTS AND ORTHOPEDIC POLYMERS.....	1
1.1 TOTAL JOINT REPLACEMENTS	1
1.2 ULTRA-HIGH MOLECULAR WEIGHT POLYETHYLENE	3
1.3 POLY-ETHER-ETHER-KETONE (PEEK) AND CARBON-FIBER REINFORCED (CFR) PEEK	4
1.4 DISSERTATION AIMS AND STUDY DESIGN	5
CHAPTER 2 – A METHODOLOGICAL FRAMEWORK FOR NANOMECHANICAL CHARACTERIZATION OF SOFT BIOMATERIALS AND POLYMERS	7
2.1 INTRODUCTION TO NANOINDENTATION RESEARCH	7
2.2 NANOINDENTATION: MATERIALS RESEARCH AND OTHER SMALL-SCALE TESTING TECHNIQUES.....	9
2.3 NANOSCALE MECHANICAL CHARACTERIZATION TECHNIQUES (WHEN IS IT APPROPRIATE?)	10
2.4 NANOINDENTATION BACKGROUND	13
2.5 PROBE GEOMETRY AND SIZE	13
2.6 LOAD FUNCTIONS	18
2.7 LOAD-CONTROL VS. DISPLACEMENT CONTROL	20
2.8 LOAD-DISPLACEMENT CURVES	21
2.9 OVERVIEW: CONTACT MODELS IN NANOINDENTATION.....	23
2.10 HERTZ LINEAR ELASTIC ANALYSIS	24
2.11 OLIVER AND PHARR	25
2.12 ADHESION-BASED MODELS (JKR, MD, MDT).....	26
2.13 EXPERIMENTAL CHALLENGES AND ERRORS.....	29
2.14 SURFACE ROUGHNESS	30
2.15 PROBE CONTAMINATION.....	31
2.16 ADHESION	31
2.17 FALSE ENGAGEMENT	31
2.18 SUBSTRATE EFFECTS.....	32
2.19 FRAMEWORK FOR DESIGNING A NANOINDENTATION EXPERIMENT.....	33
CHAPTER 3 – COMPARING NANO-MECHANICAL PROPERTIES ACROSS LENGTH-SCALES AND MICROSTRUCTURAL PROPERTIES OF ULTRA HIGH MOLECULAR WEIGHT POLYETHYLENE	39
3.1 INTRODUCTION	39
3.2 METHODS.....	39
3.3 RESULTS.....	42
3.4 DISCUSSION AND CONCLUSIONS.....	50
CHAPTER 4 – COMPARING NANO-MECHANICAL PROPERTIES ACROSS LENGTH-SCALES AND MICROSTRUCTURAL PROPERTIES OF PEEK AND PEEK COMPOSITES.....	52
CHAPTER 5 – A CHARACTERIZATION TECHNIQUE FOR IMPLANT RETRIEVALS: NANO-MECHANICAL CHARACTERIZATION OF TOTAL KNEE RETRIEVALS	65
CHAPTER 6 – DISCUSSION AND FUTURE DIRECTION	72
REFERENCES.....	74
APPENDIX A – SEMINAL PAPERS PROVIDING THE BASIS FOR UTILIZING THE MAIN EQUATIONS FOR ANALYSIS OF LOAD-DISPLACEMENT CURVES	87

APPENDIX B – SEMINAL PAPERS FOR THE DEVELOPMENT AND ADVANCEMENT OF THE OLIVER AND PHARR INDENTATION THEORY	87
APPENDIX C– SEMINAL PAPERS FOR THE DEVELOPMENT AND ADVANCEMENT OF THE ADHESION BASED NANOINDENTATION THEORY	89

List of Figures

Figure 1 - (a) Healthy knee joint (b) damaged knee joint (c) knee joint with a prosthesis. Image adapted from: <https://orthoinfo.aaos.org/en/diseases--conditions/osteoarthritis/>.....1

Figure 2 - Hip prosthesis with a metal-on-polyethylene, metal-on-metal, ceramic-on-ceramic. Image adapted from <https://www.jnjmedtech.com/en-US/companies/depuysynthes>2

Figure 3-(a) projected number of primary total hip arthroplasty (THA) and total knee replacement (TKR) (b) projected number of revision total hip arthroplasty (THA) and total knee replacement (TKR) [4].....3

Figure 4- Progression of nanoindentation research in the field of thin-films (yellow), alloys (green), ceramics (green-blue), polymers (blue), and biomaterials (dark-blue). The materials encompassed in the biomaterials category include hydrogels and biological materials, for example cartilage and tissues.....10

Figure 5- Load (uN) and indentation depth (um) ranges for AFM, nanoindentation and micro-indentation, including load-depth nanoindentation data points of representative materials to illustrate the range of properties being measured. Materials include polymers, biological materials, thin films, and ceramics/glasses. The load-indentation depth values were obtained from the literature [59,73,82–86,74–81].12

Figure 6 - General guideline to help determine whether nanoindentation is within range to characterize the sample [87]. In this an analysis, P_{max} is the maximum load, R is the radius of conospherical probe, and h_{max} is the estimated maximum depth. E_r is the unknown reduced elastic modulus (in this condition it is the plane strain modulus) that is determined from an indentation test and is limited by the macroscale elastic modulus of the material.13

Figure 7 - Schematic illustration of the various probe geometries used in nanoindentation – Berkovich, Conospherical, Conical, Cone punch, and Flat punch, . In this diagram, P is the applied load, d or h is the distance from the surface of the sample to maximum penetration depth, a is the radius of the projected contact between the tip and the sample, and b is the radius of the flattened end of the cone punch.14

Figure 8 - Calculating the impact of diamond probe, glass probe and neglecting indenter properties on the determination of the reduced elastic modulus of soft polymers (1 MPa, 50 MPa). In Eq. A, E_r is the reduced modulus (in GPa), E_i is the indenter modulus, ν_i is the Poisson’s ratio of the indenter, E_s is the sample modulus, and ν_s is the Poisson’s ratio of the sample.18

Figure 9 - Load (displacement)-time profile for (a) triangular loading profile composed of a simple load-unload cycle, (b) a trapezoidal load-hold-unload profile, and (c) a trapezoidal load-hold-unload profile incorporating a lift-off at the beginning of indentation testing (Segment A) and at the end of indent testing (Segment D). (d) Load-displacement response of a viscoelastic material exhibiting a “nose” at peak load for a viscoelastic material tested using a triangular load-time profile (a). (e) Load-displacement response of a viscoelastic material for trapezoidal load-time profile (b), eliminating the “nose” during initial unloading at peak load. (f) Load-displacement response of a viscoelastic material for Trapezoidal II profile (c), with the red box indicating the data that would have been captured using the standard trapezoidal profile (b) without the lift-offs. Including the lift-offs allows determination of the zero displacement point to correct for sink-in.....20

Figure 10 - Representative load-displacement curve (this is a load-controlled indent), illustrating the loading, unloading, hysteresis and slope of unloading curve (dP/dh). Note that the full adhesive load-displacement curve would only be collected using a loading profile with initial and final liftoff, as shown in Figure 9c. An indent with the profile shown here would only capture the data shown in the red box in Figure 11.22

Figure 11 – (a) Trapezoidal time-profile in displacement control and associated load-displacement behavior for (b) elastic-plastic and (c) viscoelastic materials. (d) Trapezoidal II time profile in displacement control typically used for testing an adhesive material, and the associated load-displacement behavior (e). The portion of the load-displacement curve contained in the red box is the data that would be collected using the basic trapezoidal displacement-time profile in Figure 8a.22

Figure 12 - Representative load-displacement behavior of a material exhibiting adhesion during the indentation process, with accompanying displacement-time profile. By including the lift-offs in segments A and D of the displacement-time profile, the indentation data captures the entire indent process. First, the probe approaches the sample (1), which is followed by a snap-on (2) process as it makes contact with the sample. In steps (3-5), the probe engages with the sample and step (6) shows the probe pulling from sample and experiencing adhesion (material sticking to probe as it is withdrawn).....23

Figure 13 - Nano-JKR method used to analyze samples experiencing adhesion. There are three approaches: Displacement Method I, Displacement Method II, and curve fitting. In all equations, R is the radius of the conospherical probe. The other variables used to calculate the reduced modulus, E_r , in Displacement Methods I and II are labeled on the figure. In the curve fit equation, $P_{adhesion}$ is the maximum negative load reached during pull-off (at $\delta_{adhesion}$), a_0 is the projected contact radius between the probe and the sample at zero load (at $\square\delta_0$), and

$\delta_{contact}$ is a variable included to rezero the displacement to optimize the fit. P_{adh} , a_0 , and $\delta_{contact}$ are solved for using a non-linear curve fit of the load-displacement ($P - \delta$) data from the unloading curve.28

Figure 14 – Illustration of potential challenges that may be encountered during nanoindentation, (a) surface roughness, (b) contaminated probe, (c) adhesion, (d) false probe-sample engagement, and (e) substrate effects, accompanied by their respective load-displacement behavior.....30

Figure 15 - Part I: Framework provides a guideline for selecting a nanoindentation probe (geometry, size and material). The tip geometry is important to indentation testing; for example, sharp probes are preferred to use on stiff materials to maximize spatial resolution, while blunt probes are preferred to use on soft materials to avoid sample puncture and facilitate sample detection. However, the use of blunt probes comes at the expense of spatial resolution. As for tip material, there is a variety of materials to choose from when testing soft materials and many researchers might choose a tip material that mitigates adhesion and is cheap and easy to manufacture rather than the traditional diamond probes.36

Figure 16 – Part II: Framework provides the experimental set-up for nanoindentation testing. First, it provides a guide for identifying the appropriateness of using a displacement-controlled vs load-controlled experiment. Second, it provides a guide for identifying the maximum load or displacement to apply during indentation testing. Third, it provides a general framework for developing the time-profiles based on whether a material is viscoelastic, whether the indent will need re-zeroing from sink-in effects or whether the material is prone to adhesion.....37

Figure 17 – Part III: This portion of the framework illustrates the potential challenges manifested in load-displacement curves. Further, the framework provides solutions for addressing these challenges. Finally, this framework focuses on the data analysis methods that should be employed after indentation testing to ascertain the mechanical properties, showing that the type of model used will depend on whether adhesion is present38

Figure 18 - Correlating compression modulus to nanoindentation and tensile modulus. The correlation strength is based on spearman rank correlation coefficient. The spearman rank correlation coefficient for compression and tensile true elastic modulus is 0.839.* While the spearman rank correlation coefficient between compression and nanoindentation is 0.587. The * denotes $P \leq 0.01$49

Figure 19 – (a) Correlating crystallinity (%) to elastic modulus (compressive and tensile). (b) correlating crystallinity to true and engineering yield strength (compressive and tensile). (c) correlating lamellar thickness to elastic modulus (tensile and compressive). (d) correlating lamellar thickness to true and engineering yield strength (compressive and tensile).....50

Figure 20 - Surfaces of PEEK composites before and after polishing. Surface roughness (average \pm standard deviation) before polishing is $1.48 \mu\text{m} \pm 0.15 \mu\text{m}$, and after polishing the surface roughness (average \pm standard deviation) is $0.42 \mu\text{m} \pm 0.05 \mu\text{m}$ 54

Figure 21 - Illustration of (a) the indentation load-time profile and (b) a representative load-displacement curve.....55

Figure 22 - (a) Plot showing the spearman rank correlation coefficient between ($r = 0.975$) between $1.5 \mu\text{m}$ indentation modulus versus nanoindentation modulus using an indenter tip of $20 \mu\text{m}$ (b) Load-displacement behavior for one indentation cycle performed on Unfilled PEEK (annealed to $275 \text{ }^\circ\text{C}$) using a $20 \mu\text{m}$ and a $1.5 \mu\text{m}$ radius conospherical tip59

Figure 23 - Bar graph illustrating the indentation modulus (median \pm std. error) using an indenter tip of $1.5 \mu\text{m}$ (a) Indentation modulus for Unfilled PEEK (b) Indentation modulus for PAN CFR PEEK (c) Indentation modulus for Pitch CFR-PEEK59

Figure 24 - Load displacement curves for Unfilled PEEK and CFR PEEK composites (not heat treated) (a) load unload path for PEEK unfilled measured using a $20 \mu\text{m}$ radius conospherical indenter (b) load unload path for PEEK unfilled measured using a $1.5 \mu\text{m}$ radius conospherical indenter (c) load unload path for pitch-based carbon fiber PEEK measured using a $20 \mu\text{m}$ radius conospherical indenter (d) load unload path for pitch-based carbon fiber PEEK measured using a $1.5 \mu\text{m}$ radius conospherical indenter (e) load unload path for PAN-based carbon fiber PEEK measured using a $20 \mu\text{m}$ radius conospherical indenter (f) load unload path for pitch-based carbon fiber PEEK measured using a $1.5 \mu\text{m}$ radius conospherical indenter60

Figure 25 - Indentation modulus measured using a $1.5 \mu\text{m}$ -radius indenter tip.62

Figure 26 - (a) Scanning electron microscopy image of CFR PEEK [152]. (b) Load-Displacement curve for PEEK with PAN-carbon fibers (CF) (c) Load-Displacement curves for PEEK with Pitch-CF (d) The nanomechanical properties for the matrix, matrix-fiber interface and fiber measured with a $1.5 \mu\text{m}$ -radius indenter tip and subsequently processed using k-means.....62

Figure 27 - (a) Plot showing the spearman rank correlation coefficient between ($r = 0.9498$) microindentation modulus versus nanoindentation modulus using an indenter tip of $20 \mu\text{m}$ (b) Plot showing the spearman rank correlation coefficient between ($r = 0.9825$) between microindentation modulus versus nanoindentation modulus using an indenter tip of $1.5 \mu\text{m}$63

Figure 28 - Plot showing the spearman rank correlation coefficient between (r) between percent crystallinity [48] and nanoindentation modulus using an indenter tip of 1.5 μm64

Figure 29 – Frequency distribution for the indentation reduced elastic modulus for (a) implant 1611143 and (b) Implant 18032742.68

Figure 30 –Frequency distribution for the indentation reduced elastic modulus for (a) implant 2011844 and (b) Implant 18032544.69

Figure 31- Welch test to compare the reduced modulus of implants at the (a) articulating surface (Implant A and B) and (b) cross-section (Implant C and D).70

List of Tables

Table 1 - Review papers on static nanoindentation of soft materials and biological materials (hydrated and non-hydrated) spanning from early 2003 to 2020.....	7
Table 2 – Advantages and disadvantages for using atomic force microscopy (AFM) and nanoindentation as a mechanical characterization technique. As for the instrumentation, in AFM, the approach is angled, while nanoindentation is a vertical approach.....	11
Table 3 – Presentation of the advantages and disadvantages of commonly used nanoindentation probes in tissues and polymers and a summary of the materials that are best suited for characterization with given probe geometries.....	15
Table 4 – Summary of literature pertaining to nanoindentation of biomaterials. Table includes probe geometry, probe material, probe radius, biomaterial characterized and indentation elastic modulus.	15
Table 5 – Characteristics of load control and displacement control experimentation during nanoindentation.....	21
Table 6 - Area function Equations for Berkovich, conical probes [84], spherical and cylindrical flat punch. Where h_c is the contact depth, θ is the semi-angle for a Berkovich indenter (65.27°), α is the effective cone angle for a conical indenter, and a is the radius of the flat punch tip.....	26
Table 7- Commonly used adhesion-based models for analyzing contact mechanics data with adhesion.....	27
Table 8 – Research utilizing JKR theory to analyze nanoindentation load-displacement curves and research that advances the nanoindentation research for soft materials.....	28
Table 9 - Microstructural property summary for GUR 1020, GUR 1020 35kGy, GUR 1020 75kGy+Remelted, GUR 1020 AO, GUR 1020 AO 80kGy, GUR 1020 Vitamin E.....	43
Table 10- Microstructural property summary for GUR 1020 VE 50kGy, GUR 1020 VE 75kGy, GUR 1020 VE 100kGy, GUR 1020 VE 125kGy, GUR 1050, GUR 1050 75kGy + Remelted.....	43
Table 11 - Summary of mechanical properties for GUR 1020, GUR 1020 35kGy, GUR 1020 75kGy+Remelted, GUR 1020 AO, GUR 1020 AO 80kGy, GUR 1020 Vitamin E.....	46
Table 12 - Summary of mechanical properties for GUR 1020 VE 50kGy, GUR 1020 VE 75kGy, GUR 1020 VE 100kGy, GUR 1020 VE 125kGy, GUR 1050, GUR 1050 75kGy + Remelted.....	47
Table 13 - Compression and nanoindentation (mean \pm standard deviation) for the following materials: GUR 1020, GUR 1020 35kGy, GUR 1020 75kGy RM, GUR 1020 AO, GUR 1020 AO 80kGy, GUR 1020 VE.....	48
Table 14 – Compression and nanoindentation properties (mean \pm standard deviation) for the following materials: GUR 1020 VE 50kGy, GUR 1020 VE 75kGy, GUR 1020 VE 100kGy, GUR 1020 VE 125kGy, GUR 1050, GUR 1050 75kGy RM.....	48
Table 15- PEEK and carbon fiber reinforced PEEK composites (Invisio, Lankashire, UK) used in this research along with the properties of the carbon fibers [130,132]. The carbon fibers are short and randomly distributed in the PEEK matrix (Unfilled PEEK).	54
Table 16- The nanomechanical properties (median indentation modulus) of PEEK and CFR-PEEK composites heat treated to different annealing temperatures. The indentation modulus recorded were attained using a 1.5 μm or a 20 μm conospherical tip.....	58
Table 17 – A summary of researchers using small length scale characterization technique to assess retrievals.	67
Table 18 - Sample size, indentation reduced elastic modulus (mean \pm standard deviation), standard error of mean for E of Implant 18032742 and 1611143.....	68
Table 19 – Sample size, indentation reduced elastic modulus (mean \pm standard deviation), standard error of mean for E of Implant 20111844 and 18032544.....	69

Chapter 1 – Introduction to total joint replacements and orthopedic polymers

1.1 Total Joint Replacements

Joints are essential components of the musculoskeletal system, enabling articulation and stability. While there are hundreds of joints in the human body, synovial joints are the most common. Synovial joints have one or more articulating surfaces enveloped by a fibrous sac; this sac contains synovial fluid. A viscous synovial fluid's presence dampens the impact of body forces and provides nutrients to the avascular cartilage tissues[1]. Further, the joint cavity differentiates synovial joints from fibrous and cartilaginous joints. Examples of synovial joints are the ball-and-socket hip and the bicondylar knees (Knee is often considered complex hinge with rotation, rolling and sliding). These synovial joints contain cartilage tissue that coats the bone surfaces and provides a medium for force absorption (Figure 1a). Damage to the cartilage on these joints results in pain for the patient. A healthy knee joint (Figure 1a) shows a joint space surrounded by synovial fluid and healthy articular cartilage. By contrast, a damaged knee joint (Figure 1b) exhibits damage to the articular cartilage. Cartilage does not have a nerve supply. However, once the cartilage is worn, exposure to the innervated bone can result in pain. To reduce pain and improve mobility, surgeons recommend joint replacement (Figure 1c), a standard surgical procedure, to replace the arthritic or damaged joint with a prosthesis. A prosthesis replicates the natural joint and provides stability and motion range during daily activity.

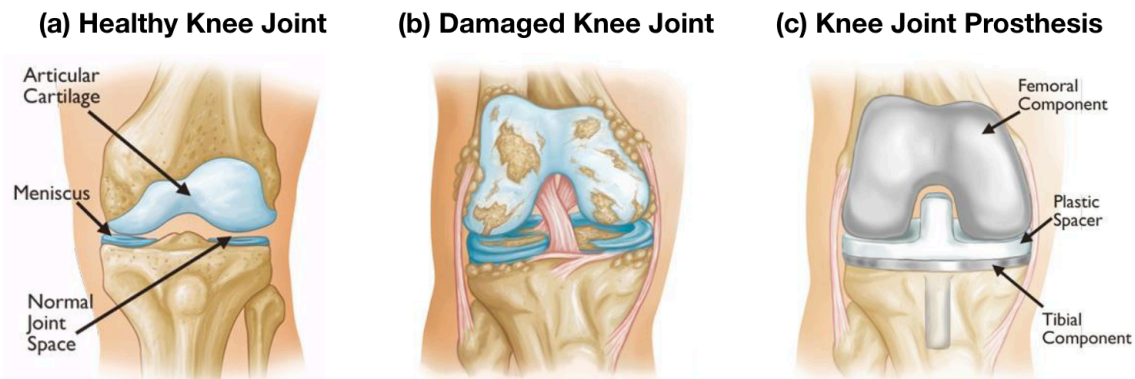


Figure 1 - (a) Healthy knee joint (b) damaged knee joint (c) knee joint with a prosthesis. Image adapted from: <https://orthoinfo.aaos.org/en/diseases--conditions/osteoarthritis/>

Typically, total joint replacements (knee, hip, shoulder) comprises a polymeric component with a metallic or ceramic counter-counter bearing. In particular, the polymeric component is ultrahigh molecular weight polyethylene (UHMWPE), and the metallic part is cobalt chrome, among other alloys. The most common couple bearing is polymeric-metallic and was introduced by Sir John Charnley in the 1960s. Sir John Charnley noted desirable qualities in the polymeric-metallic couple, such as low coefficient of friction, high degree of toughness, and reduced biological attack [2]. Other bearing couples are metal-on-metal, ceramic-on-ceramic, and ceramic-on-polymer (Figure 2). Nevertheless, UHMWPE continues to remain the gold-standard material for orthopedic applications.

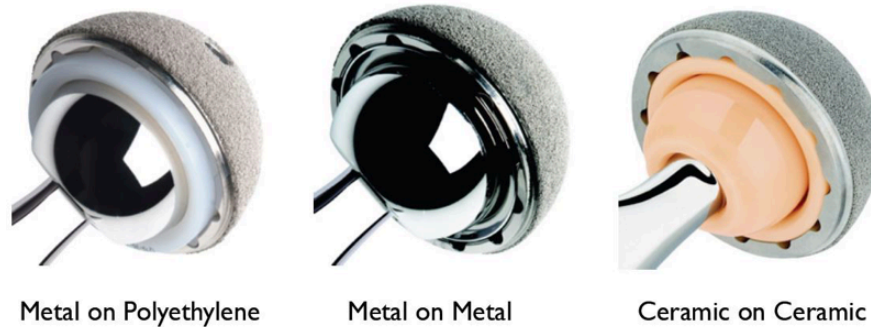


Figure 2 - Hip prosthesis with a metal-on-polyethylene, metal-on-metal, ceramic-on-ceramic. Image adapted from <https://www.jnjmedtech.com/en-US/companies/depuysynthes>

Primarily, the metal-on-metal and ceramic-on-ceramic implants restore function under greater loads in the joint. Nevertheless, metal-on-polyethylene continues to dominate the market because pathological issues of metal debris toxicity and squeaking challenge the success of metal-on-metal and ceramic-on-ceramic designs.

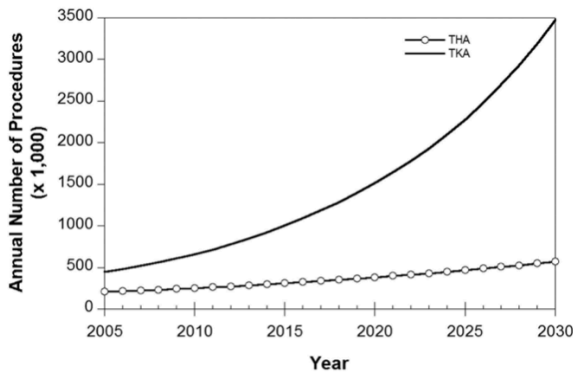
There is a need to improve implants' longevity and accommodate varying lifestyles to enable patients with a high quality of life post total joint replacement surgery. Further, there is substantial demand for total joint replacement as the baby-boom population begins to age, increased rates of obesity, and improved confidence in these devices – over 90% of joint replacements (knee and hip) survive beyond ten years [3]. Figure 3 shows the growth of total knee and hip procedures and revision surgeries [3].

Revision procedures are more burdensome to patients and require a higher financial cost than primary surgeries [4]. The changing demographics of total joint replacement (TJR) patients threaten the success rate of orthopedic systems. Primarily, Sir John Charnley designed these devices for older sedentary patients. However, these devices expanded to include both younger and more active patients over time. Younger patients are often at higher risk for revision due to higher activity levels and longer lifespan than elderly patients.

As revision surgeries are on the rise for total hip arthroplasty (THA) and total knee arthroplasty (TKA), the primary reasons for revision remain consistent. For example, common causes for revision are instability, mechanical or aseptic loosening, infection, implant failure or breakage, dislocation (THR), bearing surface wear, and periprosthetic fracture [5–7].

To improve the longevity of these medical devices and to mitigate revisions over a patient's lifetime, there has been a significant push to tailor the microstructure of UHMWPE to minimize wear and oxidative degradation and improve fatigue crack resistance [8–13]. In particular, improving the wear resistance of UHMWPE is the main driving force for current innovation (For hips, yet there is awareness that fatigue is an ongoing challenge in knees). Wear debris harms the human body, as its particles can elicit complex immunological responses [14,15]. For example, wear debris induced osteolysis (bone loss) can lead to prosthetic loosening and premature failure of the device [16].

(a) Projected number of primary THA and TKR



(b) Projected number of revision THA and TKR

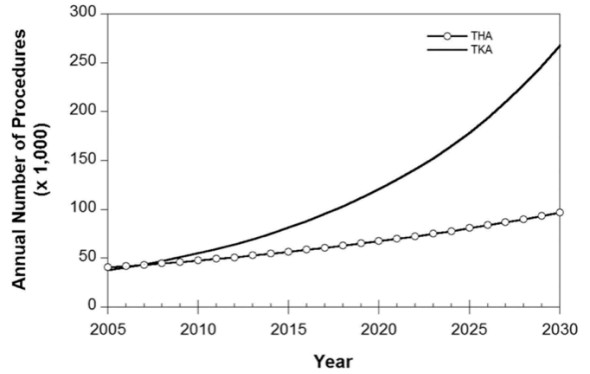


Figure 3-(a) projected number of primary total hip arthroplasty (THA) and total knee replacement (TKR) (b) projected number of revision total hip arthroplasty (THA) and total knee replacement (TKR) [4].

1.2 Ultra-High Molecular Weight Polyethylene

UHMWPE is the material of choice for total joint replacements. Primarily, because of its desirable material properties, biocompatibility, and microstructure [17–19]. As such, UHMWPE is a linear and semicrystalline polymer containing crystalline and amorphous domains since it is difficult for polymers to be fully crystalline. As such, UHMWPE has a crystallinity of 45 and 65% and uses covalent bonds and secondary interactions. Further, the ability for the chains to pack regularly, side-by-side, to form crystalline domains is a reflection of the chain architecture, backbone chemistry, and molecular weight. By contrast, the amorphous region in the polymer lacks order throughout its structure [20].

The crystallinity and molecular weight (4-6 million g/mol) affect the mechanical properties of UHMWPE [20]. Further, implant design challenges the optimization of material properties. Other factors that contribute to the performance of the implant include clinical issues, regulatory issues, and processing and materials selection [20]. Tailoring the mechanical properties of UHMWPE is done through processing conditions and altering the microstructure [20].

There are a variety of material formulations, each aimed to address issues of oxidative degradation, wear, and fatigue. While many material formulations exist, the balance of oxidation, wear, and fracture properties is a continual concern for orthopedic polymers used as bearing surfaces [21].

In the late 1990s, researchers crosslinked UHMWPE via gamma radiation to reduce wear debris and debris-induced osteolysis [22–24]. The radiation breaks up the intramolecular bonds and produces free radicals that promote crosslinking across the polymer chains. At the microstructural level, crosslinking increases the overall density and improves wear characteristics [9,25–27]. While crosslinking improves UHMWPE's adhesive and abrasive wear resistance, high levels of crosslinking affect mechanical properties such as ultimate strength, failure strain, fracture toughness, and fatigue crack propagation resistance [21,28,29].

When crosslinking occurs, it happens in the amorphous phase of UHMWPE [30]. However, the remaining free radicals produced in the process cause oxidative instability [31–35]. The remaining free radicals are undesirable because they can react with oxygen and may compromise the material properties over time [32,36,37]. As a result, researchers and manufacturers proposed using thermal treatments post crosslinking to avoid oxidative degradation and preservation of mechanical properties. Thermal treatments include either annealing below the

melting point of UHMWPE or melting above the melting temperature ("remelting") after irradiation [38,39]. During the remelting process, there is a quenching of the free radicals. While remelting can result in improved oxidative stability, reducing crystallinity and lamellae quantity, and diminishing the fatigue crack propagation resistance. By contrast, annealing preserves the material's important microstructure and mechanical properties [21,40].

Another effort to mitigate oxidative degradation in crosslinked UHMWPE is the infusion or blending of antioxidants such as Vitamin E [23,41–43]. Researchers noted that blending of Vitamin E reduces oxidation for crosslinked UHMWPE while retaining crystallinity quality and quantity [21,40]. However, blending Vitamin E also diminishes the crosslinking efficiency, thereby improving the fatigue resistance of crosslinked UHMWPE but at the expense of optimal wear resistance [44,45]. Wear, oxidative and fatigue resistance are essential properties that affect the longevity of total joint replacements. However, more work is needed to fully understand the polymer microstructures necessary for optimizing properties such as wear, oxidation, fatigue, and fracture [21,41].

1.3 Poly-ether-ether-ketone (PEEK) and carbon-fiber reinforced (CFR) PEEK

While UHMWPE has traditionally been the material of choice for medical implants, poly-ether-ether-ketone (PEEK) shows great promise as a superior implant material [46]. Where PEEK may excel over UHMWPE is in its highly tailorable mechanical properties [47]. Since fibers can be incorporated into PEEK to make new composites, the overall material's properties may be optimized by altering the fiber volumetric fraction or the fiber material choice (carbon fibers, glass fibers, etc.) [46]. This opens the design space of possible biocompatible materials and enables engineers to design new materials which better match the surrounding bone mechanics.

Carbon-fiber reinforced PEEK (CFR-PEEK) may offer many advantages by replacing metallic components. For instance, patients with metallic sensitivity may be positively affected from polymeric-based components. Furthermore, PEEK-based implants may be monitored *in vivo*, as they are radiolucent.

There are two types of carbon fibers that are suitable for load-bearing applications in orthopedics - Pitch-based and polyacrylonitrile (PAN) based carbon fibers. There are a few advantages to using these carbon fibers over UHMWPE and metallic-based materials in total joint replacements. Firstly, PEEK can maintain its mechanical properties during commonly employed sterilization processes (i.e., gamma, steam autoclave, vaporized hydrogen peroxide, and ethylene oxide) [46]. Secondly, CFR-PEEK can be a suitable alternative to load-bearing metallic components as it can reduce stress shielding, because CFR-PEEK components have a closer modulus match to bone properties. The mechanical properties of CFR-PEEK are strongly correlated to the microstructure [48].

Microstructural research of PEEK and PEEK composites notes that PEEK chains form an orthorhombic structure in the lamellar regions [49]. The thickness of the lamellae and the size and density of spherulites depend on the thermal history. As previously mentioned, thermal treatments can induce morphological changes, resulting in tunable mechanical properties [49]. For example, researchers show annealing causes an increase in crystallinity by a combination of thickening of the existing lamellae and nucleation and growth of new, thinner lamellae [49].

1.4 Dissertation Aims and Study Design

My dissertation is based on the hypothesis that nanoindentation offers an appropriate methodology to test the suitability of medical grade polymers for application in total joint reconstruction. I am to test this hypothesis by conducting nanoindentation to better (a) understand the structure-property behaviors and (b) develop the relationship between mechanical properties across various microstructural scales (spanning nano-micro-macro). Additionally, the dissertation seeks to implement a framework to allow researchers new to nanoindentation to develop best practices and obtain reliable measurements.

Chapter 2 discusses the development of a framework to characterize soft biomaterials and polymers using nanoindentation. Nanoindentation utilizes a hard indenter probe to deform the sample surface to measure local properties, such as indentation modulus and hardness. Initially intended for characterization of elastic and elastic-plastic materials, nanoindentation has more recently been utilized for viscoelastic solids as well as hydrated and soft biological materials. An advantage to nanoindentation is the ability to determine the nano- and microscale properties of materials with complex microstructures as well as those of limited sample dimension. Nanoindentation finds utility in the characterization of structural tissues, hydrogels, polymers and composites. Nevertheless, testing complexities such as adhesion and surface detection exist in nanoindentation of compliant viscoelastic solids and hydrated materials. These challenges require appropriate modifications in methodology and use of appropriate contact models to analyze nanoindentation data. A full discussion of protocol adjustments has yet to be assembled into a robust nanoindentation testing framework of soft biomaterials and polymers. We utilize existing nanoindentation literature and testing expertise in our laboratories to (1) address challenges and potential errors when performing indentations on soft or hydrated materials, (2) explore best practices for mitigating experimental error, and (3) develop a nanoindentation framework that serves researchers as a primer for nanoindentation testing of soft/hydrated biomaterials and polymers.

Chapter 3 investigates the mechanical behavior (i.e. tensile, compressive, and nanomechanical) and microstructural properties (i.e., crystallinity, lamellar thickness) of clinical formulations of UHMWPE. Correlations between mechanical and microstructural properties are developed to ascertain the structure-property relationships that are imperative to understand the behavior of UHMWPE in orthopedic implants.

Chapter 4 discusses the use of nanoindentation as a method to characterize mechanical behavior of clinical grade PEEK and PEEK composites. We examine PEEK formulations with pitch and PAN fibers and evaluate a range of thermal treatments known to influence the microstructure of the polymer. In this research, I vary the tip diameter of the indenter to determine indentation modulus over different length scales. The findings are correlated with previous characterization on the same systems using microindentation. The novelty of the research is that we identify the modulus of the various constituents present in the PEEK composite system. This research demonstrates that nanoindentation is an effective characterization tool for discerning fiber-matrix interactions and measuring the mechanical behavior in response to thermal treatment and carbon fiber type in PEEK composites. Nanoindentation is shown to be a viable tool for characterizing complex biomaterials and can serve as an effective technique to guide optimization of microstructures for long-term structural applications in the body.

Chapter 5 discusses a novel approach to assessing the surface properties of retrieved knee implants. In this investigation, it is the first attempt to use nanoindentation to understand the

changes of nanomechanical properties of retrievals and develops a protocol for future retrieval testing. Surface testing is important in the field of retrievals, as it allows for assessment of local properties and understand the impact of *in vivo* conditions on the mechanical behavior.

Chapter 6 discusses the ongoing challenges and future research direction for implementing nanoindentation as a method for analyzing medical-grade polymers and retrievals. Accompanying nanoindentation with microstructural analysis may provide insight into the effects of *in vivo* behavior. Future studies should focus on addressing the effects of tilt on nanoindentation measurements and comparing the nanomechanical properties of retrievals to standardized mechanical testing methodologies. Assessing the local properties of retrievals may provide insight into important questions in the field, like understanding wear mechanisms.

Chapter 2 – A methodological framework for nanomechanical characterization of soft biomaterials and polymers

This chapter was previously published by Journal of the Mechanical Behavior of Biomedical Materials [50].

2.1 Introduction to Nanoindentation Research

Nanoindentation techniques were developed primarily for linearly elastic, isotropic and homogenous materials [51]; yet, there is ongoing interest in utilizing this tool for the characterization of soft, hydrated materials with hierarchical microstructures [52]. Nanoindentation probes materials at the nano- and micro- length-scales, proving advantageous for mechanical characterization of samples with limited dimensions or complex microstructures. An advantage of nanoindentation is its ability to map the local mechanical behavior of heterogeneous materials [53]. However, a few disadvantages to nanoindentation may be localization, surface sensitivity, and variable skin depth issues. Nevertheless, nanoindentation is particularly appealing as a mechanical characterization tool of biological tissues with heterogeneous microstructures, irregular dimensions and compliant anisotropic behaviors [54]. Soft, hydrated biomaterials such as hydrogels [55–57] and cartilage [58,59] have employed nanoindentation methods to ascertain local mechanical properties such as modulus and hardness. As research in the fields of biomaterials, tissues and nature-inspired materials increases, there is ongoing demand for nanoscale characterization techniques that can elucidate structure-property relationships in these complex systems [60].

The lack of standardized guidelines for performing nanoindentation on soft, hydrated materials is an ongoing roadblock to validating nanoindentation and poses a risk of reporting erroneous nanomechanical measurements. Standardized procedures for characterizing the nanomechanical properties of metallic and stiff materials (i.e. MEMS, semiconductor components and protective coatings) exist (ASTM E 2546 and ISO 14577); yet, these lack experimental modifications and appropriate models for collecting and analyzing nanoindentation data for soft and hydrated biomaterials [61]. Variability in testing protocols may arise from the presence of adhesion, difficulty in detecting surfaces, fluid-probe interactions, or viscoelastic behaviors [62]. Further, a lack of standardization leads researchers to use inappropriate data collection and analysis, or each to develop their own protocol, so it is difficult to compare results between studies in different groups or know how the indentation modulus should compare to materials properties (such as modulus) measured through bulk testing methods like tension and compression. In sum, standard procedures for characterizing soft, hydrated and heterogeneous systems are needed. In the interim, we review the literature to offer a methodological framework for nanomechanical characterization of soft, hydrated biomaterials and polymers.

Table 1 - Review papers on static nanoindentation of soft materials and biological materials (hydrated and non-hydrated) spanning from early 2003 to 2020.

Reference	Material	Aims
Perepelkin et al. 2020 [63]	Soft Materials	<ul style="list-style-type: none">• Discussion of various depth sensing indentation approaches• Exploration of factors contributing to erroneous measurements• Provide an overview of methods that account for adhesion
Qian et al. 2018 [64]	Soft Biological Materials	<ul style="list-style-type: none">• Discussion of constitutive behavior of soft biomaterials

		<ul style="list-style-type: none"> • Discussion of experimental methodology and challenges from nanoindentation of soft biomaterials • Exploration of the applications of nanoindentation
Chang et al. 2016 [65]	Biological Materials	<ul style="list-style-type: none"> • Discussion of other small-length scale testing techniques • Examination of the potential errors and parameters that may influence nano-mechanical measurements • Provide an overview of contact mechanisms • Provide a guideline for experimental settings
Oyen 2015 [66]	Hydrated Biological tissues and hydrogels	<ul style="list-style-type: none"> • Discussion of the challenges associated with handling and testing hydrated materials • Discussion on the models used to extract mechanical properties • Provide a review of key results from recent nanoindentation experiments • Discussion on the outlook for the future of nanoindentation
Ebenstein et al. 2006 [52]	Biological materials	<ul style="list-style-type: none"> • Provide a review of the research impact of nanoindentation • Discussion of the mechanics of nanoindentation • Discussion of probe selection, adhesion, surface preparation and hydration
Haque 2003 [67]	Biological materials, biomaterials	<ul style="list-style-type: none"> • Exploration of the applications of nanoindentation • Discussion of the materials already explored by nanoindentation

A limited number of review papers address the complications associated with testing soft, hydrated or viscoelastic biomaterials. In the seminal nanoindentation review paper on nanoindentation in biomaterials, Ebenstein and Pruitt emphasize the susceptibility of adhesive interaction between the probe and sample [52]. A practical guide for analyzing nanoindentation data with an emphasis on biological materials was later published by Oyen and Cook [68] and serves as an introduction to various deformation modes found during indentation - elastic, plastic, viscous and fracture; however, it does not focus on the intricacy of studying the nanomechanical properties of soft biomaterials. Oyen later highlights the future of nanoindentation in her review of nanoindentation of hydrated materials and tissues [66]. Oyen recognizes that soft-biological materials are prone to adhesion effects and may have different failure modalities that pose experimental challenges where analysis of data needs further elaboration for obtaining reliable results. More recently, Chang and co-workers explore the potential errors and parameters that may influence nanomechanical measurements and provide a brief discussion on the contact mechanics within the applications of nanoindentation [65]. These review articles serve as a foundation to introduce the complex multi-faceted approach of performing a nanomechanical analysis of biological materials. However, they provide few practical pointers on how to select the best methods for data collection and analysis when studying a new material.

As the use of nanoindentation expands to other fields, there is a pressing need to provide an educational paper that is accessible to those not fully versed in the field of nanomechanical characterization. This work aims to serve as a comprehensive guide for edifying novices to nanoindentation on proper testing practices, thereby minimizing experimental errors and ensuring efficacy in measurements. Through this review, we develop a framework that encompasses a broad range of nanoindentation users who seek to employ nanoindentation in diverse research fields. We aim to encourage accessibility while ensuring efficacy and reliability in the nano-mechanical measurements. As such, the framework provides guidance on all aspects of the nanoindentation experiment, including probe selection, experimental set-up, and data analysis methods, highlighting common data collection challenges and how to address them.

2.2 Nanoindentation: materials research and other small-scale testing techniques

Since its inception in the 1980s, nanoindentation research has expanded from thin films to ceramics, alloys, polymers and biomaterials. We performed a systematic literature review focused on nanoindentation research for the following materials – hydrogels, soft polymers, soft biological materials, soft cartilage and thin-films. Each result was carefully reviewed to ensure that depth sensing nanoindentation instrumentation was used in the research. As illustrated in Figure 4, in the 1990s, nanoindentation emerged as a tool for measuring and mapping the mechanical properties of thin films, as at the time it was the only standardized technique that measured properties of small volumes of stiff materials.

Nanoindentation was primarily designed for testing elastic and elastic-plastic materials and this trend is reflected in the extensive number of early research materials (Figure 4). An uptick of nanoindentation research for other materials ensued in the late 1990's with the advancement of nanoindentation analytical models for analyzing load-displacement curves, namely after Oliver and Pharr published their seminal paper on nanoindentation [69]. Further, an increase in nanoindentation research may also be a consequence of the technology becoming more affordable and accessible and technological advancements leading to improved capability of capturing local nano-length scale mechanical properties.

The proportion of publications each year for nanoindentation of biomaterials is small compared to thin films and alloys (Figure 4). Nanoindentation research for hydrogels, soft biological and soft cartilage materials is fairly recent; the earliest publications appeared in the early 2000s but research in this realm is expanding (Figure 4). Similarly, an increasing trend is observed for nanoindentation research of soft polymers. The abundance of literature that exists for non-biomaterial systems is likely owed to the established experimental testing protocols that promote confidence in and reliability of data. Since biomaterials are a newly developing field for nanoindentation, there is a need to address the challenges and errors in order to advance nanoindentation research of soft, hydrated biomaterials and polymers. Numerous review publications highlight the utility of nanoindentation as a method that can assist in the physical understanding of materials and the local properties of surfaces, interfaces and highly hierarchical structures [41,52,64,66,70], so nanoindentation is likely to be applied to diverse materials in the future. As nanoindentation becomes more prolific in other fields, it is imperative to develop a framework that can assist researchers make the appropriate choices for obtaining reliable nanomechanical measurements.

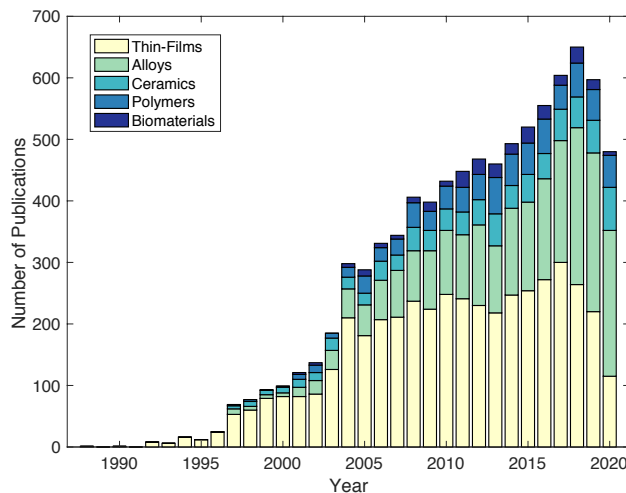


Figure 4- Progression of nanoindentation research in the field of thin-films (yellow), alloys (green), ceramics (green-blue), polymers (blue), and biomaterials (dark-blue). The materials encompassed in the biomaterials category include hydrogels and biological materials, for example cartilage and tissues

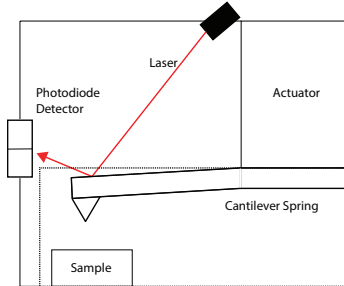
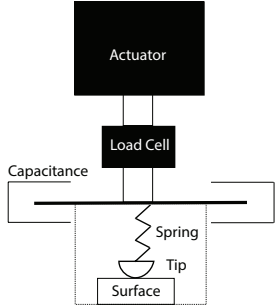
2.3 Nanoscale mechanical characterization techniques (When is it appropriate?)

Many biological materials and biomaterials have a structural hierarchy that influences their bulk mechanical behavior. There is growing interest in mechanical characterization of structure-property relationships, in particular across multi-scaled or hierarchal length scales, for synthesis of tailored nature-inspired or hierarchical materials for specific use in load-bearing applications [71]. This need motivates the urgency for robust testing across nano- and micro-scale domains. Nanoindentation provides an appealing option for understanding the mechanical properties across multiple length scales of biological systems and biomaterials.

Aside from nanoindentation, other methods for mechanical testing of small and soft materials include pipette aspiration and atomic force microscopy. A handful of researchers have compared the mechanical behavior of soft, hydrated biological and biomaterials across various testing modalities. For example, nanoindentation has been coupled with traditional methods of confined and unconfined compression in the characterization of articular cartilage [72]. Buffinton et al. compared the mechanical behavior of polyacrylamide gels measured using pipette aspiration, and bulk uniaxial compression to nanoindentation. In the same study, the researchers compared the properties of silicone elastomers (<1 MPa) measured using nanoindentation to properties measured via pipette aspiration, compression, and tension [73]. The findings from Buffinton and co-workers concluded pipette aspiration and nanoindentation to be suitable mechanical characterization techniques for soft biomaterials [73].

Comparisons of nanoindentation and atomic force microscopy (AFM) are more prevalent in the biomaterials literature, since both have been used extensively to indent soft materials. For this reason, we compare AFM with nanoindentation (Table 2). AFM utilizes a nanoscale-sized pyramidal probe attached to a small cantilever; as the cantilever bends, a laser diode and a split photodetector detects the bending. This bending is indicative of the probe-sample interaction force. In AFM, the indenter penetrates the sample at a slight angle to the surface; by contrast, the indenter travels to the surface vertically in nanoindentation. Similar to AFM, nanoindentation can measure the stiffness of soft and hydrated materials, however, it is more limited in load and displacement range. Furthermore, AFM was developed for scanning (topographic characterization) and adapted to mechanical analysis, while nanoindentation was developed for mechanical testing and adapted to scanning. While AFM has better spatial resolution it is more challenging to get accurate mechanical properties. Conversely, nanoindentation has less spatial resolution for scanning and testing, but there exists more accurate mechanical models.

Table 2 – Advantages and disadvantages for using atomic force microscopy (AFM) and nanoindentation as a mechanical characterization technique. As for the instrumentation, in AFM, the approach is angled, while nanoindentation is a vertical approach.

	Atomic Force Microscopy	Nanoindentation
Advantages	<ul style="list-style-type: none"> Higher load and depth resolution Suitable for ultra-soft materials Suitable for very thin materials Superior image and spatial resolution Easier to test in fluids 	<ul style="list-style-type: none"> Larger load and displacement range Suitable for stiff materials More accurate mechanical models and mechanical properties Suitable image resolution on stiff materials
Disadvantages	<ul style="list-style-type: none"> Limited load and displacement range Challenging to extract accurate mechanical properties Sample dimension constraints Intensive sample preparation Slow scan time 	<ul style="list-style-type: none"> Lower load and depth resolutions Not optimized for ultra-soft materials nor testing in fluids
Instrumentation	<p style="text-align: center;">Angled-Approach</p> 	<p style="text-align: center;">Vertical Approach</p> 

A noteworthy observation is that the location on the load vs. indentation may differ for the same sample material. This is due, in part, to the variety of indentation parameters used when indenting the materials showcased in Figure 5, such as maximum load, maximum displacement, loading rate, probe geometry, and probe size. For example, for the same stiffness material and maximum indent load, the maximum indent depth is expected to increase as the diameter of a conospherical probe decreases. Similarly, in viscoelastic materials for which the stiffness increases with indentation loading rate, even if the maximum indent depth is held constant, the maximum load is expected to increase as the loading rate increases. These examples show that careful attention is necessary when studying complex materials' nanomechanical properties and comparing results across studies with different experimental parameters.

Further, Figure 5 shows how the nanoindentation load and displacement ranges compare with AFM and microindentation ranges. It is interesting to note that although the displacement range of nanoindentation spans all three testing methods, the load range (~10 uN – 10 mN) is unique. It is also notable that all the nanoindentation data collected with blunt, larger diameter probes (e.g., conospherical, flat punch) fall within the microindentation displacement range. In comparison, the data predominantly collected using sharper probes (e.g., Berkovich) fall in the AFM range. These results suggest that nanoindentation, AFM, or microindentation are suitable for characterizing some materials. However, the testing parameters need to be different so that the loads fall into the optimal ranges for those systems.

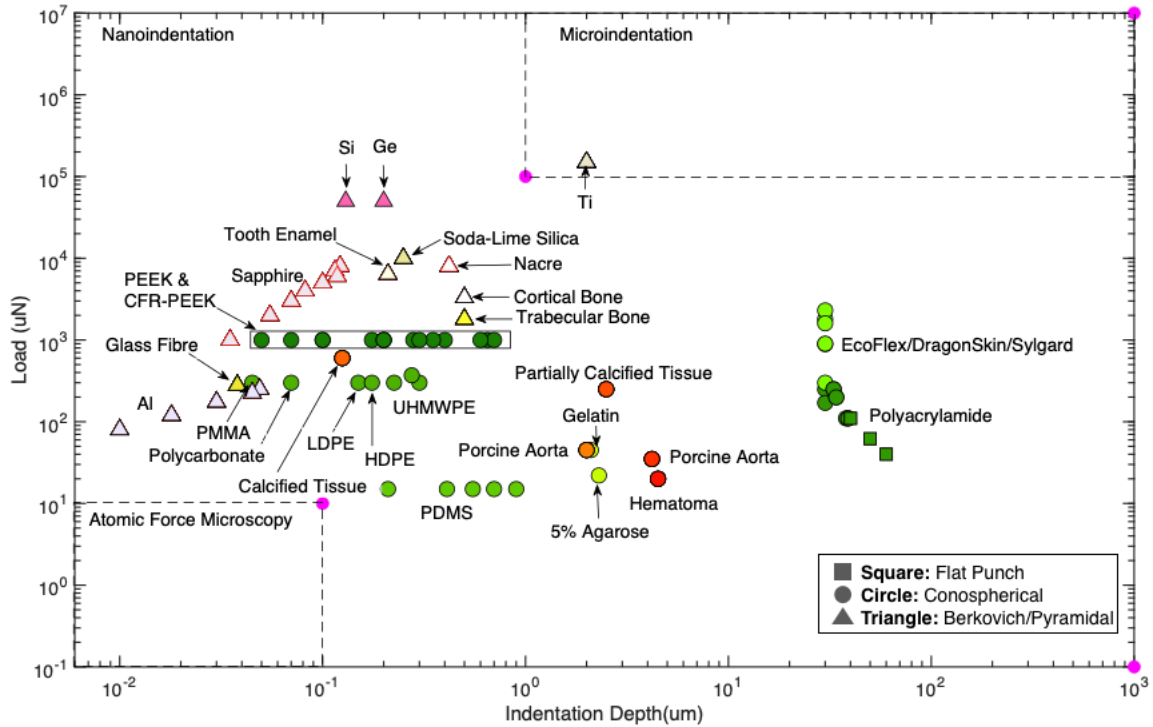


Figure 5- Load (μN) and indentation depth (μm) ranges for AFM, nanoindentation and micro-indentation, including load-depth nanoindentation data points of representative materials to illustrate the range of properties being measured. Materials include polymers, biological materials, thin films, and ceramics/glasses. The load-indentation depth values were obtained from the literature [60,74–87].

When deciding on the best small-scale characterization technique, knowledge of the macroscale elastic modulus of the material helps identify whether the indentation depth or indentation load is within the resolution limits of the testing system. Oyen [88] provides a general back-of-the-envelope calculation to aid in determining whether a material is suitable for nanoindentation; the process is illustrated in Figure 6. This method makes use of the maximum-load (P_{max}) equation that is based on the Hertz relationship between load and displacement for a spherical indenter. By using this method, we can get a quick assessment of the material suitability for nanoindentation based on the knowledge of the macroscale properties and the radius of the indenter probe. Use of this equation requires the following assumptions: (1) the material exhibits minimal adhesion to the probe; (2) the material deforms within its linear elastic regime under the applied stress and strain rate produced by spherical probe of radius, R ; (3) any effects of finite thickness are neglected for the indent depth, h ; and (4) the probe is made from a comparably rigid material, such that the elastic properties of the probe can be neglected. The calculation serves as a rough estimate of suitability for using nanoindentation (Figure 6). Once the approximate maximum load or maximum displacement has been calculated, the values can be compared against the range of the nanoindenter instrument. While the load and displacement range may vary across different manufacturers, customarily the displacement may fall within $10^{-2} - 10^3 \mu\text{m}$ and the load within $10^{-1} - 10^7 \mu\text{N}$, dependent on instrumentation. Lastly, careful selection of the probe geometry and size is imperative to the overall gathering of data, and guidance on selecting a suitable probe geometry and size will be discussed in subsequent sections.

Identifying whether expected load or displacement is within the equipment's range

$$P = \frac{4}{3} E_r R^{\frac{1}{2}} h^{\frac{3}{2}} \quad \text{Eqn: Hertz relationship}$$

P: load; E_r : reduced modulus; R: Radius of conospherical probe; h: depth

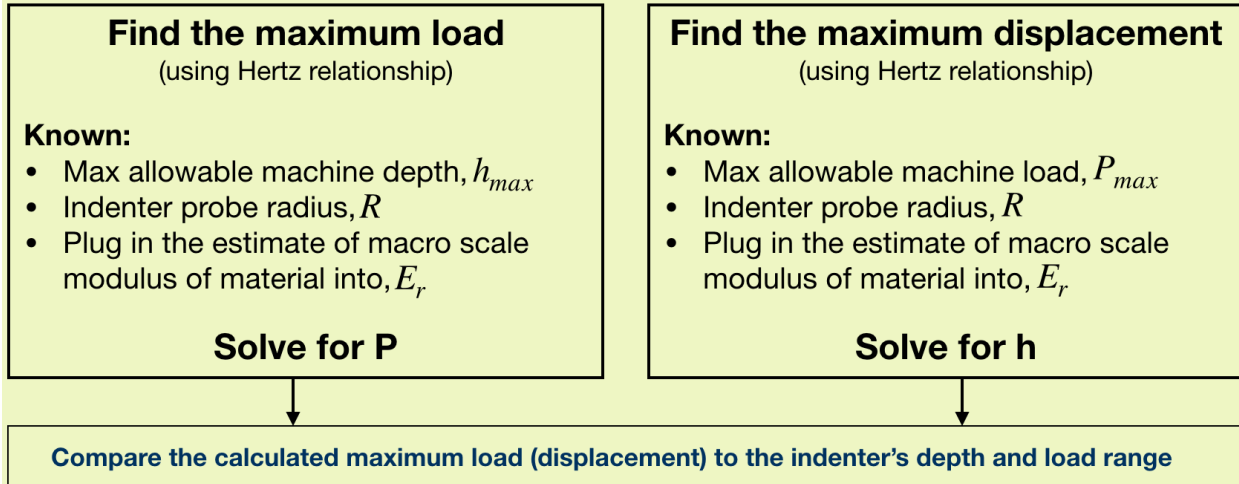


Figure 6 - General guideline to help determine whether nanoindentation is within range to characterize the sample [88]. In this analysis, P_{max} is the maximum load, R is the radius of conospherical probe, and h_{max} is the estimated maximum depth. E_r is the unknown reduced elastic modulus (in this condition it is the plane strain modulus) that is determined from an indentation test and is limited by the macroscale elastic modulus of the material.

2.4 Nanoindentation background

In depth-sensing nanoindentation, the load and displacement are monitored continuously as a small probe is pressed into a sample following a user-prescribed profile. The load-displacement data can later be analyzed using an appropriate contact mechanics model to extract mechanical properties such as modulus and hardness. Before an indenter can perform an indent, the probe needs to know when it is in contact with the surface. A common method for surface detection is the use of a set-point force. Using this method, the indenter probe is slowly stepped towards the surface until a predefined force, the set-point force, is sensed by the instrument. Once that force is detected, the instrument assumes the probe is in contact with the sample and will begin the indent and data collection process.

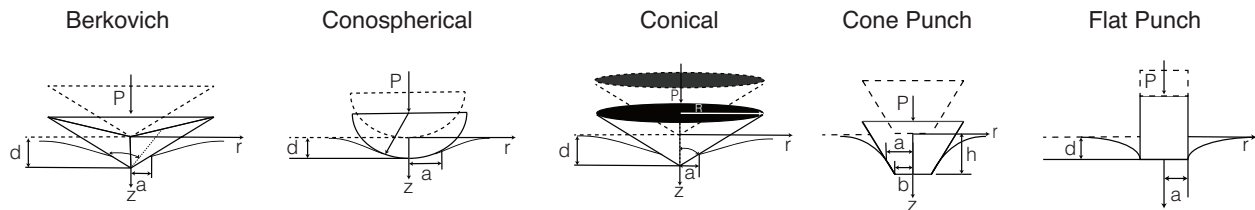
The first crucial step in the design of a nanoindentation protocol is identifying an indenter geometry and size that is most appropriate for the scope of the research and the material in question. The next step is setting up the time profile, which provides the instructions (testing parameters) to the nanoindenter – rate, maximum load/displacement, holding times and whether the test is in load or displacement control. Lastly, the data analysis of nanoindentation involves selecting a suitable model to analyze the load-displacement curves and extracting the mechanical properties. This review will explain in detail the importance of each step of the indentation process and provide suggestions to ensure collection of reliable mechanical properties.

2.5 Probe geometry and size

Judicious choice of probe geometry and size is essential for acquiring reproducible and accurate measurements of the desired material. The probe geometry and size influences the

nanomechanical measurement for a number of reasons including the variation in contact stress beneath the indenter relative to the length scales of underlying material constituents. The most common probe geometries used for nanoindentation include Berkovich, conospherical, conical, flat-end conical and flat punch (see Figure 7). Berkovich (3-sided pyramidal probes) and conical probes are commonly considered sharp probes. Flat punch, flat-end conical and conospherical indenters are examples of blunt probes; however, the acuity of conospherical probes may be increased by decreasing the probe diameter.

Figure 7 - Schematic illustration of the various probe geometries used in nanoindentation – Berkovich, Conospherical, Conical, Cone punch, and Flat punch, . In this diagram, P is the applied load, d or h is the distance from the surface of the sample to maximum penetration depth, a is the radius of the projected contact between the tip and the sample, and b is the radius of the flattened end of the cone punch.



Geometry of probes is an important consideration for nanoindentation. The advantages and disadvantages of flat punch, spherical and pyramidal indentation probes is summarized in Table 3. Spherical probes (Figure 7) are advantageous in that there is a delayed onset of plastic deformation while the sharper conical or pyramidal probes induce elastic-plastic deformation even at small displacements. Flat punch probes are advantageous in that they provide a constant, known contact area, while contact area changes with depth for all other probe geometries. However, the issues with a flat punch are the presence of stress concentration at edges and the challenge with achieving full contact, as it is very difficult to achieve a perfect parallel surface on samples. Another probe geometry utilized in characterizing soft materials, the flat-ended cone punch (Figure 7), offers the benefits of using a flat-punch while reducing the high stress concentration at the corners. In contrast to flat punches, flat-ended cones are easier to manufacture, and can offer a constant contact area for small displacements, simplifying the analysis [82]. The flat-ended cone punch has been successfully used in the characterization of cartilage and polyurethane [59].

	Advantages	Disadvantages	Materials
Flat Punch	<ul style="list-style-type: none"> + Data interpretation is straightforward + Detecting and measuring the contact area is simpler than other tip geometries + Contact area is less likely to get affected by thermal drift or creep 	<ul style="list-style-type: none"> - Most limited in spatial resolution (compared to sharp indenters) - Not suitable for characterizing fine features - Alignment of tip parallel to sample surface is important and challenging - Stress singularities present at the edges 	<ul style="list-style-type: none"> • Large diameter flat punches are preferred for testing very soft materials
Spherical	<ul style="list-style-type: none"> + Can use analytical models (e.g. JKR) + Delay onset of plastic deformation + Geometric similarity + Offers increased contact stiffness without high stress concentrations + Wide range of diameters available (for multiscale analysis or to probe constituents or tissue level properties) 	<ul style="list-style-type: none"> - Reduced spatial resolution (compared to sharp indenters) - May not be ideal for probing really fine features 	<ul style="list-style-type: none"> • Large diameter spherical probes are preferred for testing very soft materials • Smaller diameter spherical probes are preferred for testing stiffer materials • Preferred for testing depth-dependent materials
Pyramidal	<ul style="list-style-type: none"> + Yields much smaller contact area + Geometric similarity + Suitable to probe fine features 	<ul style="list-style-type: none"> - Sharp edges may damage soft materials - Harder to detect surface of soft materials 	<ul style="list-style-type: none"> • Most suitable for fine features • Preferred for stiffer materials • Most commonly used probe geometry

Table 3 – Presentation of the advantages and disadvantages of commonly used nanoindentation probes in tissues and polymers and a summary of the materials that are best suited for characterization with given probe geometries.

A compendium of literature related to nanoindentation of biomaterials is provided in Table 4, which offers relevant information on the probe utilized including its geometry, material, and probe-size (radius), followed by the biomaterial and the measured elastic moduli. As demonstrated in Table 3, the conospherical probe is widely employed for a variety of softer biomaterials. In contrast, the Berkovich is prevalently used for characterizing bone-tissue [89] and stiff PDMS formulations [90].

One factor to consider when deciding on an indentation probe is the stiffness of the material to be tested – *is the sample a soft material or a stiff material?* As an example, we consider indentation of gels using a flat punch. For stiff gels whose modulus is on the order of 100 kPa and above, the general recommendation is to use smaller diameter punches whose diameter is on the order of 500 μm [91]. In contrast, as the gel stiffness decreases toward the 1 kPa range, a larger diameter punch of 1.75-2 mm is recommended [91]. The challenge with using a diameter that is too small on a soft material is that the low contact stiffness makes it difficult to properly identify the contact interface and reach a stable equilibrium during surface detection, thereby, preventing the initiation of the indentation test. Similarly, using a diameter that is too large for a material whose surface is not nominally flat hinders achieving a complete contact [91]. In general, the softer the material, the blunter the probe recommended.

Table 4 – Summary of literature pertaining to nanoindentation of biomaterials. Table includes probe geometry, probe material, probe radius, biomaterial characterized and indentation elastic modulus.

Probe Geometry	Probe Material	Probe Radius	Material Characterized (Reference)	E (MPa)
Berkovich	Diamond		PDMS [92]	/
			Bone tissue [81]	/
Flat Punch	Sapphire	25 μm	poly-2-hydroxyethylmethacrylate (pHEMA)	/
	Sapphire	25 μm	PuraMatrix-collagen hydrogels [83]	/
	Diamond	97.72 μm	Polyacrylamide gel [82]	/

Flat ended cone		5 μm	Urethane [59]	4.73
		5 μm	Cartilage [59]	2.56
		90 μm	Urethane [59]	4.41
		90 μm	Cartilage [59]	2.32
		90 μm	Cartilage ii [59]	3.43-4.73
		190 μm	Urethane [59]	4.34
		310 μm	Urethane [59]	4.62
		310 μm	Cartilage [59]	1.26
		1000 μm	Cartilage ii [59]	1.21-1.62
Conospherical	Diamond	100 μm	PEG [57]	0.6 – 8.5
	Diamond	100 μm	PDMS [54]	0.7 – 2.6
	Diamond	100 μm	Hematoma, Fibrous Tissue, Calcified Tissue [93]	0.02-2.6, 0.05-21.5, 0.04-21300
	Diamond	100 μm	Porcine Costal Cartilage [94]	1-2.4
	Diamond	1 μm	Plaque [81]	0.06-9
	Diamond	50 μm	PDMS [95]	1.9 \pm 2.3
	Diamond	55 μm	pHEMA [96]	\
	Diamond	55 μm	PS-4 Polymer [53]	\
	Borosilicate G	100 μm	PDMS [57]	\
	Borosilicate G	75-150 μm	PDMS [97]	0.2 – 2.2
	Sapphire	283 μm	Cartilage, Bone [53]	\
	Sapphire	400 μm	PS-4 Polymer [53]	\
	Sapphire	200 μm	Silicon [98]	\
	Sapphire	500 μm	Polyacrylamide Gels [98]	\
	Glass Sphere	500 μm	Polyacrylamide gel [82]	\
	Alumina	400 μm	Poly(acrylamide) gels [55]	\

A second factor to consider when deciding on an indentation probe is the size scale of the features of interest in the sample material – *are you interested in tissue level / bulk properties, or the properties of individual constituents?* For heterogenous or porous materials, nanomechanical measurements can vary significantly depending on whether a sharp or blunt probe is used, and can also be affected by the radius of the blunt probe [53]. Varying the dimension of the probe enables the mechanical characterization across macro-, micro-, and nano- length scales; however, increasing the dimension of probes decreases spatial resolution [52]. The selection of probe geometry and size are parameters that depend on the length scale of the microstructure or constituents present in the material and the goal of the research. For instance, a large diameter spherical probe ($> 50 \mu\text{m}$) is better suited for measuring tissue level properties in soft tissues because the diameter is larger than typical dimensions of cells and structural fibers [60]. On the other hand, if the mechanical properties of the individual constituents are needed then the dimension of the probe should be adjusted to maximize the spatial resolution and allow measurement at precise locations [52].

A small body of work has explored the role of indenter size on the measured elastic modulus of soft materials. For example, Oyen and co-workers investigated the size effects in indentation of hydrated biological tissues by utilizing micro- and nanoindentation techniques. They discovered that elastic properties were consistent across length-scale but the time-dependent mechanical response were substantially different between large and small contact radii for the same tissue specimen [53]. Additionally, Simha and co-workers explored the effects of probe size on the mechanical properties of bovine cartilage and polyurethane [59]; they observed that the modulus measurements obtained using larger (2 mm and 4 mm) indenter probes agreed with the literature values. By contrast, the modulus measured using a smaller (90 μm diameter) probe overestimated the reported values. Hence, measured modulus may have a dependence on indenter probe size, especially when probe sizes span constituent length scales. Many tissue studies seeking

to characterize constituent behavior choose an indenter size that is less than 10% of the expected length-scale of the modulus variation, as this enables accurate prediction of the mechanical variations in tissues with significant modulus heterogeneity [99].

In summary, researchers have the choice between different geometries, and within some of these geometries there is control over size. The stiffness of the material and the size of the target features influence the choice of your probe – geometry and size. When testing soft materials, a blunt or large diameter probe is preferred in order to avoid puncturing the material and to achieve sufficient contact stiffness to detect when the probe is in contact with the sample. The diameter of the blunt probe should be chosen based on the size scale of the constituents of interest or the desired spatial resolution of testing (there is a trade-off between increasing resolution and decreasing contact stiffness).

Indenter probes are made from stiff, hard materials to prevent substantial probe deformation and wear during indentation. Reducing wear ensures that the probe geometry will not change rapidly with testing, increasing the durability and consistency of the probe (AFM probes are less expensive but are less durable and need to be replaced frequently). Using a stiff material ensures that the deformation observed in the indent is dominated by the deformation of the sample rather than the probe. As such, the material recommendations for fabricating probes varies based on the stiffness and hardness of the material being indented. Typically, stiff, hard materials such as diamond or sapphire are used to fabricate commercial indenter probes, under the assumption that probes are used to test hard, stiff materials. However, lower stiffness materials such as glass and tungsten can be equally suitable when nanoindentation is applied to soft biomaterials with moduli more than three orders of magnitude lower than traditional indentation substrates. Glass has the advantage of being able to fabricate a truly spherical probe at a much lower cost than sapphire (which can also be perfectly spherical) or diamond (which is difficult to fabricate as a perfect sphere at the nano/micro scale due to its faceted crystal structure). Glass is also easy to functionalize.

Common indenter probe materials are diamond, sapphire, glass, tungsten or alumina. Commercial indenter probes are made from diamond and sapphire, while custom-made indenters include glass, tungsten or alumina. Custom-made probes are often tailored for specific researcher needs. In particular, there is ongoing research into the use of alternative probe materials to mitigate probe-sample adhesion [59]. For example, Grunlan and co-workers prepared tungsten probes of various probe diameters to compare the mechanical property measurements against those obtained using diamond [80]. They attributed observed differences to the probe-adhesion and suggested that tungsten probes may prevent adhesion effects during indentation. Others have utilized indenter probe functionalization to mitigate adhesion between the probe and sample (adhesion effects are described in subsequent sections). Slaboch and colleagues pioneered the use of keratose-functionalized probes to characterize blood clots after prior research showed a reduction of blood/tissue adhesion in medical devices [100]. While probe functionalization in the nanoindentation community is not widely employed, it is a commonly employed practice in the AFM community to mitigate probe-and-sample adhesion.

In summary, diamond-based probes are the gold standard of nanoindentation; they offer high strength and hardness as well as ease of manufacturability across various probe diameters. It is worth noting that when using diamond-based probes, conospherical probes will not be perfectly spherical due to diamond's faceted crystal structure, and some geometries such as flat punches are more challenging to manufacture in the tens of microns size range. Therefore, the use of other lower-cost and higher-fidelity probe materials, such as glass, may be preferred when fabricating

blunt probes for testing soft materials. The impact of probe stiffness on modulus measurements in soft materials is demonstrated in Figure 8. As shown in Figure 8, using different material probes (diamond vs. glass) to characterize soft polymers (between 1 MPa and 50 MPa) resulted in negligible differences in reduced modulus calculations, and the moduli were comparable to those computed when neglecting indenter properties entirely. This demonstrates that glass is a sufficiently stiff probe material to prevent substantial probe deformation during indentation of soft polymers. This provides researchers with the flexibility to utilize a variety of probe materials when testing soft materials.

Evaluating the impact of probe material on the sample modulus

Plane-strain modulus: $\frac{1}{E_r} = \frac{1 - \nu_i^2}{E_i} + \frac{1 - \nu_s^2}{E_s}$
 Re-write: $E_r = \left(\frac{1 - \nu_i^2}{E_i} + \frac{1 - \nu_s^2}{E_s} \right)^{-1}$ Eq. A

Calculate the reduced modulus for a material with the following properties?

Sample 1	Sample 2
$E_s = 0.001 \text{ GPa}$ $\nu_s = 0.2$	$E_s = 0.050 \text{ GPa}$ $\nu_s = 0.2$

Use Eq. A to calculate the sample modulus, assuming a (1) diamond indenter and (2) glass indenter (3) neglecting indenter properties

(1) diamond indenter	(2) glass indenter	(3) neglecting indenter properties
$E_i = 1143$ $\nu_i = 0.06$	$E_i = 47$ $\nu_i = 0.17$	
<p>Sample 1</p> $\frac{1}{E_r} = \frac{1 - 0.06^2}{1143} + \frac{1 - 0.2^2}{0.001}$ $E_r = 0.00104$	<p>Sample 1</p> $\frac{1}{E_r} = \frac{1 - 0.17^2}{47} + \frac{1 - 0.2^2}{0.001}$ $E_r = 0.00104$	<p>Sample 1</p> $\frac{1}{E_r} = \frac{1 - 0.2^2}{0.001}$ $E_r = 0.00104$
<p>Sample 2</p> $\frac{1}{E_r} = \frac{1 - 0.06^2}{1143} + \frac{1 - 0.2^2}{0.05}$ $E_r = 0.05208$	<p>Sample 2</p> $\frac{1}{E_r} = \frac{1 - 0.17^2}{47} + \frac{1 - 0.2^2}{0.05}$ $E_r = 0.05202$	<p>Sample 2</p> $\frac{1}{E_r} = \frac{1 - 0.2^2}{0.05}$ $E_r = 0.05208$

Figure 8 - Calculating the impact of diamond probe, glass probe and neglecting indenter properties on the determination of the reduced elastic modulus of soft polymers (1 MPa, 50 MPa). In Eq. A, E_r is the reduced modulus (in GPa), E_i is the indenter modulus, ν_i is the Poisson's ratio of the indenter, E_s is the sample modulus, and ν_s is the Poisson's ratio of the sample.

2.6 Load Functions

The applied load or displacement profile is another critical experimental parameter in indentation testing. Triangular and trapezoidal profiles are most commonly utilized in nanoindentation (Figure 9). The triangular profile consists of load and unload segments (Figure 9a), while a trapezoidal profile includes a holding period at peak load or displacement (Figure 9b). The use of the trapezoidal time profile elucidated in (Figure 9b) is commonly employed for viscoelastic materials because creep related artifacts manifest in nanoindentation as a “nose” on the unloading curve (Figure 9d), as reported by Briscoe and colleagues [101]. This nose is observed on an indentation load-displacement curve when a material continues to increase in displacement after the applied load is reduced, posing a challenge for accurately determining the unloading curve slope. A trapezoidal loading curve has been shown to mitigate this creep artifact in polymeric materials (Figure 9e) [84].

An alternative profile is shown in Figure 9c, and it incorporates an initial lift-off from the sample (Segment A), a loading segment (Segment B), a hold period at peak displacement (Segment C), and an unloading segment that also lifts-off from the sample (Segment D). This displacement profile is commonly used for testing soft materials to correct for probe sink-in (when the probe is

already several hundred nanometers into a sample before the surface is detected) or characterize probe-sample adhesion [57]. The advantage of this displacement profile is that it captures the entire indent process from indent approach and surface detection through full separation of the tip from the sample, even in the presence of adhesion, rather than starting data collection after surfaced detection.

A related aspect of consideration when developing a time profile is deciding upon the magnitude of the setpoint force used to find the initial surface contact; once the surface is found by the probe sensing the setpoint force, the zero displacement is established. A setpoint force, usually between 0.1 and 10 μN , is specified in the process of developing the time profile [102]. The higher the setpoint force, the deeper the probe will sink into the sample when detecting the surface. The displacement resulting from the preload can be quite significant for compliant materials [95]. Hence, the lowest value of setpoint force that you can use that avoids false engagement with the surface is recommended. Typical values are 0.1-2 μN ; using values as high as 10 mN is only recommended when necessary for testing in fluids (to avoid false surface detection due to changing capillary forces on the shaft, as will be discussed in a later section) and should only be used in conjunction with the time profile with lift-off segments (Figure 9c) to allow for proper identification of the true zero of displacement. In summary, including the lift-off segment (Segment A) at the start of an indent aids in establishing the true “zero point” of contact between the probe and the sample to correct for sink-in, while the lift-off at the end of the indent (Segment D) can be used to ensure that you capture the full indent until the probe fully separates from the sample when there is significant adhesion between the probe and the sample. The load-displacement response of a viscoelastic material using a Trapezoidal II profile (Figure 9c) is illustrated in Figure 9f, the load-displacement profile in the red box is the data that would have been captured using the standard trapezoidal profile (Figure 9b) without the lift-offs. Including the lift-offs allows determination of the zero-displacement point to correct for sink-in.

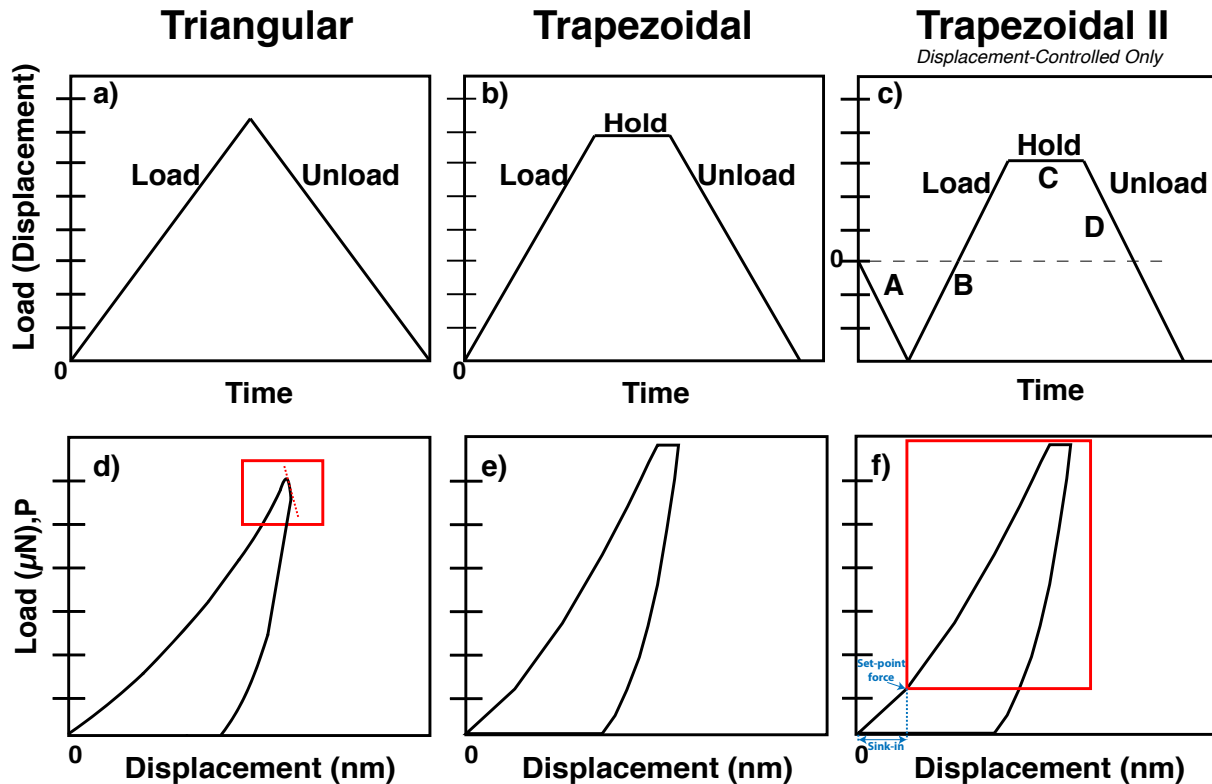


Figure 9 - Load (displacement)-time profile for (a) triangular loading profile composed of a simple load-unload cycle, (b) a trapezoidal load-hold-unload profile, and (c) a trapezoidal load-hold-unload profile incorporating a lift-off at the beginning of indentation testing (Segment A) and at the end of indent testing (Segment D). (d) Load-displacement response of a viscoelastic material exhibiting a “nose” at peak load for a viscoelastic material tested using a triangular load-time profile (a). (e) Load-displacement response of a viscoelastic material for trapezoidal load-time profile (b), eliminating the “nose” during initial unloading at peak load. (f) Load-displacement response of a viscoelastic material for Trapezoidal II profile (c), with the red box indicating the data that would have been captured using the standard trapezoidal profile (b) without the lift-offs. Including the lift-offs allows determination of the zero-displacement point to correct for sink-in.

2.7 Load-Control vs. Displacement Control

During a load-controlled experiment, the load applied during indentation is preselected and as the load changes incrementally, the displacement results depend on the stiffness of the material. The electrostatic force compensates for the stiffness of the sample and maintains a constant applied force in load-controlled tests. By contrast, during a displacement-controlled experiment, the displacement changes while the reaction force results depend on the stiffness of the material. For most indenters, the default setting is load-controlled as most components are loaded through force rather than displacement in real life applications. However, displacement-controlled experiments are preferred for testing compliant, adhesive and time-dependent materials.

One reason why displacement-controlled experiments are preferred for soft biological materials is that the properties may vary with depth because of their hierarchical structure - cartilage is a good example, because depth can make the difference between indenting just the superficial layer versus superficial to deep. When testing a soft material in load-control, it will undergo substantially more displacement in the z-direction in comparison to a stiffer sample for the same applied load. Such behavior results in measuring properties at various depths based on

material stiffness, and makes it challenging to target a specific layer of a material such as cartilage or observe variations across sample groups when comparing load-controlled indents [103]. Another advantage of displacement-controlled experiments is the ability to correct for sink-in when displacement-controlled indents are performed using the time profile shown in Figure 9c, as described in section 3.2. In addition, displacement control allows visualization and quantification of adhesion, which will be discussed in subsequent sections. Furthermore, displacement-controlled experiments simplify the analysis of viscoelastic materials that are strain rate dependent [53]. An important consideration for time-dependent materials is that displacement-controlled nanoindentation offers constant strain rate while load-controlled experiments do not [53]. A summary of the characteristics for both load-controlled and displacement-controlled nanoindentation experiment is summarized in Table 5.

Table 5 – Characteristics of load control and displacement control experimentation during nanoindentation.

	Load-Control	Displacement-Control
Characteristics	<ul style="list-style-type: none"> • Strain rate is not constant 	<ul style="list-style-type: none"> • Strain rate can be held constant • Can incorporate lift-offs to accurately define the initial contact point and detect adhesion
Materials	<ul style="list-style-type: none"> • Stiff • Not prone to adhesion 	<ul style="list-style-type: none"> • Compliant • Prone to adhesion • Time-dependent behavior

2.8 Load-Displacement Curves

An indentation load-displacement curve is commonly referred to as the “mechanical fingerprint” of the material. Figure 10 shows a generalized load-displacement curve based on a trapezoidal load-time profile. Nanoindentation load-displacement data is commonly used to ascertain basic nanomechanical properties such as elastic modulus and hardness. However, it is also possible to determine creep and stress relaxation parameters from nanoindentation data of viscoelastic materials. The path of the loading and unloading in the load-displacement curve is also indicative of whether a material is exhibiting elastic, elastic-plastic, brittle, viscoelastic or adhesive behavior.

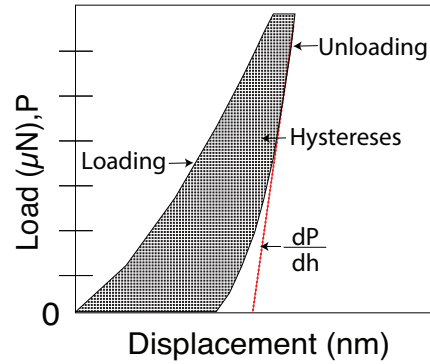


Figure 10 - Representative load-displacement curve (this is a load-controlled indent), illustrating the loading, unloading, hysteresis and slope of unloading curve (dP/dh). Note that the full adhesive load-displacement curve would only be collected using a loading profile with initial and final liftoff, as shown in Figure 9c. An indent with the profile shown here would only capture the data shown in the red box in Figure 11.

The load-displacement curve shows distinct behavior for elastic-plastic, viscoelastic and adhesive materials based on a trapezoidal load profile, as illustrated in Figure 11. For elastic-plastic materials, the unloading path does not follow the loading path as it would for a perfectly elastic material, and there is an observable hysteresis denoted by the area between the loading and unloading path. Viscoelastic materials also experience energy loss due to deformation, thereby forming a hysteresis, and also show evidence of stress relaxation (or creep, in a load-controlled test) during the hold period [68].

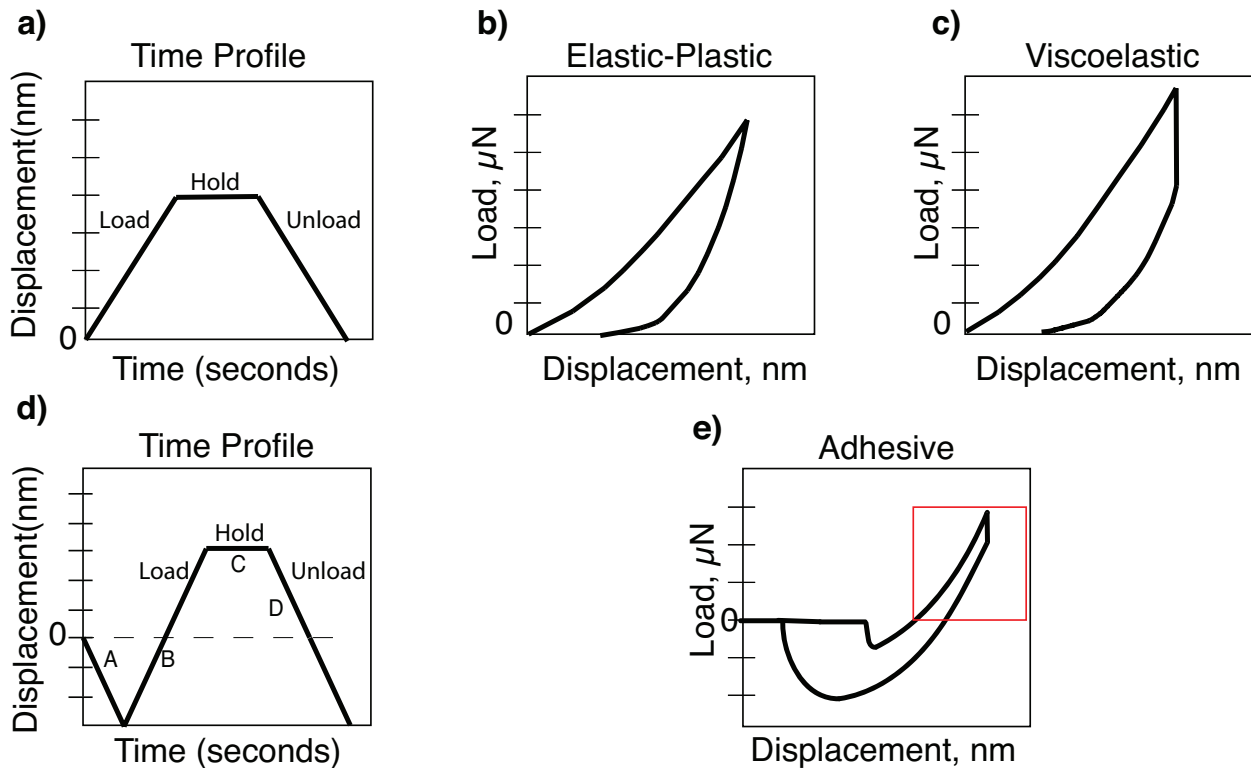


Figure 11 - (a) Trapezoidal time-profile in displacement control and associated load-displacement behavior for (b) elastic-plastic and (c) viscoelastic materials. (d) Trapezoidal II time profile in displacement control typically used for testing an adhesive material, and the associated load-displacement behavior (e). The portion of the load-displacement curve contained in the red box is the data that would be collected using the basic trapezoidal displacement-time profile in Figure 8a.

Adhesion offers another challenge in nanoindentation of soft materials. The indenter probe and sample interaction for a material exhibiting probe-sample adhesion is illustrated in more detail in Figure 12, along with the important points on the curves that are used during analysis. Note that negative forces are observed during both loading (snap-on) and unloading (pull-off) due to adhesion between the probe and the sample. This evidence of adhesive interaction is not apparent unless indenting in displacement control using a displacement-time profile incorporating lift-offs as showing in Figure 9c and Figure 12. In the presence of adhesion, the probe is experiencing three balanced forces: the resistant and adhesive forces from the sample and the externally applied force from the nanoindentation system. When the probe is brought near enough to the surface to sense the surface energy, the probe is drawn into the sample until zero force is reached (non-zero displacement). At this point, the stored elastic energy and the surface energy are balanced. This is indicative of zero external loads acting on the probe. The indent then proceeds with sample loading and unloading, and finally, as the probe is lifted off the sample, the tip and sample fully separate.

While viscoelastic effects are typically mitigated primarily by using the trapezoidal loading profiles, changes to both data collection and data analysis methods are often employed for samples exhibiting adhesion, and this behavior is addressed below.

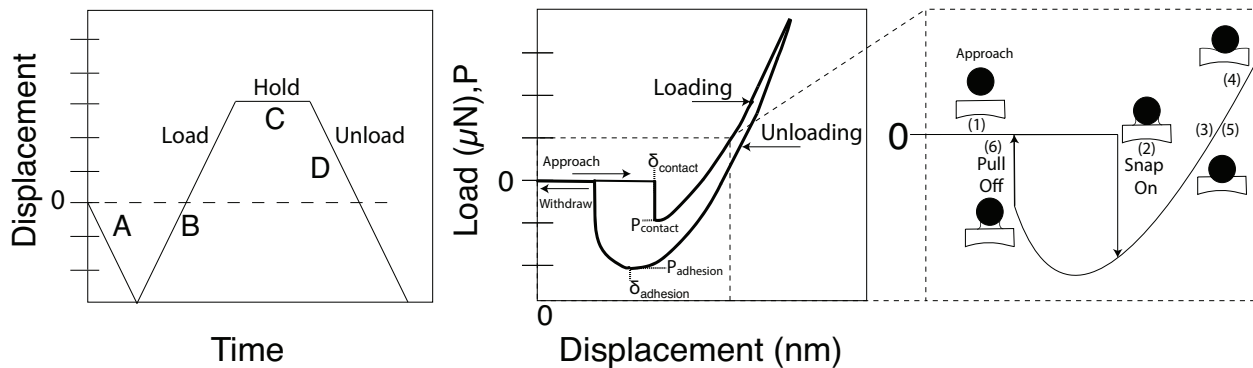


Figure 12 - Representative load-displacement behavior of a material exhibiting adhesion during the indentation process, with accompanying displacement-time profile. By including the lift-offs in segments A and D of the displacement-time profile, the indentation data captures the entire indent process. First, the probe approaches the sample (1), which is followed by a snap-on (2) process as it makes contact with the sample. In steps (3-5), the probe engages with the sample and step (6) shows the probe pulling from sample and experiencing adhesion (material sticking to probe as it is withdrawn).

2.9 Overview: Contact Models in Nanoindentation

Nanoindentation involves penetrating the specimen using an indenter probe while recording the indentation load, P , and displacement, h , for one complete loading and unloading cycle (Figure 10). The indenter penetrates the specimen at a given load or displacement rate until it reaches the desired maximum load or displacement; subsequently a hold period at maximum load or displacement may be enforced to prevent viscoelastic effects followed by an unloading portion. The loading region undergoes a mixture of elastic and plastic deformation with a resultant residual impression of the indenter probe while the unloading region exhibits elastic recovery and provides a measure of the surface modulus [104,105]. The seminal nanoindentation papers that lay the foundation for the use of load-displacement curves in determining mechanical properties are summarized in Appendix A.

The Oliver and Pharr method (see section 3.5.2) is the standard technique for analyzing the nano-mechanical behavior of stiff materials such as metals and ceramics. This method is based on

the work of Boussinesq, Hertzian contact mechanics and Sneddon's derivation that provide the general relationships among the load, displacement and contact area for any punch described as a solid of revolution of a smooth function. While the Oliver and Pharr method was developed and validated for elastic and elastic-plastic materials, it is commonly employed in the analysis of soft biomaterials and polymers [84,106]. However, this method may not always yield accurate results since adhesion is presumed to play a negligible role in the sample deformation when using the Oliver and Pharr method. For example, using a Hertzian approach to analyze materials with adhesion underestimates the contact area as well as the effective load experienced by the substrate, resulting in overestimation of sample modulus [107]. Adhesion-dominated interactions between the nanoindentation probe and sample are best analyzed with other contact models (discussed later).

2.10 Hertz linear elastic analysis

The Hertz linear elastic analysis is based on the classical Hertzian contact theory. The hertzian reduced modulus, E_r^{Hertz} , is expressed as

$$E_r^{Hertz} = \sqrt{\frac{S^3}{6RP_{max}}} \quad \text{Equation 1}$$

Where R is the nominal radius of the probe, and P_{max} is the maximum applied force that corresponds to the total penetration depth into the surface. The contact stiffness, S , is obtained from the force-displacement curve. Here E_r , the reduced modulus, is related to the elastic modulus of the substrate as defined by Equation 2

$$\frac{1}{E_r} = \left[\left(\frac{1-\nu_s^2}{E_s} \right) + \left(\frac{1-\nu_i^2}{E_i} \right) \right] \quad \text{Equation 2}$$

Here E_s is the elastic modulus of the substrate and E_i is the elastic modulus of the indenter, ν_s is the Poisson's ratio of the substrate and ν_i is the Poisson's ratio of the indenter. It is common practice to neglect the Poisson's ratio and modulus of the indenter when testing soft biomaterials, as the indenter stiffness is generally significantly larger than the substrate making the indenter term negligible. The stiffness (S) of the material is measured from the unloading segment of the force-displacement curve (Figure 10), as shown by Equation 3:

$$S = \left(\frac{dP}{dh} \right)_{h=h_{max}} \quad \text{Equation 3}$$

Combining Equations (Equation 1-3), and assuming probe deformation is negligible, provides an expression for the elastic modulus for spherical indentation (Equation 4):

$$E_S^{Hertz} = \sqrt{\frac{S^3(1-\nu_s^2)^2}{6RP}} \quad \text{Equation 4}$$

2.11 Oliver and Pharr

The Oliver and Pharr method utilizes Sneddon's relationship for a flat cylindrical punch and is generalized for any punch described as a solid of revolution for a smooth function [108]. The mathematical relation between contact stiffness, contact area and modulus are based on Sneddon's simplification from the Boussinesq equations (details can be found in Appendix B) [109]. Appendix B summarizes seminal papers on the theory and contact mechanics associated with the theory of the Oliver and Pharr method. Important elements are highlighted below.

In the Oliver and Pharr technique, the unloading portion of the load-displacement curve (Figure 10) is fit with a power-law, which is useful for materials with non-linear unloading behavior [110]. The unloading slope is estimated as the first derivative of the fitted function at the maximum displacement and is the prevalent method for analyzing indentation data (Equation 5).

$$S = \frac{dP}{dh} = \alpha(h - h_f)^m \quad \text{Equation 5}$$

Here, α and m are empirically determined fitting parameters, h is the displacement and h_f is the final displacement after complete unloading [110].

Classical indentation theory states that the contact stiffness of the material is related to the contact area, A , and reduced modulus, E_r , as expressed in Equation 6.

$$\frac{dP}{dh} = \frac{2}{\sqrt{\pi}} \sqrt{AE_r} \quad \text{Equation 6}$$

The projected contact area, A , requires precise knowledge of the shape of the indenter, which is described by a shape or area function that relates the cross-sectional area of indenter to the distance, d , from its probe. Two methods exist for determining the area function and they both involve making a series of indentations on a calibrating material over a range of indentation depth. The first method involves indentation on a soft metal and using transmission electron microscopy (TEM) to measure the size of the impression created by indentation and the accompanying load-displacement data to establish the area function. The other method involves making indentations on an isotropic material of known modulus from which the area function can be deduced from the load-displacement data alone. The advantage of using a calibrating material to identify the area function is that it eliminates the need for imaging the indents.

The use of a suitable standard calibration material is critical. Both quartz and fused silica have been explored [111]; however, the use of fused silica as a standard calibrating material has come into question when testing soft materials [112]. Klapperich and co-workers utilized polycarbonate as a standard calibrating testing material because the depths probed during calibration were similar to their compliant materials of interest [84]. To our knowledge, an alternative standard calibrating material has not been proposed for materials with moduli that are orders of magnitude softer than polycarbonate. A potential standard calibrating material for use in characterization of soft materials is polydimethylsiloxane (PDMS), an isotropic and homogenous polymeric material whose properties can be tailored via crosslinking. More research is needed in the realm of creating standard calibrating materials for soft samples.

The contact area is expressed a function of contact depth as shown in Equation 7.

$$A = C_1 h_c^2 + C_2 h_c^1 + C_3 h_c^{1/2} + C_4 h_c^{1/4} + \dots \quad \text{Equation 7}$$

The values for C_1, C_2, C_3, C_4 , etc. can be experimentally obtained by performing a series of indents at varying penetration depths on a standard calibrating material (as described above) and subsequently fitting Equation 7. Many test systems use a default area function that assumes an ideal probe geometry. The ideal area function equations for Berkovich, conical probe, spherical and cylindrical flat punch are depicted in Table 6, these assume ideal probe geometry. Klapperich and colleagues noted that the value for C_1 is approximately 24.5 when using a Berkovich indenter to probe polycarbonate [84]. This value is equivalent to the ideal Berkovich area function ($A = 3\sqrt{3} \tan^2 \theta h_c^2 = 24.5 h_c^2$) for deep indents. While using the ideal probe geometry instead of experimental calibration can be effective when performing deep indents with sharp probes or perfectly spherical probes (e.g., fabricated from glass or sapphire, not diamond), for shallow indents experimental probe calibration is needed to avoid measurement errors due to probe imperfections. For example, sharp probes do not come to perfect points as assumed in the ideal probe area function; a new Berkovich probe will typically have a radius of curvature of at least 100 nanometers, and this can increase over time due to wear if testing hard materials. Similarly, spherical probes fabricated from diamond may diverge from their ideal shape at the nm scale due to the faceted nature of diamond.

Table 6 - Area function Equations for Berkovich, conical probes [113], spherical and cylindrical flat punch. Where h_c is the contact depth, θ is the semi-angle for a Berkovich indenter (65.27°), α is the effective cone angle for a conical indenter, and a is the radius of the flat punch tip.

Probe Geometry	Area function equation
Berkovich	$A = 3\sqrt{3} h_c^2 \tan^2 \theta = 24.5 h_c^2$
Conical of half-apical angle α	$A = \pi h_c^2 \tan^2 \alpha$
Spherical	$A = \pi(2R h_c - h_c^2)$
Cylindrical flat punch	$A = \pi(a^2)$

2.12 Adhesion-based models (JKR, MD, MDT)

The models described above are valid when the interfacial adhesive forces are much lower than the applied compressive force between indenter and sample substrate. When adhesion forces are not negligible, and spherical probes are used for indentation, it is more appropriate to apply continuum mechanics models that include the adhesive effect:

$$a^3 = \frac{6R}{8E_r} f(P, F_{po}) \quad \text{Equation 8}$$

Established models for adhesion include Johnson Kendall Roberts (JKR), Maugis-Dougdale (MD), and Derjaguin-Muller-Toporov (DMT). These are summarized in Table 7.

The most widely used contact mechanics models for capturing adhesion are the Johnson-Kendall-Roberts (JKR) and Derjaguin-Muller-Toporov (DMT) theories. JKR is used for low modulus materials with high surface energy and large radius of curvature while DMT theory is applicable to high modulus materials with low surface energy and small radius of curvature.

Physically, JKR accounts for adhesion forces only within the expanded area of contact; DMT accounts for adhesion forces outside the contact area while maintaining the Hertzian gap profile. Maugis-Dougdale (MD) is a transitory model that captures the interactions between surfaces that lie between the JKR and DMT models. A more in-depth analysis is provided in Appendix C.

Tabor observed that JKR and DMT exist as two extreme limits that can be parametrized using Tabor's parameter, as defined by Equation 9.

$$\mu := \frac{d_c}{z_0} \approx \left[\frac{R(\Delta\gamma)^2}{E_r^2 z_0^3} \right]^{\frac{1}{3}} \quad \text{Equation 9}$$

Here z_0 is the equilibrium separation between the two contacting surfaces, $\Delta\gamma$ is the work of adhesion, E_r is the reduced modulus, and R is the probe radius being used for testing. The work of adhesion represents the amount of energy needed to pull two surfaces apart and is a function of probe size and adhesion forces [114]. The Tabor parameter is calculated to identify whether the contact conditions fall within the JKR ($\mu > 5$), DMT ($\mu < 0.1$) or MD ($0.1 < \mu < 5$) regimes.

Table 7- Commonly used adhesion-based models for analyzing contact mechanics data with adhesion.

Model Name	Johnson, Kendall, Roberts (JKR)	Derjaguin, Muller, and Toporov (DMT)	Maugis-Dougdale (MD)
Assumptions	The initial pressure distribution between two contacting spheres consists of repulsion close to the center and attraction at the edge of the contact area	Attraction forces are occurring outside the contact area and these forces are too weak to produce any substantial deformation of spheres	Describes the interaction potential between surfaces
Application	<ul style="list-style-type: none"> Compliant materials Large sphere radii Strong, short-range adhesion forces 	<ul style="list-style-type: none"> Stiff materials Small sphere radii Weak, long-range adhesion forces 	
Tabor's Parameter (μ)	$\mu > 5$	$\mu < 0.1$	$0.1 < \mu < 5$

The most commonly utilized theory to analyze nanoindentation load-displacement data of soft materials with adhesion is the nano-JKR method [115]. Ebenstein and Wahl compared the results of load-displacement data using several methods based on the JKR adhesion model [115]. The nano-JKR methods used to analyze the mechanical properties of materials exhibiting adhesion are captured in Figure 13. These methods rely on several important points in the load-displacement curves and are derived by evaluating the JKR equations at specific points. Table 8 summarizes relevant research in the area of adhesive-based models and nanoindentation on soft and hydrated materials. Ebenstein and Wahl found that displacement method I, which used points from the unloading curve, worked best for analyzing nanoindentation data of soft polymers using a large diameter spherical probe [64], but Method I was used by Grunlan and in analysis of AFM force

curves [80]. Curve fitting the unloading curve using equations derived from the JKR model (Figure 13) is the most reliable method, but is more labor-intensive [57].

Per review of the literature (Table 8), nano-JKR is the most commonly used model for analysis of load-displacement curves that exhibit adhesion as measured via depth sensing indentation, while the other adhesion-based contact theories are more generally employed in AFM.

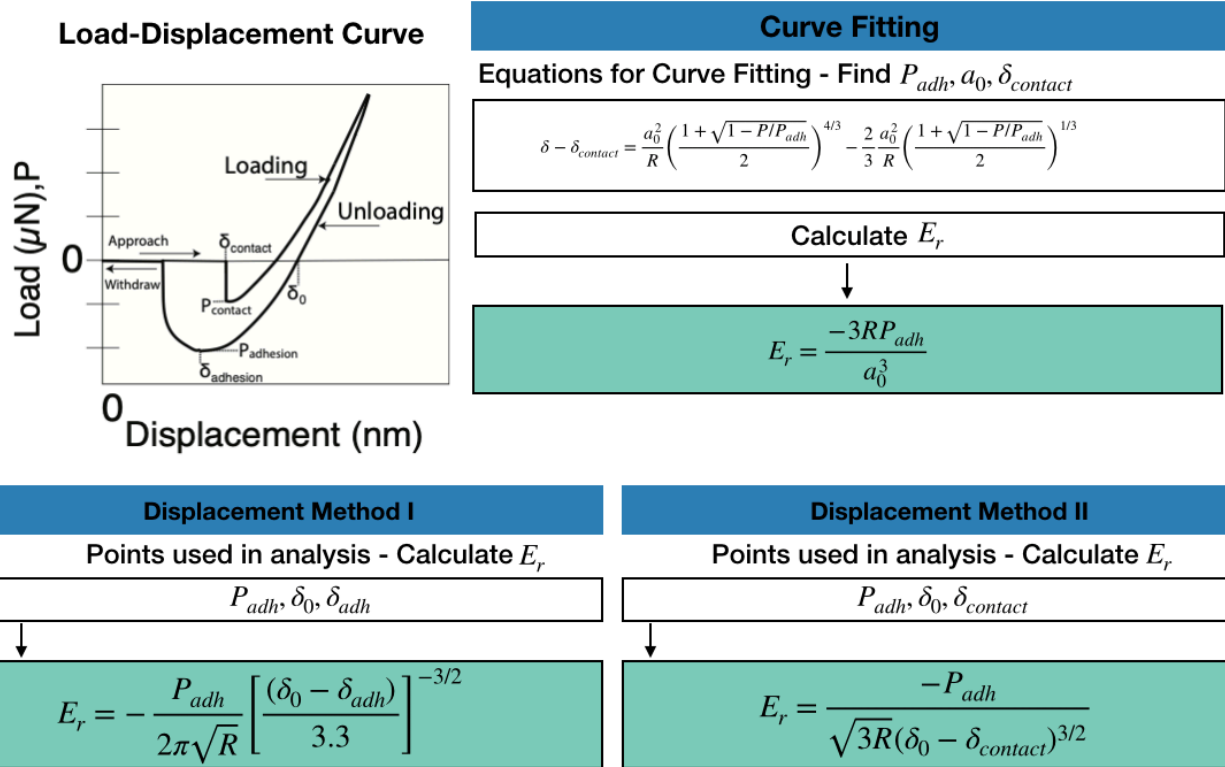


Figure 13 - Nano-JKR method used to analyze samples experiencing adhesion. There are three approaches: Displacement Method I, Displacement Method II, and curve fitting. In all equations, R is the radius of the conosphical probe. The other variables used to calculate the reduced modulus, E_r , in Displacement Methods I and II are labeled on the figure. In the curve fit equation, $P_{adhesion}$ is the maximum negative load reached during pull-off (at $\delta_{adhesion}$), a_0 is the projected contact radius between the probe and the sample at zero load (at δ_0), and $\delta_{contact}$ is a variable included to zero the displacement to optimize the fit. P_{adh} , a_0 , and $\delta_{contact}$ are solved for using a non-linear curve fit of the load-displacement ($P - \delta$) data from the unloading curve.

Table 8 – Research utilizing JKR theory to analyze nanoindentation load-displacement curves and research that advances the nanoindentation research for soft materials.

Reference	Summary
C. Jin, Z. Wang, A. Volinsky, A. Sharfeddin, N. Gallant (2016) [116]	Mechanical characterization of crosslinking effect in PDMS using nanoindentation The nano-JKR method was implemented to analyze the load-displacement curves of polydimethylsiloxane (PDMS).
D. Ebenstein (2011) [117]	Nano-JKR force curve method overcomes challenges of surface detection and adhesion for nanoindentation of a compliant polymer in air and water Addresses the challenges of testing soft and hydrated samples, provides alternative hydrating fluids to minimize adhesion effects. The research focused on characterizing polydimethyl siloxane (PDMS) and showed the JKR to be a suitable method to account for adhesion.
S. Gupta, F. Carrillo, C. Li, L. Pruitt, C. Puttlitz (2006) [118]	Adhesive forces significantly affect elastic modulus determination of soft polymeric materials in nanoindentation Investigated the nanomechanical properties of PDMS elastomers, and used the JKR contact model to analyze the data and compared the results to data analyzed from Hertz contact model. This paper

	highlighted the importance of utilizing the appropriate contact model when a sample experiences non-negligible adhesion effects.
F. Carrillo, S. Gupta, M. Balooch, S.J. Marshall, G Marshall, L. Pruitt, C. Puttlitz (2005) [54]	Nanoindentation of PDMS elastomers: Effect of crosslinking, work of adhesion, and fluid environment on elastic modulus This research used nanoindentation to characterize elastic moduli of soft, elastomeric polydimethylsiloxane (PDMS) with varying degrees of crosslinking. Adhesion contact mechanics was implemented on the indentation measurements and determined the effects of adhesion. The research highlighted the importance of considering adhesion in the calculation for determining the elastic modulus, especially for soft materials.
C. Jin, D. Eberstein (2016) [119]	Nanoindentation of compliant materials using Berkovich probes and flat probes The paper extends the nano-JKR analysis to include Berkovich and flat indenter probes. The researchers performed numerical simulations by applying adhesive interactions as interaction potential and the surface deformations coupled by half-space Green's functions discretized on the surface.
J. Kohn, D. Eberstein (2013) [57]	Eliminating adhesion errors in nanoindentation of compliant polymers and hydrogels This research provides two methods for considering adhesion in the nanoindentation analysis. The first method is the nano-JKR curve method and the second method is the surfactant method.
D. Eberstein, K J. Wahl (2006) [115]	A comparison of JKR-based methods to analyze the quasi-static and dynamic indentation force curves This research compares five approaches used to analyze quasi-static and dynamic load-displacement data obtained from instrumented indentation. The data was analyzed by direct curve fitting, three different simplified methods that are based on the JKR theory.
Q. Liao, J. Huang, T Zhu, C. Xiaong, J. Fang (2010) [120]	A hybrid model to determine mechanical properties of soft polymers by nanoindentation The development of a hybrid model – JKR and Hertz- to analyze the elastic modulus of soft polymers (PDMS) using nanoindentation techniques.
Y. Cao, D. Yang, W Soboyejoy (2005) [95]	Nanoindentation method for determining the initial contact and adhesion characteristics of soft polydimethylsiloxane (PDMS) This research illustrates the method that combines JKR and Maugis-Dugdale adhesion theories and nonlinear least squares fitting to predict the load-indentation depth characteristics of PDMS.

2.13 Experimental Challenges and Errors

This section describes challenges that are encountered during the nanoindentation process that can interfere with accurately measuring the elastic modulus, and poses potential solutions to those challenges. The challenges discussed pertain to indenter probe and sample interaction, particularly, (a) surface roughness, (b) contaminated probe, (c) adhesion, (d) false engagement, and (e) substrate effects, as depicted in Figure 14. These are all issues that can be detected by looking at the load-displacement curves.

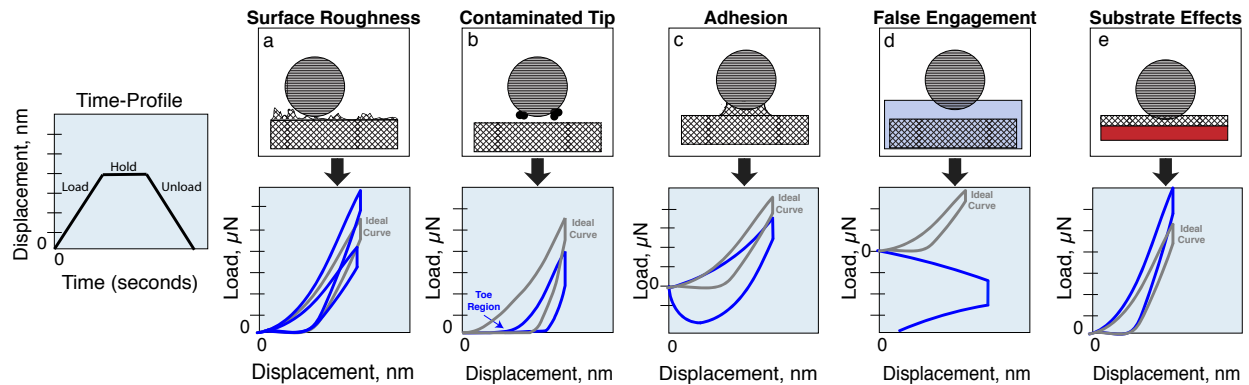


Figure 14 – Illustration of potential challenges that may be encountered during nanoindentation, (a) surface roughness, (b) contaminated probe, (c) adhesion, (d) false probe-sample engagement, and (e) substrate effects, accompanied by their respective load-displacement behavior.

2.14 Surface Roughness

Surface roughness can lead to a wide variability in indent load-displacement response, as shown in Figure 14. Surface roughness can have a significant effect on nanomechanical measurements, particularly if the arithmetical mean deviation (R_a) of the assessed roughness profile is on the same scale as the probe radius (Figure 14a). Chen and co-workers used a computational approach to investigate the effects of surface roughness on nanomechanical properties. They found a decrease in mechanical properties with increased surface roughness [121]. Since their simulation findings analyze elastic-plastic materials, the computational analysis and results may potentially differ for soft biomaterials. Nevertheless, in general, the surface roughness affects the scatter of load-displacement curves and can lead to deviation of hardness and reduced modulus (load-displacement curves illustrated in Figure 14a and Figure 14b). Researchers have proposed that large variations of the measured mechanical properties are in part produced by the surface roughness [62].

To minimize the impact of surface roughness on your indentation results, the surface should be prepared such that it is free of contamination and sufficiently smooth to allow for high quality indentation data. According to ISO 14577 (standard for nanoindentation of metals and ceramics), the arithmetic roughness of the surface should be 20 times lower than the maximum indentation depth [65]. This is in part to reduce the scatter in the measurements (ISO 14577). Since this standard was developed for metals and ceramics, surface roughness guidelines may vary for biological materials and the specific probe geometry and size. On a similar note, Farine cautions researchers performing nanomechanical measurements on biological tissues, as they cannot be considered flat, therefore, the influence of surface roughness on measurements should not be disregarded [62]. Farine's research highlights the importance of surface roughness on soft materials indentation by performing experimental and computational work to understand the effects of surface topography.

To this end, it is pivotal to implement best experimental practices to reduce surface roughness. As such, researchers have employed the following techniques to minimize surface roughness when possible: microtoming [84], lap polishing [84], or cryo-microtoming [52]. When it is not possible to reduce the roughness (i.e., testing cartilage in situ), an alternative is to increase the indent depth to improve the ratio of indent depth to arithmetic roughness.

2.15 Probe Contamination

Probe contamination can also affect load-displacement data, often presenting as a low stiffness toe region at the start of the load-displacement curves, as illustrated in Figure 14b. To avoid the likelihood of using a contaminated probe in nanoindentation, researchers encourage gently cleaning the probe after every use with isopropyl alcohol or acetone.

2.16 Adhesion

Soft biomaterials (i.e. synthetic and biological) are prone to adhesion effects, a phenomena in which the material adheres to the probe, presenting itself in the load-displacement curve as negative forces during sample approach (snap-to-contact) and withdrawal (pull-off) (Figure 14c). If modulus measurements are extracted using traditional analytical methods (i.e. Oliver and Pharr) for compliant materials with dominant adhesion interactions, an overestimation of properties has been observed [57]. Despite the demonstrated errors in modulus, many studies of soft tissues and other compliant biomaterials ignore the effects of adhesion. Adhesion phenomena is often not recognized in a load-controlled experiment or when unloading data is not recorded past zero displacement (e.g., no lift-off). One solution to verify whether adhesion is occurring is to continue collecting the data until the probe fully separates from the surface by including a lift-off at the end of the displacement-time profile (Figure 9c).

As described in Section 3.5.3, there are contact models that account for adhesion; however, nanoindentation software typically does not include these models and hence adhesion analysis needs to be performed using other software. An alternative to implementing JKR analysis to analyze nanoindentation data when adhesion is present is to utilize experimental approaches to mitigate adhesion during testing. Several researchers have submerged samples in a surfactant solution to cut adhesion - a surfactant is an amphiphilic molecule that binds to hydrophilic and hydrophobic materials to reduce the surface tension between the probe and sample [57]. Some researchers have utilized surfactants with dilauryl sulfate (SDS) to mitigate adhesion effects during indentation of hydrated bone [122] and silicone elastomers [57]. Kohn and Ebenstein used OptiFree Express® contact lens solution and others have utilized F108 pluronic surfactant to reduce adhesion during indentation of hydrogels [57,123]. The use of surfactants is a potential avenue for eliminating adhesion during testing; however, submerging samples in surfactants may result in changes in mechanical properties, especially for hydrogels [57]. Therefore there is a need for more research on the types of surfactants that can be used to minimize adhesion during nanoindentation of soft polymers, hydrogels, and tissues without changing the properties of the material. Coating of probes is another option that can help mitigate adhesion, as mentioned in Section 3. Slaboch and colleagues pioneered the use of keratose-functionalized probes in a nanoindentation study of blood clots [100]. Other chemistries could also be investigated for glass indenter probes, as there is much research on functionalization of glass. Probe functionalization is a common practice in the AFM community [100], but it is less commonly used in nanoindentation. As such, more research is needed to standardize a solution to eliminate adhesion during nanoindentation in hydrated and soft systems.

2.17 False Engagement

Issues of false probe-to-sample engagement, when the indenter setpoint force is triggered by capillary forces and data collection is initiated without the probe being in contact with the sample,

can be a confounding factor when indenting soft, hydrated materials. Meniscus forces or capillary forces during indentation can arise when testing hydrated materials, as a capillary neck forms between the probe and sample surface. More commonly these forces act on the indenter shaft when indenting submerged samples [122,124,125], and result in detection of negative forces by the nanoindenter, leading to false engagement. The load-displacement behavior for false engagement may resemble the one illustrated in Figure 14d [62], as the indent is performed in the submerging liquid rather than in the sample. As a result, properties of the sample material cannot be extracted from the load-displacement data. In other cases, mechanical properties may be extractable from the load-displacement curve, but they may be inaccurate due to the varying capillary forces.

Tang et al. suggests that the presence of liquid film may significantly affect the mechanical properties by producing an artificial drift from the reference point for probe displacement and surface-tension on the probe [125]. To mitigate capillary forces on the indenter, a common practice when testing in fluids is the use of probes with longer, small diameter shafts [124]; yet, the movement of partially submerged shafts can still affect the accuracy in the force measurements during indentation [102]. Alternatively, researchers also proposed coating the probe or using surfactants [57,67] to reduce capillary forces. However, as previously mentioned, the challenge with using surfactant is the potential effect on the nanomechanical properties, which is especially problematic in hydrogels [57]. As for coating probes to aid in reducing capillary forces, Slaboch and colleagues have been one of the few researchers to functionalize the nanoindentation probe. This highlights the need for future studies to focus on coating and functionalizing probes to reduce or eliminate capillary forces.

A final hack to minimize the likelihood of false engagement is to increase the setpoint force to reduce the possibility that capillary forces alone will trigger the indenting process. Setpoint values as high as 10 μN (vs. typical values of 0.1-2 μN [98]) have been used [57], but this leads to increased sink-in and must be used in conjunction with lift-offs in the displacement-time profile to allow re-zeroing of the displacement. This hack is also often used with other methods such as long shafts and surfactants.

Although researchers have introduced many mitigating measures, false engagement from capillary forces when testing hydrated samples is an ongoing challenge that merits more research. This novel challenge arises because nanoindentation primarily characterizes hard, dry materials, not soft, hydrated materials. Innovations in indentation instruments and experimental methodology will likely be needed to tackle this problem entirely.

2.18 Substrate Effects

Performing nanoindentation on small-dimensional specimens (i.e., thin-films) poses a challenge in nanoindentation data acquisition, as substrate effects may be pronounced and influence the nanomechanical properties. The indentation response of a thin film on a substrate is complex since it involves the mechanical response of both the film and substrate. Hence, when indenting a thin soft material on a stiff substrate, the substrate effect manifests in nanoindentation data through an artificial stiffening of the material with decreasing thickness of sample, as illustrated in Figure 14e.

Numerous investigators have used experimental and theoretical approaches to study the problem of extracting “true” film properties from nanoindentation of film/substrate composites. For example, Saha and Nix examined the influence of substrate on the properties, exploring the effects of soft films on hard substrates and hard films on soft substrates and providing potential

models to account for substrate in the analysis [126]. In order to measure “sample-only” properties, researchers recommend limiting the indentation depth to less than 10% of the film thickness [65]. While this may be feasible for some samples, for others, particularly irregularly shaped biological materials, it may be more challenging to obtain samples thick enough to minimize substrate effects. In those cases, coupling indentation with analytical [76] or computational models can allow extraction of “true” properties of the soft material.

2.19 Framework for designing a nanoindentation experiment

This review focuses on developing a framework (illustrated in Figure 16-17) to be used for designing a nanoindentation experiment to accurately measure the nanomechanical properties of soft and hydrated materials. This framework can serve as a guide for novice researchers in the field of nanoindentation. As such, it provides guidance on the following topics in the context of testing soft, hydrated materials: probe selection, experimental set-up, data collection challenges, and data analysis methods.

The first step in designing a nanoindentation experiment is usually deciding on an appropriate probe based on the material composition and properties (Figure 15). Two important factors to consider when selecting a probe are the stiffness of the sample material and the size scale of interest in the study. Blunt probes (e.g., large diameter spherical or flat punch probes) are preferred when testing soft materials both to avoid puncturing the material and to ensure a large contact size/stiffness to facilitate detecting the surface before too much sink-in occurs (Figure 6). But keep in mind that there is a tradeoff between probe diameter (or indent contact size) and spatial resolution of testing – the larger the contact size, the lower the spatial resolution of your sample mapping (Figure 15-1a). The size of the probe should be selected based on the length-scale of the research question (e.g., *are you interested in measuring the properties of the individual constituents, or in capturing the combined microstructural behavior of the material?*) and knowledge of the sample’s microstructure or the size of the various constituents of interest. The literature advises to choose an indenter size that is less than 10% of the expected length-scale of interest, as this enables accurate probing of the mechanical variations in the materials with significant modulus heterogeneity (Figure 16-1b) [99]. A summary of probes utilized in the nanoindentation of biological materials, hydrated biomaterials and soft materials with varying stiffnesses are given in Table 4.

As for selecting the type of probe material (Figure 16-1c), there are a few options. Diamond-based probes are the gold-standard for nanoindentation; yet, many researchers diverge from diamond-based indenters when indenting soft materials because (as explained in the earlier sections) soft materials do not require overly stiff probes and some alternative probe materials, such as glass and tungsten, are better suited for mitigating adhesion. Glass could be a particularly advantageous material for mitigating both probe-sample adhesion and capillary forces on the indenter when testing hydrated samples, given the large body of research on functionalizing glass. It is also sufficiently stiff to make a negligible contribution to reduced modulus for samples with moduli as high as 50 MPa. Lastly, these alternative probe materials may be preferred for soft material testing as they are cheaper and easier to manufacture into ideal conospherical geometries than faceted diamond.

The experimental set-up of nanoindentation involves creating a load or displacement profile (for load-controlled or displacement controlled experiments, respectively). This profile defines the indent parameters such as loading/displacement rate, maximum load/displacement and

hold period. As illustrated in Figure 16-2a, the choice of load-controlled vs. displacement-controlled experimentation is dependent on the sample (i.e., adhesion, stiffness and structure). For example, displacement-controlled experiments are preferred for testing compliant, adhesive and time-dependent materials, or materials that may have depth-dependent properties due to complex microstructures (e.g., cartilage). Displacement-controlled experiments can aid in detecting the surface of soft materials and simplify the analysis of viscoelastic materials that are strain rate dependent [53].

The next step is choosing the maximum applied load or displacement, which depends on the research question being asked and the material being characterized (Figure 16-2b). Shallow indentations require smooth surfaces to avoid artifacts of surface roughness while substrate effects can become an issue when performing deep indentations into the sample. Additionally, the desired penetration depth may also depend on the sample, as some materials can exhibit depth dependent properties. Finally, the combination of peak load or displacement, sample stiffness, and probe radius should satisfy the criteria shown in Figure 6 to ensure that the indent loads and displacements fall within the range of the nanoindentation instrument.

As illustrated in Figure 16-2c, many features of the time profile depend on the behavior of the material. For example, a hold period is recommended on the time-profile when testing viscoelastic materials. This is done to reduce the creep related artifacts manifesting in nanoindentation as a “nose” on the unloading curve, as observed by Briscoe and colleagues [101]. Almost all polymers and biomaterials will exhibit sufficient time-dependent properties to mandate the trapezoidal time profile, but the time at peak load/displacement will vary by material (from a few seconds to a few minutes). If the hold time is too short, the “nose” will be visible in the load-displacement data and inhibit data analysis (Figure 17-3B).

If the material exhibits adhesion to the probe (as observed as negative forces on the indenter probe during unloading), the sample should be tested in displacement control using a modified displacement profile that includes a lift-off at the start and end of the indent (Figure 16-2c). This allows collection of the full interaction between the probe and the sample, starting from snap-to-contact and ending after pull-off (Figure 17-4). This full data is required to extract accurate modulus values during data analysis using the nano-JKR method. Alternatively, the researcher can engage measures to reduce or eliminate the adhesive interaction between the probe and sample, such as testing in a surfactant solution or coating the probe with a material that reduces adhesion.

Accurate surface detection is a prevalent challenge when characterizing the surface properties of soft (or hydrated) samples, due to the low contact stiffness when testing soft materials, and, in the case of hydrated samples, capillary forces acting on the indenter probe. As a result, some researchers have implemented the high-set point method to find the surface and avoid false engagement under these conditions (Figure 16-2c). Using the set-point method to detect the sample surface, the indenter approaches the surface until a small predetermined set-point force is detected, typically 0.1 – 2 μN [83,97,127–129]. Since transient capillary forces can exceed these typical values, when testing in fluid some researchers have used set-point loads as high as 10 μN to avoid false engagement (triggering the indent before the probe is in contact with the sample). The high set-point method should only be used in conjunction with a displacement profile with an initial lift-off as a high set-point force will lead to substantial sink-in, sometimes greater than 1 μm in a soft sample. Hence, the initial lift-off will be needed for accurate determination of the zero point of displacement for data analysis.

In addition to surface detection challenges, experienced nanoindentation researchers have acknowledged other sources of errors when characterizing soft and hydrated biomaterials – surface

roughness, contaminated probe, adhesion, false engagement, and substrate effects. The experimental errors are manifested in the load-displacement behavior (illustrated in Figure 17-3). Suggestions of changes to make in sample preparation and/or experimental set-up to overcome these challenges are explained in detail in the text (Section 3 and Section 4, Figure 14) and summarized in Figure 14-3B.

As nanoindentation continues to rise in utility for testing soft polymers, it becomes imperative to recognize the assumptions and limitations in the traditional methods for analyzing load-displacement curves, and consider other contact mechanics models for analyzing data. The presence of adhesion requires application of adhesion models for analysis of nanoindentation data, as Oliver-Pharr and Hertz models all assume negligible adhesion (Figure 17). Choosing between the MD, DMT and JKR adhesion models depends on the value calculated for Tabor's parameter. Per review of the literature (

Table 8), nano-JKR is the most commonly used model for analyzing load-displacement curves that exhibit adhesion (measured via depth sensing indentation), while the other adhesion-based contact theories are more generally employed in AFM. More details on how to implement nano-JKR analysis can be found in the text (Figure 13).

In summation, as nanoindentation continues to rise in utility and expand across many disciplines from medicine to materials science, it remains of utmost importance to understand the multifactorial parameters involved in nanoindentation of soft or hydrated materials. This decision framework can serve as a guide for novice researchers in the field of nanoindentation to facilitate determination and dissemination of reliable, accurate nanoindentation moduli when testing soft or hydrated materials.

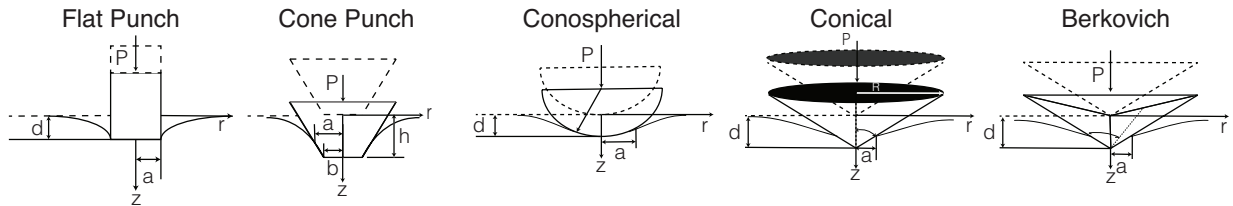
1

Tip Selection

a. Tip Geometry

What is the stiffness of your material?

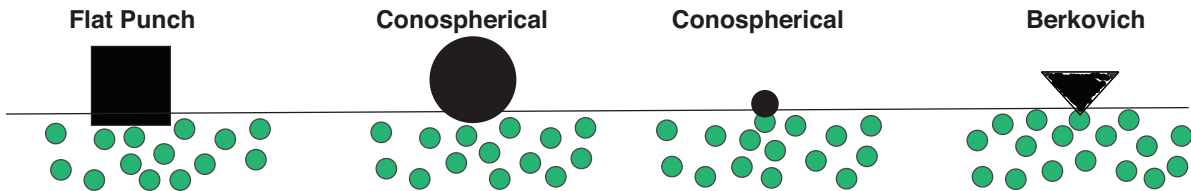
Low Material Stiffness → Low Probe Acuity → Low Spatial Resolution
 High Material Stiffness → High Probe Acuity → High Spatial Resolution



b. Tip Size

What is the lengthscale of interest for the material?

Contact area >> single constituent Contact area = single constituent Contact area < single constituent



c. Tip Material



Figure 15 - Part I: Framework provides a guideline for selecting a nanoindentation probe (geometry, size and material). The tip geometry is important to indentation testing; for example, sharp probes are preferred to use on stiff materials to maximize spatial resolution, while blunt probes are preferred to use on soft materials to avoid sample puncture and facilitate sample detection. However, the use of blunt probes comes at the expense of spatial resolution. As for tip material, there is a variety of materials to choose from when testing soft materials and many researchers might choose a tip material that mitigates adhesion and is cheap and easy to manufacture rather than the traditional diamond probes.

2

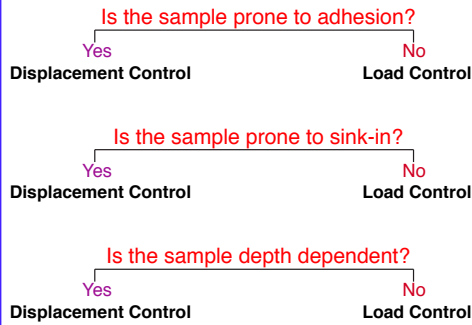
Experimental Set-Up

a. Displacement-Controlled vs. Load-Controlled b. Identifying a maximum load or displacement



Issues to consider:

- ① Surface Roughness
- ② Sample Thickness
- ③ Depth Dependence
- ④ Vertical Resolution
- ⑤ Research Question
- ⑥ Resolution on Indenter

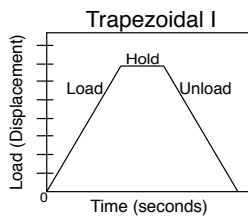


Use Hertz relationship to estimate whether indenter has the appropriate limits for the experiment

See Section 2.2

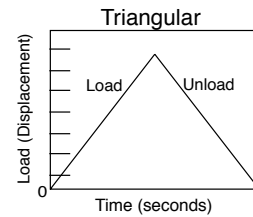
c. Time - Profile

Is the sample a viscoelastic material?

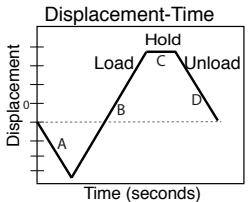


Yes → Add a **hold** period @max load/displacement

No → No hold period

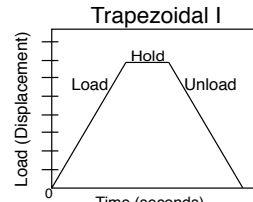


Will the indent need re-zeroing because of sink-in (e.g., soft sample or high set point testing)?



Yes → Add a **lift-off** @start of indent

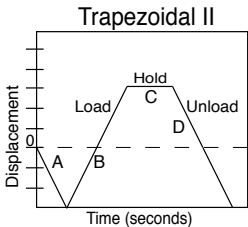
No → Trapezoidal I



*Preload = 1-2 uN (up to 10 uN for indents in water)

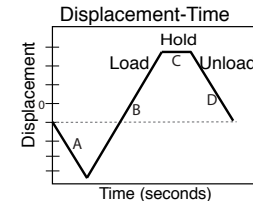
*Preload = 1-2 uN

Is the sample prone to adhesion?



Yes → Add a **pull-off** @end of indent

No → No pull-off



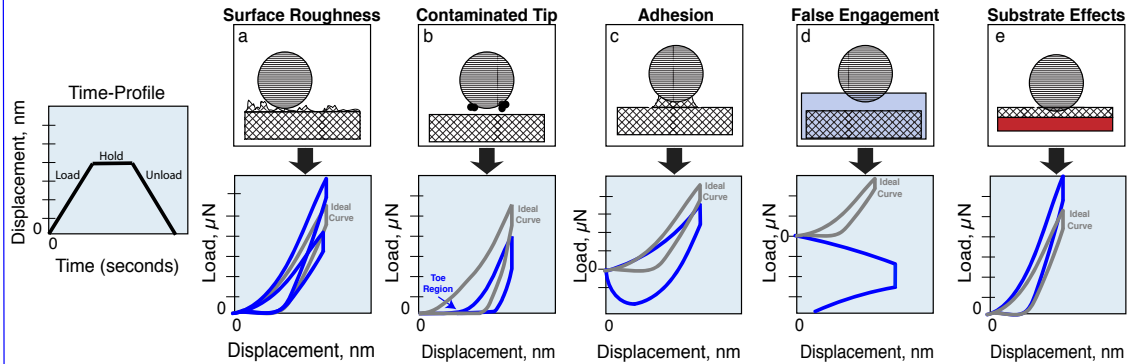
*Preload = 0.1-2 uN (up to 10 uN for indents in water)

Figure 16 – Part II: Framework provides the experimental set-up for nanoindentation testing. First, it provides a guide for identifying the appropriateness of using a displacement-controlled vs load-controlled experiment. Second, it provides a guide for identifying the maximum load or displacement to apply during indentation testing. Third, it provides a general framework for developing the time-profiles based on whether a material is viscoelastic, whether the indent will need re-zeroing from sink-in effects or whether the material is prone to adhesion.

3

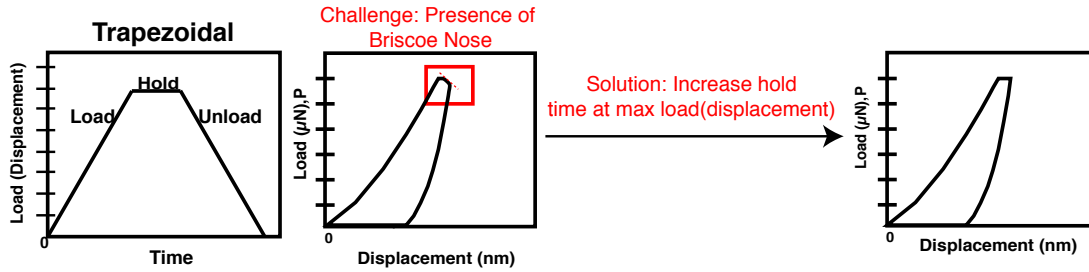
Potential Challenges

A. Load-Displacement Behavior of Common Indentation Challenges



B. Potential Solutions for Addressing Experimental Challenges

Surface Roughness	Contaminated Tip	Adhesion	False Engagement	Substrate Effects
<ul style="list-style-type: none"> Polish Microtome Cryo-microtome 	<ul style="list-style-type: none"> Gently clean the probe with isopropyl alcohol or acetone 	<ul style="list-style-type: none"> Use surfactants Coat the probe Implement appropriate nano-mechanical models 	<ul style="list-style-type: none"> Use probes with longer, smaller diameter shafts Coat the probe Use surfactants Increase setpoint force 	<ul style="list-style-type: none"> Limit the indentation depth to less than 10% of the film thickness



4

Data Analysis

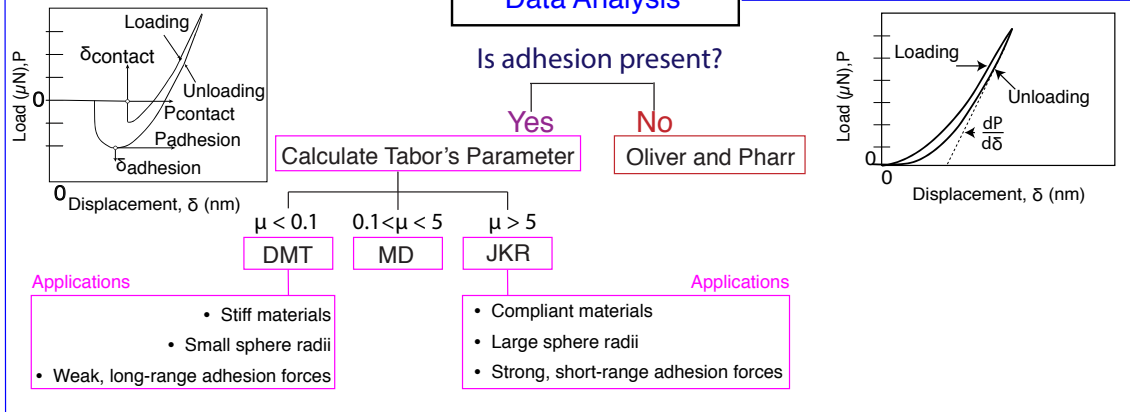


Figure 17 – Part III: This portion of the framework illustrates the potential challenges manifested in load-displacement curves. Further, the framework provides solutions for addressing these challenges. Finally, this framework focuses on the data analysis methods that should be employed after indentation testing to ascertain the mechanical properties, showing that the type of model used will depend on whether adhesion is present

Chapter 3 – Comparing nano-mechanical properties across length-scales and microstructural properties of Ultra High Molecular Weight Polyethylene

This chapter is adapted from [130], previously published by Journal of the Mechanical Behavior of Biomedical Materials.

3.1 Introduction

UHMWPE continues to remain the gold-standard material for total joint replacements. Modern UHMWPE formulations vary across crosslinking dosages, antioxidant chemistry, and types of heat treatments [11,23,30,131,132]. A significantly high amount of UHMWPE formulations attempt to address clinical complications like wear-mediated osteolysis and oxidation embrittlement [22,34,133]. Wear, fatigue, fracture, and oxidation continue challenging the clinical performance of UHMWPE. As such, researchers continue to seek an optimized formulation of UHMWPE to improve TJR longevity and clinical performance. With so many available formulations of UHMWPE, it is imperative to understand the effect of formulation processing and content on orthopedic performance. Since its original introduction as an orthopedic polymer in the 1960s, UHMWPE has undergone various iterations of processing (i.e. crosslinking, heat treatments, and infusion of antioxidants) to address clinical challenges [22,34,133]. While addressing the issue of wear by crosslinking the polymer, researchers showed a reduction in ductility and increased susceptibility to oxidation [38]. However, crosslinked polymer still remains a material that is used in orthopedic bearings. Additionally, thermal treatments such as annealing or remelting post crosslinking is an alternative to reduce oxidative degradation while it is in the body. However, these methods do not fully eradicate the free radicals and affect the microstructure, such that it affects fatigue resistance[17]. The numerous UHMWPE formulations that are tailored to address a specific clinical issue may alter other properties that may have affect other properties. As a result, it is imperative to understand how varying the microstructure either by crosslinking and subsequent thermal treatments affect the structural properties and clinical performance as orthopedic bearings. However, insight into the structure-property relationship and their inter-dependence across all temporal length scales remain limited. This research is first of its kind to develop a compendium of structure-property relations and assess the influence of testing methodology on the mechanical properties.

3.2 Methods

Microstructural Analysis

Microstructural properties were analyzed using a DSC or SAXS according to ASTM standards. The detailed protocol is outlined in Malito et al. 2018 [130]. In sum, differential scanning calorimetry (DSC) measures the degree of crystallinity in polymers based on ASTM F625-10 (2016). DSC equipment is a TA Instruments Q2000 DSC (New Castle, DE). And Small-Angle X-ray Scattering (SAXS) is used to determine the lamellar size properties.

Tension testing and constitutive modeling

Tensile testing measured the elastic modulus (engineering and true), yield stress, yield strain, non-linear hardening coefficients, ultimate engineering stress, true ultimate stress, true ultimate strain, and energetic toughness, per ASTM D638. Per ASTM standards, the specimens are Type IV tensile bar specimens and were machined such that the gauge length was parallel to the long axis of the stock material. The preparation protocol followed the one outlined in Malito et al. 2018 [130]. In summary, tensile testing used a Shimadzu AGS-X electromechanical load frame (Kyoto, Japan) at 50 mm/min with test temperature maintained at $23\pm 2^\circ\text{C}$. A custom software measures a true axial strain, true transverse strain, and instantaneous cross-sectional area.

Linear least-squares regression on the region between 0.005 to 0.009 strain from the true stress-strain curve determined the elastic modulus.

Another linear least squares regression on the upper strain limits (0.02 and 0.04) determined the elastic modulus variations across various material formulations. Per ASTM standard and protocol from Kurtz et al. 2000, the true and engineering stress-strain curve measured the yield stress (0.002 offset from the elastic region) [134].

From previous research, using a 0.002 offset line to predict yielding is in alignment with a two-segment elastic-plastic model, as described below.

The two segment elastic-plastic material model is given by:

$$\sigma = \begin{cases} E\varepsilon, & \varepsilon \leq \varepsilon_y \\ \alpha + \beta \exp(\gamma\varepsilon), & \varepsilon_y < \varepsilon \leq 0.12 \end{cases}$$

Where σ (MPa) is the true stress, E (MPa) is the elastic modulus, ε is the true axial strain, ε_y is the true yield strain, α (MPa) is the asymptotic true stress at infinite strains, β (MPa) is the rate at which the stress approaches the asymptotic limit and γ presents the curvature of the true stress-strain curve. The non-linear coefficients for the plastic model are determined using a least squares regression from true offset yield strain to 0.12 true strain. This is in accordance with previous studies that found the maximum equivalent strain of an UHMWPE tibial component is around 0.12. By creating the two segment elastic plastic model and intersecting at the yield point produces the following equation, which eliminates the α parameter:

$$\alpha = E\varepsilon_y - \beta \exp(\gamma\varepsilon_y)$$

Additional properties obtained from tensile testing are true ultimate stress, engineering ultimate stress and energetic toughness.

Poisson's ratio measurement

The protocol for measuring the Poisson's ratio follows the one established by ASTM D638. The tensile testing apparatus is an MTS Mini-Bionix II load frame using a 5kN load cell and a displacement rate of 5 mm/min. Since the Poisson's ratio is a relationship between true axial and transverse strain, a 5 mm gauge length is used to measure the axial and transverse strain measurements. The relationship below is Poisson's relationship:

$$\nu = \frac{\frac{d\varepsilon_t}{dP}}{\frac{d\varepsilon_a}{dP}}$$

Where $d\varepsilon_t$ is the absolute change in transverse strain, $d\varepsilon_a$ is the absolute change in axial strain, and dP is the change in the applied load. A linear regression of the data from 0.0005 true axial strain to the true offset yield strain calculated the slopes of $\frac{d\varepsilon_t}{dP}$ and $\frac{d\varepsilon_a}{dP}$.

Compression testing protocol

Compression testing measured the material samples' elastic modulus, yield stress, and true yield strain. The compression protocol follows the one set by Kurtz et al. (2002, 1998), based on the ASTM D695. The compression specimens ($n=5$) are cylindrical (10 mm diameter, 15 mm height). An Instron 8871 load frame (Norwood, MA) with a 5 kN load cell tested the samples in compression at a rate of 18 mm/min (0.02/s) and a temperature of 25°C. The relationship of stress as a function of load and initial cross-sectional area calculated the engineering stress:

$$\sigma_0 = \frac{|P|}{A_0}$$

Where P is the load and A_0 is the initial cross-sectional area of the sample. A compressometer is a device that measures the platen displacement accuracy. Kurtz noted that homogenous compression without barreling can occur up to 0.12. Therefore, volume constancy can be assumed up to that point, allowing for true strain measurement from the platen displacement to 0.12 strain. The relationship below measures the true strain:

$$\varepsilon = \frac{|\delta|}{l_0}$$

Where δ is the platen displacement, and l_0 is the starting platen separation. The relationship below converts the engineering stress:

$$\begin{aligned}\varepsilon &= -\ln(1 - e) \\ \sigma &= \sigma_0(1 - e)\end{aligned}$$

Where e , is the engineering strain, and solving for true stress, σ , in terms of true strain to produce

$$\sigma = \sigma_0 \exp(-\varepsilon)$$

Finally, a custom MATLAB script analyzed the data

A least-squares regression from 0.0005 to 0.009 strain determines the elastic modulus. An offset line drawn 0.002 from the elastic region determines the yield stress and yield strain.

Nanoindentation testing protocol

Nanoindentation was utilized to determine the surface hardness and reduced elastic modulus across the UHMWPE formulations ([69,112,135]. Samples were fabricated into 4 mm cubes and then microtomed with a glass blade to obtain optically smooth surfaces. The tip-area function during indentation is described by the following equation:

$$A_c(h_c) = C_0 h_c^2 + C_1 h_c^1 + C_2 h_c^{1/2} + C_3 h_c^{1/4}$$

Where A_c is the contact area, h_c is the contact depth, and C_0, C_1, C_2, C_3 are calibration coefficient obtained using a polycarbonate standard [112,135].

Indentations are performed on a TI900 Hysitron TriboIndenter (Minneapolis, MN) at room temperature using a conospherical diamond tip with a nominal 20 μm radius. Indentations are load controlled with a loading rate of 30 $\mu\text{N/s}$. Implementing a ten-second hold at each maximum load minimizes creep effects during indentation [112,135].

Each sample group ($n = 5$ specimens per material group) comprised 15 indents with a prescribed maximum load of 150 – 650 μN in equally spaced intervals [84]. A custom MATLAB code calculated the elastic modulus and contact hardness based on the following equations:

Where S is the stiffness, dP/dh is the slope of the initial unloading portion of the indentation load versus displacement curve, E_r is the reduced elastic modulus, and H_c is the hardness. For calculations of elastic modulus, we assume a Poisson's ratio of 0.46.

$$S = \frac{dP}{dh} = \frac{2\sqrt{A_c}}{\sqrt{\pi}} E_r$$
$$\frac{1}{E_r} = \frac{1 - \nu_s^2}{E_s} + \frac{1 - \nu_i^2}{E_i}$$
$$H_c = \frac{P_{max}}{A_c}$$

Statistical analysis: comparing mechanical behavior to microstructural measurements

A non-parametric Spearman rank correlation coefficient (MATLAB) is used to determine the relationship between mechanical properties and microstructural properties, based on the protocol by Atwood [136]. The correlations are based on median values for the mechanical properties.

3.3 Results

Microstructural Measurements

In summary, the average crystallinity measurements, obtained from DSC scans, are between 52.4% to 61.2%. A more complete summary of the microstructural properties, namely crystallinity and lamellar thickness are denoted in Table 9 and Table 10. The material with the

highest measured crystallinity (61.2%) belonged to GUR 1020, AO 80kGy, by contrast the material group with the lowest measured crystallinity belonged to GUR 1020 75kGy remelted.

As for lamellar thickness measurements, the lamellar thickness ranged from 23 – 30.4 nm. And again, the thickest lamellar thickness belonged to GUR 1020 AO 80kGy. And the smallest lamellar thickness measurement belonged to GUR 1020 75kGy RM.

Table 9 - Microstructural property summary for GUR 1020, GUR 1020 35kGy, GUR 1020 75kGy+Remelted, GUR 1020 AO, GUR 1020 AO 80kGy, GUR 1020 Vitamin E

Microstructural Property	GUR 1020	GUR 1020 35kGy	GUR 1020 75kGy RM	GUR 1020 AO	GUR 1020 AO 80kGy	GUR 1020 VE
Crystallinity (%)	57.7	57.8	52.4	57.5	61.2	60
Lamellar Thickness (nm)	26.3	26.1	23	26.6	30.4	29.3

Table 10- Microstructural property summary for GUR 1020 VE 50kGy, GUR 1020 VE 75kGy, GUR 1020 VE 100kGy, GUR 1020 VE 125kGy, GUR 1050, GUR 1050 75kGy + Remelted

Microstructural Property	GUR 1020 VE 50kGy	GUR 1020 VE 75kGy	GUR 1020 VE 100kGy	GUR 1020 VE 125kGy	GUR 1050	GUR 1050 75kGy RM
Crystallinity (%)	56.5	60.7	60.7	60.8	55.8	55.8
Lamellar Thickness (nm)	25.9	29.3	27	28.1	28	27.7

Tensile Measurements and Constitutive Behavior

The experimental findings confirm that tensile mechanical properties are affected by resin type, antioxidant type, and degree of crosslinking.

Table 11 and

Table 12 illustrate the mechanical properties. In summary, the elastic modulus ranged from 655 to 1077 MPa. The lowest elastic modulus of 655 MPa belonged to GUR 1020 75kGy remelted, while the highest elastic modulus is from GUR 1020 AO 80kGy. The order of these properties is related to the microstructural properties, as GUR 1020 AO 80kGy had the highest crystallinity and lamellar thickness.

The UHMWPE materials (GUR 1020 and GUR 1050) that had undergone crosslinking followed by a remelting process observed a decrease in elastic modulus.

Noteworthy, the viscoelasticity in UHMWPE hinders a clear distinction of the elastic region, and the properties are dependent on the deformation rate. As a result, defining a single value for the elastic modulus is misleading. Primarily, the elastic modulus is a comparison tool for understanding the effect of crosslinking, resin type, and changes in the formulation.

Table 11 - Summary of mechanical properties for GUR 1020, GUR 1020 35kGy, GUR 1020 75kGy+Remelted, GUR 1020 AO, GUR 1020 AO 80kGy, GUR 1020 Vitamin E

Mechanical Properties	UHMWPE Material Formulations					
	GUR 1020	GUR 1020 35kGy	GUR 1020 75kGy + RM	GUR 1020 AO	GUR 1020 AO 80kGy	GUR 1020 VE
Tensile true elastic modulus (MPa)	799.5 ± 26.2	758.2 ± 39.4	655.1 ± 42.7	925.9 ± 64.5	1076.8 ± 53.6	921.2 ± 13.6
Poisson's ratio	0.459 ± 0.015	0.483 ± 0.046	0.493 ± 0.034	0.544 ± 0.056	0.532 ± 0.013	0.633 ± 0.042
Engineering yield stress (MPa)	23.8 ± 0.2	23.6 ± 0.2	21.7 ± 0.2	24.3 ± 0.1	26.2 ± 0.1	24.5 ± 0.3
Tensile true 0.002 offset yield stress (MPa)	10.8 ± 1.2	12.0 ± 0.8	10.7 ± 0.5	12.5 ± 1.0	15.3 ± 0.5	13.5 ± 0.4
Tensile true 0.002 offset yield strain (mm/mm)	0.016 ± 0.002	0.018 ± 0.002	0.018 ± 0.002	0.016 ± 0.002	0.015 ± 0.002	0.017 ± 0.001
β	-19.8 ± 0.7	-19.0 ± 1.3	-18.3 ± 0.5	-19.2 ± 1.2	-20.5 ± 0.5	-19.6 ± 0.4
γ	-29.3 ± 0.8	-28.2 ± 0.6	-28.0 ± 1.4	-29.9 ± 0.9	-34.9 ± 0.9	-28.9 ± 0.2
Engineering ultimate stress (MPa)	45.2 ± 2.7	46.2 ± 2.9	44.4 ± 4.3	39.7 ± 2.4	46.5 ± 1.8	52.9 ± 1.4
True ultimate stress	188.2 ± 17	184.3 ± 16.1	156.3 ± 20.4	156.4 ± 15.2	152 ± 10.8	229.1 ± 9.7
True ultimate strain	4.0 ± 0.1	4.0 ± 0.2	3.2 ± 0.1	3.8 ± 0.1	2.9 ± 0.1	4.2 ± 0.05
Energetic Toughness (MJ/mm ³)	297.9 ± 24.7	301.3 ± 28.7	193.9 ± 20.9	253.6 ± 22.8	190.9 ± 14.5	361.5 ± 14.7

Table 12 - Summary of mechanical properties for GUR 1020 VE 50kGy, GUR 1020 VE 75kGy, GUR 1020 VE 100kGy, GUR 1020 VE 125kGy, GUR 1050, GUR 1050 75kGy + Remelted

Mechanical Properties	UHMWPE Material Formulations					
	GUR 1020 VE 50kGy	GUR 1020 VE 75kGy	GUR 1020 VE 100kGy	GUR 1020 VE 125kGy	GUR 1050	GUR 1050 75kGy+RM
Tensile true elastic modulus (MPa)	885.0 ± 31.5	1060.6 ± 37.4	1008.5 ± 36.6	865.4 ± 56.3	810.6 ± 26.2	762.3 ± 32
Poisson's ratio	0.499 ± 0.017	0.421 ± 0.027	0.464 ± 0.025	0.461 ± 0.040	0.540 ± 0.076	0.521 ± 0.043
Engineering yield stress (MPa)	24.9 ± 0.1	26.0 ± 0.1	25.2 ± 0.2	25.8 ± 0.1	22.9 ± 0.2	24.2 ± 0.2
Tensile true 0.002 offset yield stress (MPa)	14.1 ± 1.7	14.8 ± 0.3	14.7 ± 0.7	14.1 ± 1.1	13.2 ± 0.7	11.7 ± 0.4
Tensile true 0.002 offset yield strain (mm/mm)	0.018 ± 0.002	0.016 ± 0.001	0.017 ± 0.001	0.018 ± 0.0005	0.018 ± 0.001	0.017 ± 0.001
β	-18.5 ± 2.3	-20.3 ± 0.7	-19.7 ± 0.8	-19.3 ± 1.5	-18.0 ± 0.6	-19.7 ± 0.9
γ	-29.6 ± 1.6	-33.2 ± 0.8	-31.7 ± 1.1	-31.7 ± 1.1	-27.6 ± 0.7	-31.5 ± 1.1
Engineering ultimate stress (MPa)	45.1 ± 1.5	50.7 ± 1.7	44.4 ± 2.8	49.1 ± 1.7	50.5 ± 5.7	45.7 ± 3.0
True ultimate stress	167.1 ± 7.1	178.9 ± 10.1	146.4 ± 13.6	158.8 ± 9.7	202.8 ± 29.9	127.9 ± 12.8
True ultimate strain	3.6 ± 0.1	3.3 ± 0.1	2.9 ± 0.1	2.9 ± 0.1	3.7 ± 0.3	2.4 ± 0.1
Energetic Toughness (MJ/mm ³)	246.1 ± 11	241.8 ± 16.4	183.0 ± 16.7	187.9 ± 13.6	311.1 ± 50.4	137.4 ± 16

Compressive and Nanoindentation Measurements

Table 13 and Table 14 illustrate the compressive and indentation properties. For compressive modulus, the values ranged between 521 and 1130 MPa. Like the tensile behavior, the highest compressive modulus belonged to GUR 1020 AO 80kGy. And the lowest modulus belonged to GUR 1020 75kGy remelted (521 MPa). Further, indentation modulus also observed the most significant value from GUR 1020 AO 80kGy, and the smallest value from GUR 1020 75kGy RM. While the elastic modulus obtained from tensile, compression, and nanoindentation were not the same, there is still a correlation between the three characterization methods.

Table 13 - Compression and nanoindentation (mean \pm standard deviation) for the following materials: GUR 1020, GUR 1020 35kGy, GUR 1020 75kGy RM, GUR 1020 AO, GUR 1020 AO 80kGy, GUR 1020 VE

Mechanical Properties	UHMWPE Formulations					
	GUR 1020	GUR 1020 35kGy	GUR 1020 75kGy RM	GUR 1020 AO	GUR 1020 AO 80kGy	GUR 1020 VE
Compressive true elastic modulus (MPa)	900 \pm 49.4	539 \pm 68.2	521 \pm 23.4	925 \pm 114	1130 \pm 23.1	870 \pm 35.5
Compressive 0.002 true offset yield stress (MPa)	12 \pm 0.28	14 \pm 4.1	10.9 \pm 1.1	12.8 \pm 0.8	15.3 \pm 0.4	13.1 \pm 0.7
Compressive 0.002 true offset yield strain (mm/mm)	0.015 \pm 0.001	0.029 \pm 0.014	0.023 \pm 0.003	0.016 \pm 0.003	0.016 \pm 0.001	0.018 \pm 0.001
Nanoindentation modulus (MPa)	728.5 \pm 110.7	787.0 \pm 184.3	660.6 \pm 137.2	745.3 \pm 187.5	918.4 \pm 240.1	611.2 \pm 205.4
Nanoindentation hardness (MPa)	37.0 \pm 9.0	37.6 \pm 10.0	35.8 \pm 9.5	35.0 \pm 9.3	43.8 \pm 13.5	29.6 \pm 9.9

Table 14 – Compression and nanoindentation properties (mean \pm standard deviation) for the following materials: GUR 1020 VE 50kGy, GUR 1020 VE 75kGy, GUR 1020 VE 100kGy, GUR 1020 VE 125kGy, GUR 1050, GUR 1050 75kGy RM

Mechanical Properties	UHMWPE Formulations					
	GUR 1020 VE 50kGy	GUR 1020 VE 75kGy	GUR 1020 VE 100kGy	GUR 1020 VE 125kGy	GUR 1050	GUR 1050 75kGy RM
Compressive true elastic modulus (MPa)	982 \pm 28.2	1090 \pm 14.2	953 \pm 36.2	1040 \pm 61.6	851 \pm 71.8	591 \pm 31.0
Compressive 0.002 true offset yield stress (MPa)	13.2 \pm 0.8	14.4 \pm 4.1	12.4 \pm 0.6	14.0 \pm 0.8	13.8 \pm 1.5	12.6 \pm 1.3
Compressive 0.002 true offset yield strain (mm/mm)	0.017 \pm 0.001	0.017 \pm 0.001	0.019 \pm 0.001	0.017 \pm 0.003	0.019 \pm 0.002	0.023 \pm 0.003
Nanoindentation modulus (MPa)	815.1 \pm 141.6	912.8 \pm 147.4	717.1 \pm 96.0	880.7 \pm 129.7	776.35 \pm 118.2	837.98 \pm 152.2
Nanoindentation hardness (MPa)	33.5 \pm 5.3	41.1 \pm 9.7	32.6 \pm 5.0	36.2 \pm 7.8	40.4 \pm 8.65	30.8 \pm 6.19

Correlations

Malito et al. 2018 [130] stated that bulk mechanical properties correlated across various testing modalities. While nanoindentation hardness did not correlate with bulk mechanical properties, the compressive and nanoindentation modulus were weakly correlated (Figure 18). The differences in size in the analysis may attribute to the weak correlation between bulk and nanoindentation. As shown in Figure 18, the spearman rank correlation coefficient for compression and tensile true elastic modulus is 0.839 ($P \leq 0.01$).

Correlation of modulus: Tension, compression, nanoindentation

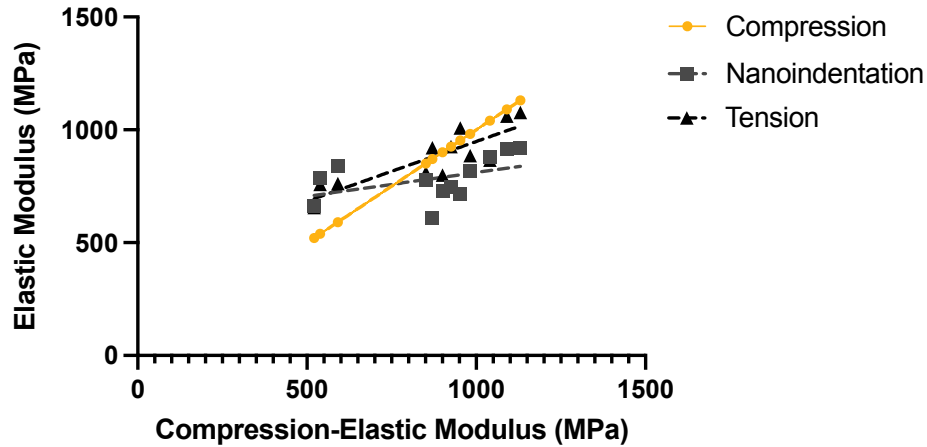


Figure 18 - Correlating compression modulus to nanoindentation and tensile modulus. The correlation strength is based on spearman rank correlation coefficient. The spearman rank correlation coefficient for compression and tensile true elastic modulus is 0.839.* While the spearman rank correlation coefficient between compression and nanoindentation is 0.587. The * denotes $P \leq 0.01$.

Correlating the crystallinity to the compressive and tensile elastic modulus resulted in a spearman correlation strength of 0.718 and 0.704, respectively (Figure 19a). Figure 19b illustrates the correlations between the crystallinity and yield strength (engineering and true) for tension and compression. The crystallinity and engineering yield strength correlation are highest amongst the true tensile and true compressive yield strength. In Figure 19c, we observe no statistical significance between compressive true elastic modulus and lamellar thickness. However, there is a correlation strength of 0.636 for lamellar thickness and tensile true elastic modulus. Similarly, we observe a correlation between lamellar thickness and yield strength (Figure 19d).

Correlations between non-linear model parameters and yield strength show a strong negative correlation. As the yield strength increases, β (-0.860, 0.0006) and γ (-0.685, 0.02) decrease. These correlations are an effort to understand the plastic hardening behavior in UHMWPE. The results illustrate that the rate the material plastically deforms increases as the yield strength increases. A lower beta signifies the material reaches the asymptotic yield stress limit at a higher rate. The observations are only valid up to 0.12 strains in UHMWPE.

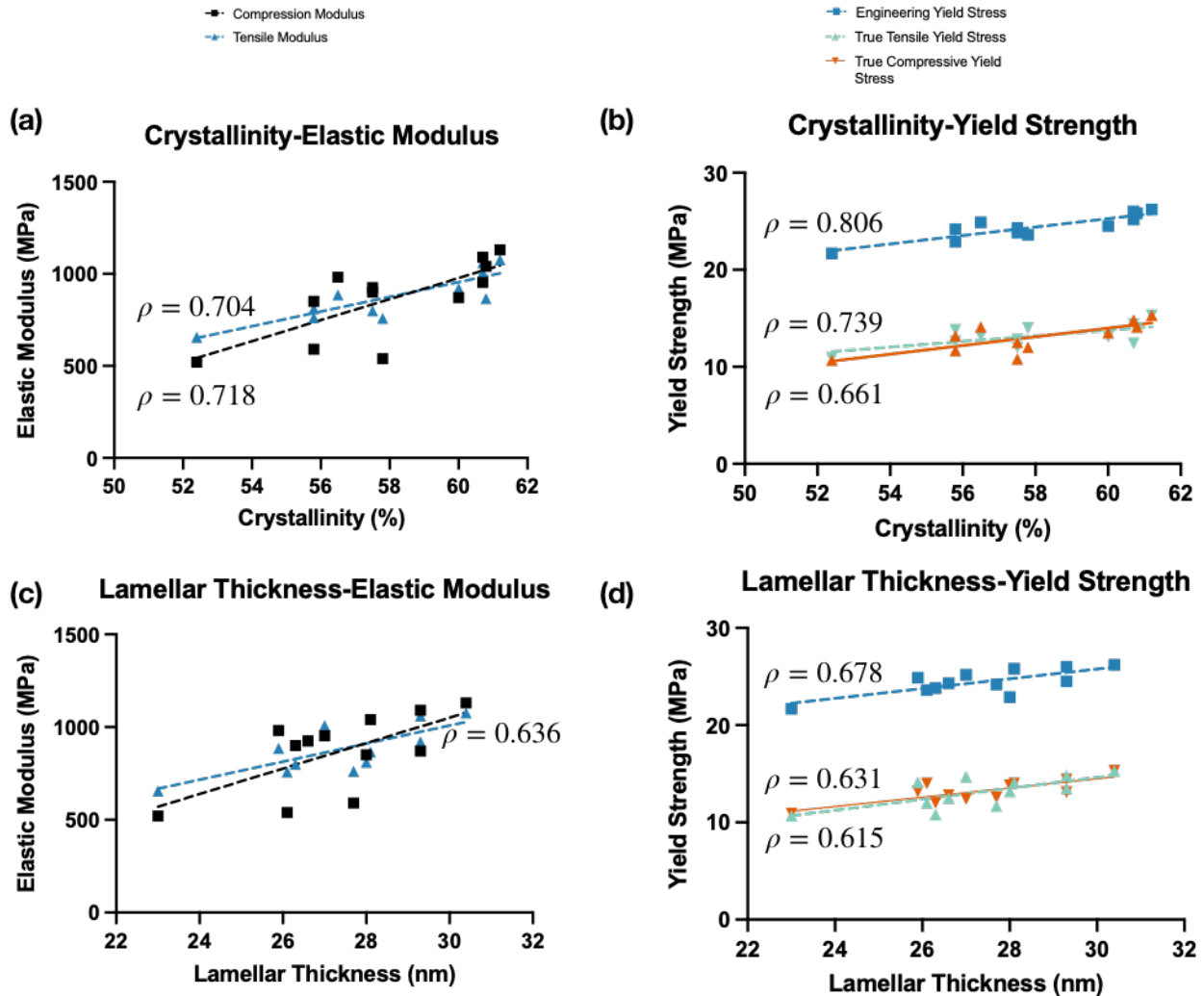


Figure 19 – (a) Correlating crystallinity (%) to elastic modulus (compressive and tensile). (b) correlating crystallinity to true and engineering yield strength (compressive and tensile). (c) correlating lamellar thickness to elastic modulus (tensile and compressive). (d) correlating lamellar thickness to true and engineering yield strength (compressive and tensile).

3.4 Discussion and Conclusions

The motivation behind characterizing medical-grade polymers is to understand the mechanical behavior and identify any anisotropic behavior that may affect the clinical performance of the material in the body. Further, basic mechanical properties obtained from true stress-strain curves are essential for simulating material deformation. This research motivates further research into the anisotropic behavior of the material, as these materials experience wear and fatigue, which can be affected by orientation. Notably, Ohta found increased wear resistance when there was a preferential crystal alignment [137].

In conclusion, mechanical properties positively correlate with microstructural properties. Further, nanoindentation offers an opportunity to analyze the surface properties and insight into property variations from microstructural changes. While indentation and compression properties are not identical, they offer correlating trends across UHMWPE formulations. And can potentially be used for retrieval analysis and assessing properties of materials where the material is limited.

Microstructure evaluation of UHMWPE is imperative for assessing the clinical outcome. Microstructure changes, namely lamellar size thickness and spacing, change crack propagation mechanisms and impact fracture resistance. A database containing mechanical and microstructural properties is highly beneficial to designers and engineers in the medical device field.

Chapter 4 – Comparing nano-mechanical properties across length-scales and microstructural properties of PEEK and PEEK composites

This chapter was previously published by Journal of the Mechanical Behavior of Biomedical Materials [74].

4.1 Introduction

Polyetheretherketone (PEEK) is a semi-crystalline polymer that emerged for use in spinal cages [138,139] and is widely sought out for biomedical purposes owing to the desirable properties; notably, strength, stiffness, toughness, radiolucency, biocompatibility and resistance to harsh *in vivo* conditions [1]. PEEK systems provide a viable option to replace metal components used in modern total joint replacements (TJR) where clinical concerns related to modulus match to surrounding bone tissue [140] and long-term complications with corrosion are ongoing in orthopedics [141,142].

Incorporating carbon fibers into the PEEK matrix expands its applications beyond bone interfacing elements into the realm of the articulating components of TJR [46]. Studies have shown improved wear resistance in carbon fiber-reinforced PEEK (CFR PEEK) composites in comparison to Cobalt-Chrome systems when articulating against ultra-high molecular weight polyethylene (UHMWPE) [143]. Extensive wear testing of PEEK and CFR PEEK have shown lower wear rates than UHMWPE formulations for the same counter-bearings [144,145]. The improved wear results of CFR PEEK expand the opportunity for a broad range of orthopedic applications [139,146,147]. Resultingly, by the late 1990s, PEEK became a leading material for replacing metal implant components in orthopedics [139]. Furthermore, isoelastic implant systems, such as PEEK and PEEK composites, have made significant contribution as bone replacements [148], fracture fixation devices [139], cranial defect repairs [149], trauma [150] and dental applications [151,152].

The majority of testing on PEEK systems comprise bulk mechanical characterization, wear studies and fatigue analysis [153,154]. It is notable that while there exists an expansive body of literature on the tribological and mechanical behavior of PEEK formulations used for orthopedic bearings, studies addressing nano-length scale behavior of these PEEK systems are lacking. The paucity of such research indicates an opportunity to explore fiber-matrix behaviors over length scales that are clinically relevant to orthopedics, especially as submicron particle debris has been implicated in a number of chronic inflammatory responses that limit longevity of TJR [155,156].

Micromechanical testing of orthopedic-grade PEEK systems indicates that annealing, carbon fiber type and quantity can be an effective strengthening mechanisms [48]. Regis and coworkers examined PAN- and pitch- based carbon fiber reinforced PEEK with microindentation; however, they found no significant difference between the matrix and the fiber-matrix interface modulus [48]. The lack of discrimination in mechanical behavior between the matrix and fiber-matrix interface is complicated by scatter in the data scatter owing to length scale of the indenter tip and its proximity to the fiber-matrix interface [48]. We hypothesize that nanoindentation techniques may assist in characterizing the mechanical behavior of the various constituents present in CFR PEEK composites and yield insight into the interphase behaviors.

Nanoindentation is a nano-length scale mechanical characterization technique for measuring the near-surface mechanical properties. Over the past few decades, the utility of nanoindentation research has been established as a viable characterization tool across a diverse cohort of

biomaterials including structural tissues, natural materials and medical polymers [157]. The appeal of nanoscale testing over macroscale testing is the ability to characterize and isolate constituent relationships in complex microstructures [52]. Nanoindentation can capture local gradients in elastic properties and aid in developing structure-property relationships for a number of complex biomaterial systems including PEEK systems.

The nanomechanical properties of PAN and pitch-based carbon fiber reinforced PEEK remain poorly understood. Nanoscale characterization facilitates the measurement of local properties of the composite constituents and provides insight into the role of varying annealing temperatures and carbon fiber type on interphase properties. The aims of this study are to use nanoindentation techniques in PEEK and PEEK composites to evaluate (i) constituent and interphase properties using the load-displacement behavior and a statistical clustering method, (ii) the relationship between indentation tip geometry and the indentation modulus, and (iii) the suitability of nanoindentation techniques for measuring the mechanical behavior of medical grade composites.

4.2 Methods

Material formulations

This research characterizes the nanomechanical properties of medical grade PEEK and PEEK composites (Invibio Inc, Lancashire, UK). A summary of physical properties is shown in Table 1. Three material groups are evaluated: (i) Unfilled PEEK, (ii) Polyacrylonirile (PAN) carbon-fiber reinforced PEEK (PAN CFR PEEK), and (iii) pitch carbon-fiber reinforced PEEK (PITCH CFR PEEK). The carbon fiber reinforced PEEK contains short and randomly distributed carbon fibers throughout the PEEK matrix.

Pre-formed granules with integrated carbon, provided by Invibio, were re-oriented in the molten matrix during the injection molding process. Prior to injection molding, the granules were first preheated to 70°C to remove residual moisture. To develop injection molded plates (250 x 25 x 2.5 mm), the nozzle temperature was set constant at 400°C and the mold at 250°C. The samples were subsequently cooled in air at room temperature and indentation samples (24 x 25 x 2.5 mm) were water-jet machined from the injection molded plates.

Six heat treatments were examined across the PEEK formulations to investigate the effects of post-processing thermal treatment on the nanomechanical properties. The samples were heated at a constant rate of 5°C/min, and held at a selected annealing temperature for 5 hours and then air cooled to 20 °C. The set of annealing temperatures are 200°C, 225°C, 250°C, 275°C and 300°C. A non-annealed group served as a control.

Table 15- PEEK and carbon fiber reinforced PEEK composites (Invibio, Lankashire, UK) used in this research along with the properties of the carbon fibers [48,158]. The carbon fibers are short and randomly distributed in the PEEK matrix (Unfilled PEEK).

Material Formulation (Tradename)	Density (g/cm ³)	Carbon fiber: content and type	Carbon fiber characteristics: modulus, diameter, length, density
Unfilled PEEK (PEEK-OPTIMA™ LT1)	1.3	None	-
PAN CFR PEEK (PEEK-OPTIMA Reinforced™)	1.3	30% wt. polyacrylonitrile (PAN) carbon fibers	Modulus: 540 GPa Diameter: 6 ± 2 μm Length: 230 ± 23 μm Density: 1.8 g/cm ³
Pitch CFR PEEK (PEEK-OPTIMA Wear Performance™)	1.4	30% wt. pitch carbon fibers	Modulus: 280 GPa Diameter: 10 ± 2 μm Length: 230 ± 13 μm Density: 2.0 g/cm ³

Surface preparation: Polishing Methodology

A multi-step polishing protocol was utilized in this study in order to: (i) remove the skin-core structure resulting from the injection molding process, (ii) reduce the surface roughness and (iii) mitigate erroneous measurements [159]. Samples were polished via a series of re-polishing step utilized a lapping process with 1 μm aluminum oxide paper to achieve a smooth surface-finish. Polishing was performed using a lapper (South Bay Technology) at an RPM range of 160-50 under hydrated conditions. Polishing reduced the surface roughness and revealed the microstructure of the PEEK and CFR PEEK surfaces (Figure 20).

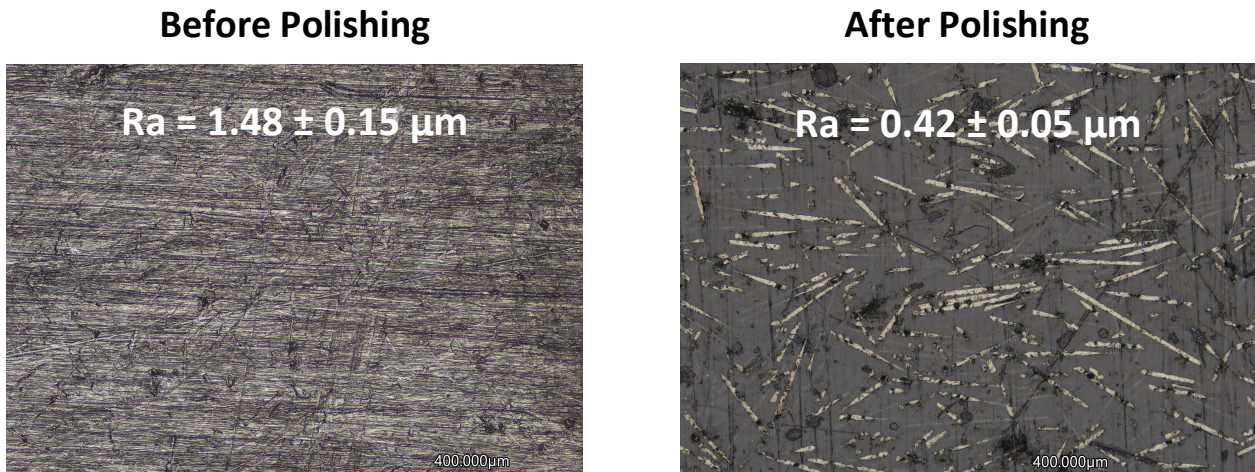


Figure 20 - Surfaces of PEEK composites before and after polishing. Surface roughness (average ± standard deviation) before polishing is 1.48 μm ± 0.15 μm, and after polishing the surface roughness (average ± standard deviation) is 0.42 μm ± 0.05 μm

Nanoindentation characterization: Methodology

A TI 900 TriboIndenter (Hysitron, Minneapolis, MN) was used to perform indentations at ambient temperature using a conospherical diamond tip. We utilized two nanoindentation tips, a conospherical tip of radii 1.5 μm and a conospherical tip of 20 μm radii (90 degree cone angle), to determine indentation modulus and to evaluate which indenter tip had better correlation with microindentation [48]. The indentations were load-controlled with a rate of 30 $\mu\text{N/s}$. A trapezoidal loading-unloading function was used with a ten-second hold at each maximum load to minimize creep effects [84,101]. Creep related artifacts manifest in nanoindentation as a “nose” on the unloading curve, as observed by Briscoe and colleagues [101]. This nose forms when a material continues to increase in displacement after the applied load is reduced, the presence of a “nose” becomes a challenge for accurately determining the slope from the unloading curve. Hence, a trapezoidal loading curve has been shown to mitigate this problem in polymeric materials [84,101].

The specimens tested for each material group had an average of 431 indentations (std. dev 80) were performed on each material group at a maximum load prescribed of 1000 μN . Hundreds of indentations were performed at the same maximum load and constant loading rate in order to obtain statistically acceptable values at the maximum contact load, the statistical analysis is described in a future section.

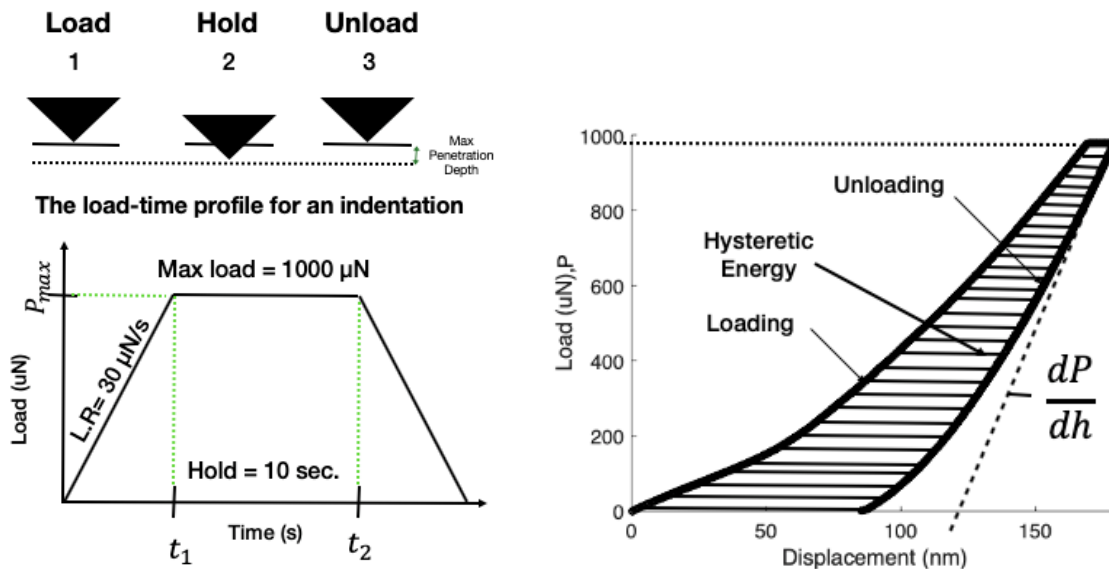


Figure 21 - Illustration of (a) the indentation load-time profile and (b) a representative load-displacement curve.

Nanoindentation – Indentation Mechanics

Nanoindentation involves penetrating the specimen using a diamond tip, while recording the indentation load, P , and displacement, h , for one complete load and unloading cycle (Figure 21). The indenter penetrates the specimen at a given loading rate and once it reaches the desired maximum load, there is a hold period at maximum load (Figure 21a). The loading region undergoes a mixture of elastic and plastic deformation with a resultant residual impression of the indenter tip. By contrast, the unloading region exhibits elastic recovery and provides a measure of the material's surface modulus (Figure 21b). The elastic unloading portion of the load-displacement curve may

be used to relate the experimental measured quantities such as the contact area, displacement and load [104,105].

The Oliver and Pharr technique curve fits the unloading portion of the load-displacement curve with a power-law and is useful for materials with non-linear unloading behavior [5]. The unloading slope is estimated as the first derivative of the fitted function at the maximum displacement and is a prevalent method for analyzing indentation data (Equation 1). In Equation 1, α and m are empirically determined fitting parameters, h is the displacement and h_f is the final displacement after complete unloading [110].

$$S = \frac{dP}{dh} = \alpha(h - h_f)^m \quad (\text{Eq. 1})$$

Classical indentation theory relates the contact stiffness of the material, S , to the contact area, A , and reduced modulus E_r , as described by Equation 2. The geometric relations are generalized for any punch described as a solid of revolution of a smooth function by Oliver and Pharr following from the work of Sneddon's relationships for a flat cylindrical punch [108]. This mathematical relation between the contact stiffness and the contact area and modulus are based on Sneddon's simplification from the Boussinesq equations [109].

$$\frac{dP}{dh} = \frac{2}{\sqrt{\pi}} \sqrt{A} E_r \quad (\text{Eq. 2})$$

Where A is the surface contact area at maximum displacement and E_r is the reduced modulus, which is related to the elastic modulus by Equation 3,

$$\frac{1}{E_r} = \frac{(1-\nu^2)}{E} + \frac{(1-\nu_i^2)}{E_i} \quad (\text{Eq. 3})$$

E and ν are the elastic modulus and Poisson's ratio of the indented sample, while E_i and ν_i are the elastic modulus and Poisson's ratio of the indenter. The reduced modulus accounts for elastic displacement contribution of both the indented sample and the indenter [69].

Statistical Analysis and Clustering of Data

A rank-based non-parametric test, specifically, the Kruskal-Wallis H test, was used to determine the statistical significance across a variety of thermal treatment and carbon fiber type. By contrast, a nonparametric spearman rank correlation coefficient (MATLAB) was employed to measure the strength of the relationship between micro- and nanoindentation modulus measurements, and correlation between the two indentation tip diameters. Statistical tests used the median values of the measured properties to correlate the strength and statistical significance amongst material groups.

The complexity of determining the average modulus of the constituents present in PEEK composites (matrix, fiber-matrix interface, and fiber) warrants the use of k -means clustering, an unsupervised machine learning technique [160]. The k -means function partitions the elastic modulus data set into three clusters, and identifies three centroids. The modulus value in the data set locates the nearest cluster by measuring the Euclidean distance and the algorithm iterates until

it finds the three centroids that minimizes the distance between the points and their corresponding centroids.

4.3 Results and Discussion

Nanomechanical properties of PEEK and CFR PEEK

In this research, we observe an indenter tip sensitivity on the nanomechanical measurements. The average difference in indentation modulus for a 20 μm and a 1.5 μm radius conospherical indenter tip is 0.97 GPa for PEEK and CFR-PEEK composites (Table 16). While there may be differences in indentation modulus that vary based on the size of the indentation tip, we still observe a strong correlation between the nanomechanical properties of a 20 μm and a 1.5 μm tip (Figure 22a).

The load-displacement curves in Figure 22b demonstrates the difference in load and unloading path between the 1.5 μm and 20 μm radius indenter tip for unfilled PEEK (annealed to 275 °C). Based on the load and unload path, the indentation performed using a conospherical tip of radius 1.5 μm is experiencing greater hysteretic effects in comparison to the indentation performed using a tip of 20 μm . The hysteretic effect is noted as the area between the load-unloading path in the load displacement curves [113]. It is common for viscoelastic polymers to dissipate energy during an indentation [113,154,161]. PEEK exhibits time-dependent behavior and annealing may enhance its creep resistance and mechanical properties [162] [163]. While the effects of annealing on the long-term viscoelastic behavior of PEEK remains poorly understood, researchers have quantified the constraints on polymer chain mobility [164]. Since the focus of this study is not on the viscoelastic properties, we fixed the indentation loading and unloading rate for all indentation tests. Furthermore, PEEK has a high glass transition temperature (145 °C) [49] and we believe the differences in load-displacement behavior are also owed to differences in stress states that exist owing to variances between both the size and geometry of the indenter tips. For a given load, a smaller size indenter can deliver an elevated stress state beneath the indenter tip that may enable greater penetration depths into the material. Such behavior is demonstrated in Figure 22b for PEEK. For a prescribed load of 1000 μN , the smaller indenter penetrates the sample to depths of 500 nm from the surface, while a 20 μm radius indenter tip only reaches depths of 100 nm. Similarly, sharper indenters produce smaller contact radius and thus provide a localized highly stressed or plastic zone, enabling greater penetration depths with greater energy dissipated [113].

Understanding the relationship between plastic zone size and indentation depth is important for nanomechanical analysis of composites. Chen and colleagues established a relationship between the radius of the plastic zone and the maximum penetration depths for elastic-perfectly-plastic bulk materials [165]. Our future studies will focus on quantifying the plastic zone for conospherical indentation of composites in order to elucidate mechanisms of deformation beneath the indenter and owing to variations in tip dimensions.

An advantage to using a nano-length scale characterization technique is the ability to measure the changes in mechanical behavior resulting from thermal treatments and carbon fiber type. Based on our nanoindentation measurements using a 1.5 μm radius conospherical tip (Figure 23), we observe that unfilled PEEK annealed to 200 °C, 225 °C and non-heat treated are not statistically different from each other (Figure 23a). However, they are statistically different from unfilled PEEK annealed to 250°C, 275°C and 300 °C. By contrast, the non-heat treated samples of PEEK with PAN-based carbon fibers were statistically different to the samples annealed to 200°C,

225°C, 250°C, 275°C, 300 °C (Figure 23b). On a similar note, the non-heat treated samples of PEEK with pitch-based carbon fibers were statistically different to the samples annealed to 225°C, 250°C, 275°C, 300 °C (Figure 23c). Based on our nanomechanical measurements and subsequent statistical analysis (Kruskal-Wallis H Test), a change of 25°C in annealing temperature did not result in statistically different indentation modulus for the PEEK samples reinforced with carbon fibers. Contrary to the microindentation measurements by Regis [48], in which substantial data scatter of carbon fiber reinforced PEEK prevented producing statistically significant differences in the nanoindentation modulus with increasing annealing temp; nanoindentation techniques has the ability to discern differences in indentation modulus for some sample cohorts. The ability to discern differences in mechanical behavior resulting from various annealing temperature motivates nanoindentation techniques for understanding the effects on the mechanical properties.

Further differences in load-displacement behavior are also evident in CFR-PEEK composites, Figure 24. Noteworthy, the diversity in loading and unloading paths from nanoindentation may exist across tip geometries and across indentation diameter of the same tip geometry. As illustrated in Figure 24, the load-displacement behavior using a 1.5 µm conospherical tip varies from the 20 µm conospherical tip. Further, the nanoindentation data show significant differences in load-displacement behavior that are also dependent on the fiber reinforcement type and thermal annealing treatment. The nanoindentation modulus of PEEK with PAN-CFR is higher than that of PEEK with pitch-CFR. These results are consistent with the bulk mechanical properties Table 15.

Table 16 summarizes the nanomechanical properties (median indentation modulus) of PEEK and CFR-PEEK composites subjected to different annealing temperatures. The indentation modulus increases with decreasing indenter size for all groups. The nanomechanical modulus increases with annealing temperature for PEEK and CFR PEEK, and this finding is in congruence with the findings by Regis and colleagues [48]. Similarly, the indentation modulus increases with increasing fiber stiffness. The findings of this work indicate that nanomechanical measurements can detect changes owing to differences in indenter stress state as well as changes owing to constituents and thermal processing conditions.

Table 16- The nanomechanical properties (median indentation modulus) of PEEK and CFR-PEEK composites heat treated to different annealing temperatures. The indentation modulus recorded were attained using a 1.5 µm or a 20 µm conospherical tip.

Nanomechanical Properties of PEEK and CFR-PEEK composites					
		Tip R = 1.5 µm		Tip R = 20 µm	
	Heat Treatment	E (median) (GPa)	Standard Dev. (GPa)	E (median) (GPa)	Standard Dev. (GPa)
Unfilled PEEK	No Heat Treatment	3.39	0.39	2.25	0.29
	300 °C	3.87	0.29	2.92	0.45
PAN CFR PEEK	No Heat Treatment	3.98	2.77	3.00	1.57
	300 °C	4.59	2.96	3.68	1.56
Pitch CFR PEEK	No Heat Treatment	3.89	1.57	2.85	1.32
	300 °C	4.23	2.78	3.44	1.43

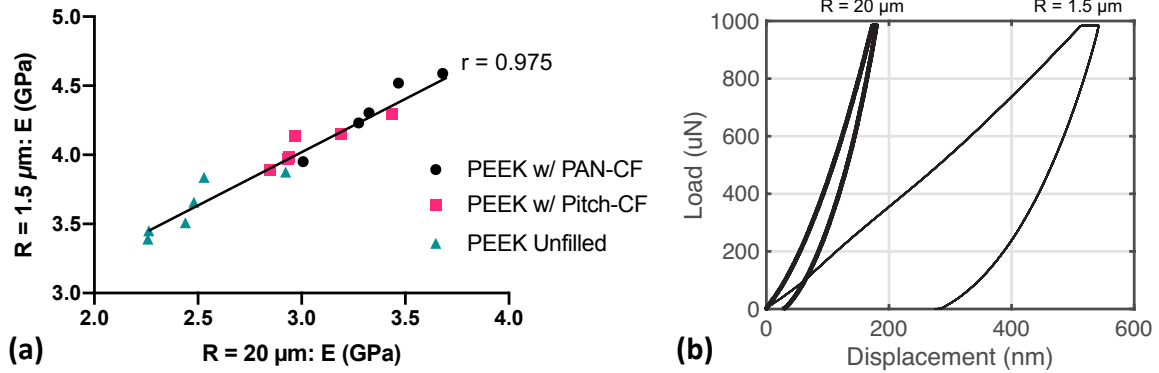


Figure 22 - (a) Plot showing the spearman rank correlation coefficient between ($r = 0.975$) between $1.5 \mu\text{m}$ indentation modulus versus nanoindentation modulus using an indenter tip of $20 \mu\text{m}$ (b) Load-displacement behavior for one indentation cycle performed on Unfilled PEEK (annealed to 275 °C) using a $20 \mu\text{m}$ and a $1.5 \mu\text{m}$ radius conospherical tip

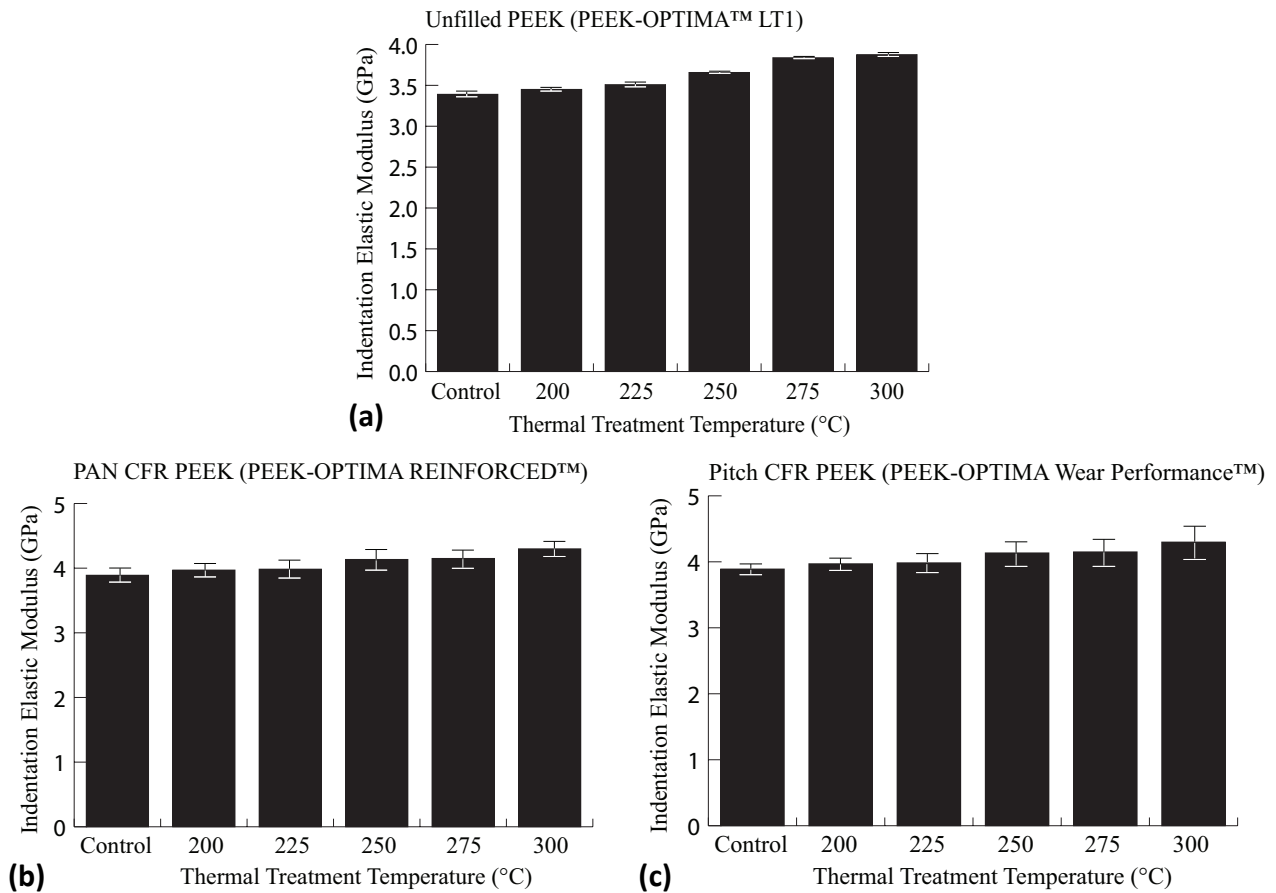


Figure 23 - Bar graph illustrating the indentation modulus (median \pm std. error) using an indenter tip of $1.5 \mu\text{m}$ (a) Indentation modulus for Unfilled PEEK (b) Indentation modulus for PAN CFR PEEK (c) Indentation modulus for Pitch CFR-PEEK

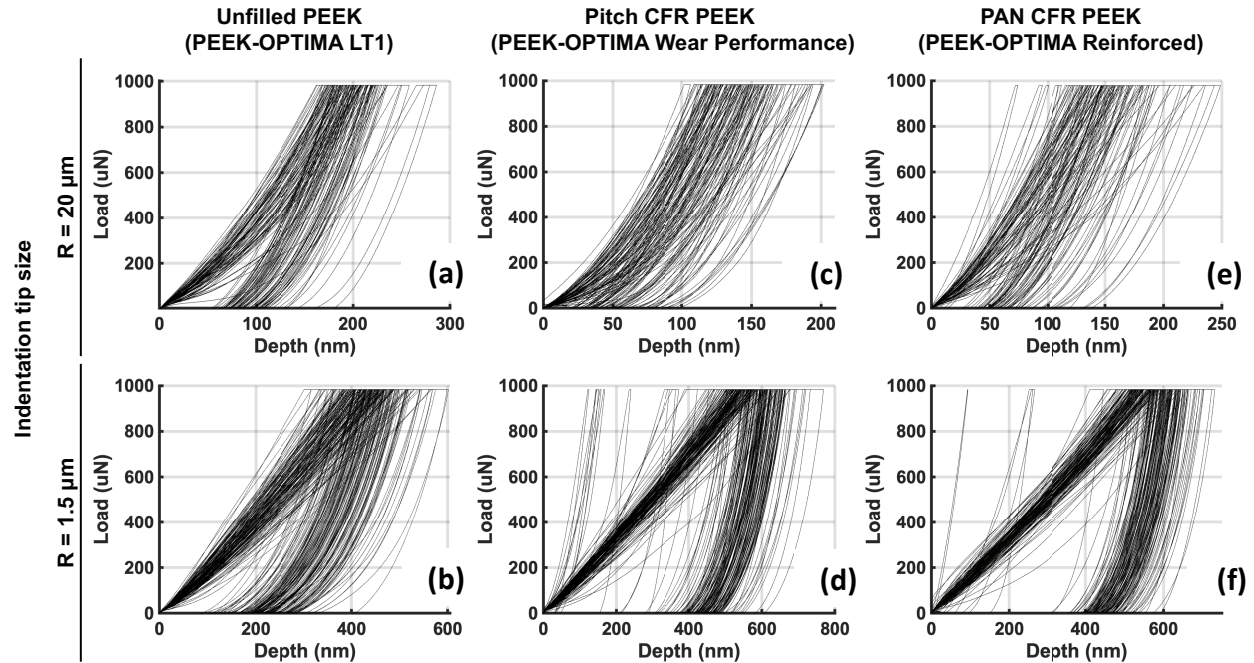


Figure 24 - Load displacement curves for Unfilled PEEK and CFR PEEK composites (not heat treated) (a) load unload path for PEEK unfilled measured using a 20 μm radius conospherical indenter (b) load unload path for PEEK unfilled measured using a 1.5 μm radius conospherical indenter (c) load unload path for pitch-based carbon fiber PEEK measured using a 20 μm radius conospherical indenter (d) load unload path for pitch-based carbon fiber PEEK measured using a 1.5 μm radius conospherical indenter (e) load unload path for PAN-based carbon fiber PEEK measured using a 20 μm radius conospherical indenter (f) load unload path for pitch-based carbon fiber PEEK measured using a 1.5 μm radius conospherical indenter

Developing an analytical method for analyzing indentation curves of composites

Our findings indicate that a smaller indentation tip is able to capture the modulus of the individual component; whereas, larger diameter tips capture blended behavior owing to a mixture of fibers and matrix. Indentations performed using an indenter tip of radius 1.5 μm are able to isolate the mechanical behavior for the fiber, fiber-matrix interphase region, and the matrix region. Since the diameter of the tip is twice as small as the diameter of the PAN carbon fibers and is three times as small as the diameter of the pitch carbon fibers, we can also infer some indentations will be on carbon fibers, while others may be on the fiber-matrix region or on the matrix as indicated by the broad range of indentation depths, varying from 90 nm to 800 nm for indentations performed at a maximum peak of 1000 μN in the CFR-PEEK (Figure 24).

We believe that the diversified load and unload paths may also be complicated by the complex microstructure of CFR-PEEK where chopped carbon fibers are randomly mixed throughout the PEEK matrix (Figure 24). We can infer the diverse load-displacement curves are a result of the indenter discerning the mechanical behavior of the constituents present in the composite; however, the challenge becomes clustering the load-displacement curves to specified groups: fiber, fiber-matrix, matrix. For that reason, k-means clustering is proposed as a method to classify the indentation data into three groups to ascertain the nanomechanical behavior of the fiber, fiber-matrix and the matrix region.

By implementing the k-means clustering method, we can evaluate the indentation data to gain insight on the changes in mechanical behavior occurring as a result of thermal treatment and carbon fiber type. As shown in Figure 25, the nanomechanical modulus of the three material groups increases with annealing temperature. Furthermore, the indentation modulus of the PAN-based

CFR-PEEK is stiffer than pitch-based CFR-PEEK. These results are in congruence with the bulk properties (Table 15) [153]. Figure 26 highlights the microstructure (Figure 26a) and the various types of load-unload behavior (Figure 26b, Figure 26c) present in CFR PEEK. Meanwhile Figure 26d reveals that the indentation modulus of the matrix for the CFR PEEK is stiffer than the neat matrix of unreinforced PEEK. This finding suggests that neighboring carbon fibers in-plane and subsurface of the indentation site influence the measured stiffness of the matrix. The microstructure of CFR-PEEK (Figure 26a) complicate the nanoindentation techniques and mitigate the ability to isolate individual constituents present in CFR PEEK. Nevertheless, the diverse load and unloading path (Figure 26b, Figure 26c, Figure 24) demarcate the various constituents present in CFR PEEK composites and enable a clustering method to isolate the mechanical behaviors of constituents.

Through the use of finite element modeling, researchers studied how fiber orientation and the axial distance between fiber and indenter affects the nanoindentation response of the fibre/matrix composite [166]. Their research observed that when the ratio of fiber-to-indenter over fiber diameter is small, then the nanoindentation response depends strongly on the indenter geometry, fiber orientation, and fiber-to-indenter distance. Similarly, Gountsidou and colleagues, observed a relationship between indenter proximity to the young modulus [167]. The closer the indenter is to the fibre, the greater the young's modulus [167]. These computational results that model the indentation of reinforced materials using spherical indenters, are in congruence with the experimental results we observe. The diverse indentation behavior observed are dependant on the proximity of the indenter to a fiber or to the matrix.

While it is difficult to ascertain the experimental modulus of the individual constituents in a composite due to the effects of neighboring constituents beneath the indenter, researchers have resorted to finite element modeling. Specifically, Duan and colleagues investigated the effect of fiber orientation and indentation location on the elastic properties of the fiber reinforced composite [168]. The nanomechanical properties of the individual constituent present in the fibre/matrix composite were extracted by using a linear equation and a second-order polynomial equation based on numerical fitting [168]. By contrast, our approach uses statistical methods (machine learning) in combination with the experimental load-displacement curves from our PEEK composites to identify the modulus of the individual constituent. Future studies should focus on utilizing finite element analysis to model the nanoindentation behavior of randomly arranged carbon fibres and validate the experimental results.

Koumoulos and co-workers established a method for utilizing machine learning classification to cluster nanoindentation data using k-means clustering [169,170]. To the author's knowledge this is the first study to cluster the nanoindentation data of carbon fiber reinforced PEEK composites using k-means clustering. The nanomechanical properties for unfilled PEEK and the properties for each constituent in CFR PEEK using k-means clustering are shown in Figure 26d. This is the first known research to recognize a distinction in the load-displacement curves and to develop a methodology for clustering the data to gain insight on the nanomechanical behavior for the fiber, fiber-matrix and matrix region. Notably, the local characterization technique provides a method for understanding the changes in mechanical behavior resulting from changes in microstructure. Implementing a statistical method for systematically differentiating the nanomechanical behavior of the constituents may assist in tailoring the microstructure of composites for load bearing applications.

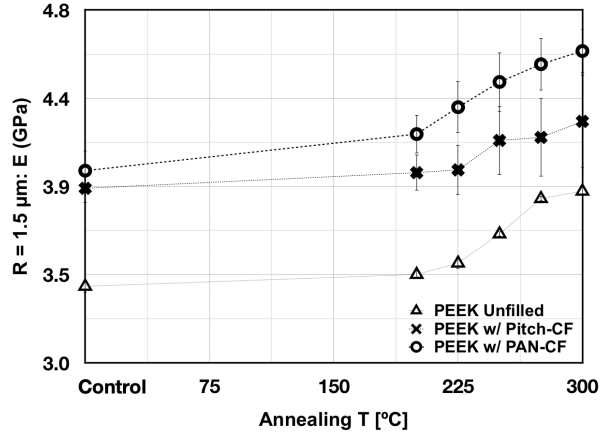


Figure 25 - Indentation modulus measured using a 1.5 μm -radius indenter tip.

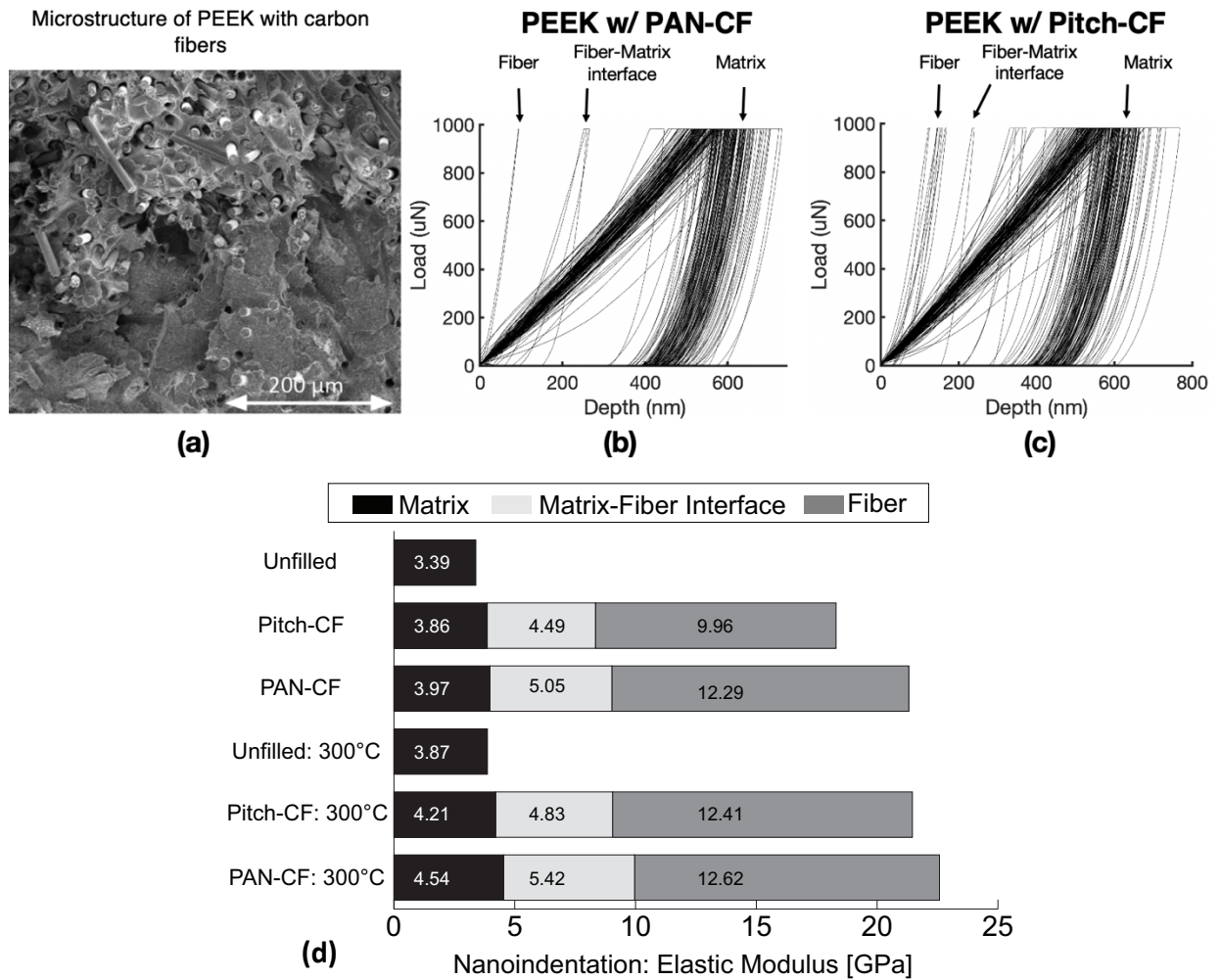


Figure 26 - (a) Scanning electron microscopy image of CFR PEEK [153]. (b) Load-Displacement curve for PEEK with PAN-carbon fibers (CF) (c) Load-Displacement curves for PEEK with Pitch-CF (d) The nanomechanical properties for the matrix, matrix-fiber interface and fiber measured with a 1.5 μm -radius indenter tip and subsequently processed using k-means.

Correlations: Micro- and Nano-mechanical properties, microstructural (crystallinity) property

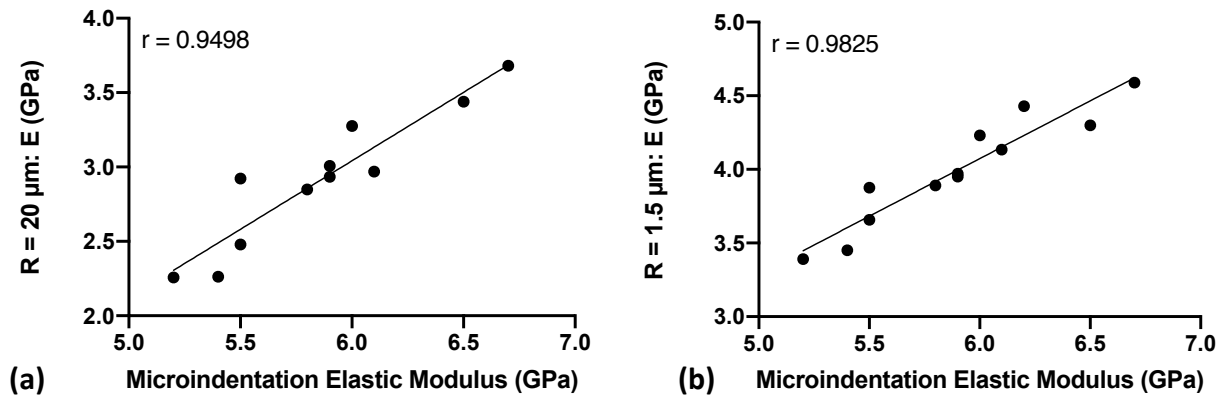


Figure 27 - (a) Plot showing the spearman rank correlation coefficient between ($r = 0.9498$) microindentation modulus versus nanoindentation modulus using an indenter tip of 20 μm (b) Plot showing the spearman rank correlation coefficient between ($r = 0.9825$) between microindentation modulus versus nanoindentation modulus using an indenter tip of 1.5 μm .

In this study we evaluate mechanical properties of PEEK and CFR-PEEK composites using micro- and nano-length scale testing. We also correlate our findings with research published by Regis and colleagues [48] on the same material systems. These researchers noted and observed increase in micro-indentation elastic modulus with annealing temperature; however, the large scatter prevented the authors from providing statistically significant differences across the micro-indentation measurements [48]. A benefit of the nanoindentation measurements is that the length scale provides the ability to discern the mechanical behavior resulting from various annealing temperatures. The smaller indenter tip used combined with the diverse load and unload paths also facilitates a mechanism to discern constituent mechanical behavior using nanoindentation.

Additionally, we evaluated the correlation between microindentation modulus and nano indentation modulus using both the 20 μm and 1.5 μm tips (Figure 27a, Figure 27b). While Figure 27a and Figure 27b show a strong spearman correlation between nanoindentation modulus and microindentation modulus, it is noteworthy to observe the minute increase in correlation strength when using a 1.5 μm tip. This behavior may potentially be attributed to the similarity of indenter geometry between the 1.5 μm nanoindentation tip and the Vickers tip used in microindentation. Further studies are needed to evaluate the role of tip geometry on the ability to correlate properties across different length scales, especially as microindentation and nanoindentation become more prevalent in biomaterials characterization.

Finally, we evaluated the correlation strength between nanoindentation modulus (1.5 μm tip) and crystallinity. Crystallinity measurements were obtained from the work by Regis and colleagues [[48]. Based on their morphological study, they observed annealing of PEEK induces an increase in crystallinity via the thickening of existing lamellae and nucleation and growth of new, thinner lamellae. The microstructural changes occurring as a result of annealing was recognized by nanoindentation through an increase in indentation modulus with increasing annealing temperature (Figure 28). Furthermore, the correlation strength between Unfilled PEEK and crystallinity (%) is greater than CFR-PEEK. We surmise this decrease in correlation strength noted in CFR-PEEK in contrast to PEEK unfilled may be attributed to the complex microstructure of a carbon fiber reinforced composite. Nevertheless, this study provides evidence on the utility of

nanindentation as an alternate characterization method for developing structural-property relationships.

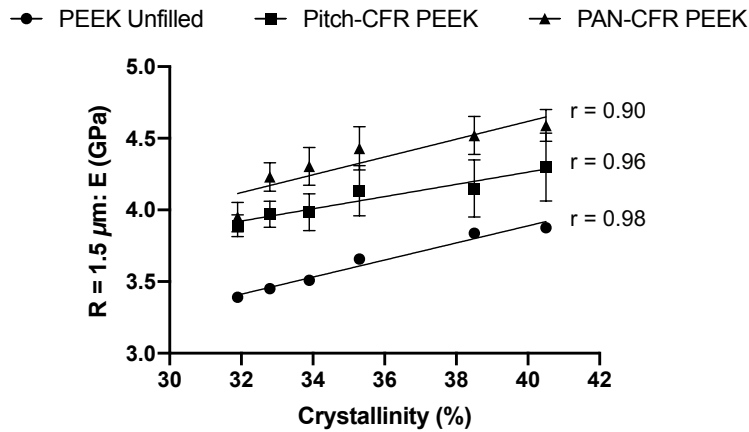


Figure 28 - Plot showing the spearman rank correlation coefficient between (r) between percent crystallinity [48] and nanoindentation modulus using an indenter tip of 1.5 μm .

4.4 Conclusion

In this study, we utilized nanoindentation as a method to characterize mechanical behavior of clinical grade PEEK and PEEK composites. In order to evaluate the ability of nanoindentation to assess microstructural changes in the PEEK systems, we assessed formulations with both pitch and PAN fibers and evaluated a range of thermal treatments known to influence polymer microstructure. We combined nanoindentation with k -means clustering to quantitatively discern the influence of heat treatment and carbon fiber type on the mechanical behavior of PEEK composites. We utilized two types of nanoindentation tips, a conospherical tip of radii 1.5 μm and a conospherical tip of 20 μm radii, to determine indentation modulus and to evaluate which indenter tip had better correlation with microindentation. Both tips captured the local mechanical behavior in response to thermal treatments; however, using an indentation tip with a smaller radius improved the ability to capture the behavior of the constituents in CFR PEEK.

The average surface roughness post polishing is a limitation of the research, as the indentation depth and average surface roughness values are on the same order of magnitude. Some researchers recommend indenting to a penetration depth that is at least five-times greater than the average roughness to obtain a reasonable value of modulus. However, in spite of the average surface roughness, the strong correlation between nano- and micro- indentation modulus and the nanoindentation modulus value are within the same order of magnitude as the microindentation modulus. These results confirm reliability of the measured indentation values. However, if accuracy and precision for each indentation sample is to be improved, then, decreasing surface roughness and penetrating the sample to appropriate depths may be needed in future studies.

In summary, we believe that nanoindentation is an effective characterization tool for discerning fiber-matrix interactions and measuring the mechanical behavior in response to thermal treatment and carbon fiber type in PEEK composites. We believe that nanoindentation is a viable tool for developing structure-property relationships and optimizing biomaterial properties for structural applications such as orthopedics.

Chapter 5 – A characterization technique for implant retrievals: nano-mechanical characterization of total knee retrievals

5.1 Introduction

Ultra High Molecular Weight Polyethylene (UHMWPE) is a gold-standard material for total joint arthroplasty due to its biocompatibility, desirable mechanical properties, and tailorability [171]. Newer formulations of UHMWPE offer the potential for enhanced longevity in total joint replacements (TJR). Existing characterization techniques focus on bulk mechanical behavior of the implants, but that does not account for understanding localized properties of UHMWPE that may provide insight on the wear or fracture of the implant. Instead, I use nanoindentation to yield insight on the surface properties [44]. Assessing the surface properties may provide insight into how the *in vivo* loading conditions affect the microstructure evolution and provide information into the wear mechanisms [172]. The following wear mechanisms, adhesive and abrasive wear, are more prevalent in conforming TJR while less conforming joints such as knees are prone to fatigue (delamination) [173]. The high contact stresses in many tibial component designs may exacerbate wear rates and can promote fatigue mechanisms in UHMWPE [173–175]. As a result, certain material formulations are only suited for knee inserts. Characterization of the surface mechanical properties provides insight into the local material properties. It offers benefits over macroscale testing that may lack the ability to detect localized mechanical property variations across the articulating surface of an implant [176]. Thus, testing techniques such as small punch testing and micro-indentation techniques measure the local behavior of retrievals and have been used for mechanical assessment [176–179]. Notably, Edidin and colleagues used small punch testing to relate UHMWPE properties to the wear mechanisms in acetabular bearings [180]. In particular, Kurtz et al. established the suitability of small punch testing for mechanical characterization of retrievals [181]. By contrast, Wernele et al. highlighted the usefulness of micro-indentation for correlating mechanical properties to oxidation levels for retrieved tibial knee bearings [10]. Micro-length scale mechanical testing proves beneficial as a characterization technique for retrievals [179,181]; yet, there is an ongoing need to develop relations between the surface behavior and wear mechanisms. Nano-scale characterization techniques enable the opportunity to map the nano-mechanical heterogeneity on the articulating surface and in the cross-section of a UHMWPE TJR component. Furthermore, nano-mechanical mapping may provide the opportunity to observe oxidation and cyclic loading effects on the local mechanical properties of explants.

This research investigates the suitability of using nanoindentation to characterize the properties at the articulating surface and the cross-section. This research will delve into the benefits and challenges of using indentation as a characterization technique of retrievals. The motivation is to understand and quantify the mechanical properties' changes. Further, quantifying local mechanical properties may provide insight into wear mechanisms on tibial inserts.

5.2 Background

Previous efforts to characterize UHMWPE and the need to understand its surface behavior

Wear formation and development is a significant concern for the long-term survivorship of contemporary knee prosthetics. The polyethylene debris generation links to osteolysis, which may lead to bone resorption and implant loosening. The three dominating wear mechanisms present in

knee prostheses are (a) microscopic, (b) macroscopic, and (c) subsurface failure. The microscopic wear process relates to polymer abrasion. By contrast, macroscopic wear involves fatigue failure of the polymer resulting from high subsurface strains. The transition between microscopic and macroscopic depends on the mechanical properties, as defined by Wang et al. In sum, wear mechanisms are sensitive to bearing topography, loading, implant geometry, and kinematic motion between the polymer-metal components.

Knee kinematics is very complex; the dominant motion is flexion, resulting in a combined cyclic loading of rolling and sliding between the bearing surface. The cyclic loading and sliding created the most significant damage, delamination, and cracking 100 μm beneath the articulating surface and subsurface cracks (2 mm below the surface) [182]. The modeled mechanism describes fatigue wear in conjunction with subsurface cracking, yielding surface delamination [182]. According to McKellop et al., a deformed and hardened polyethylene surface layer, with increased crystallinity and enhanced mechanical properties, forms from cyclic loading [183]. However, with increased loading, the surface layer reaches a state of maximum strain, which initiates debonding at the surface and hardened surface layer.

The contact areas of polyethylene have local flow or re-molding and a ripple texture, which results in surface and subsequent fatigue cracking [183]. Polyethylene implants (tibial inserts) can experience loads three times the body weight during walking conditions and four to five times the body weight during stressful activities like running. As such, loads are a particular concern to the longevity of the implant since the contact stresses can exceed the compressive yield strength of the material (UHMWPE). Research shows that excessive stresses on the polymer surface may promote delamination and pitting. Thus, the geometry and types of loading on the implant are essential for determining the contact area and size of the contact stress. Researchers such as Bartel [184], Buechel [185], and Argenson [186] determined that high conformity in implants may reduce wear rates. Such designs are standard in hip components. By contrast, the peak shear stress is closer to the surface in non-conforming contact with sliding, such as those found in knee replacements. As a result, higher conformity reduces wear, as the non-conformity implants cause more damage to the polymer surface. Clinical studies suggest the most common causes for revision are infection, loosening, instability, and patellofemoral complications. Further, failure mechanisms are related to the implant's design, notably tibial tray fracture and accelerated polyethylene wear. However, a shortcoming in the field is the limited research on the pathogenesis of the failure of total knee arthroplasty.

To better understand the properties of the articulating surface, researchers have implemented small-scale testing methodologies to ascertain the mechanical behavior of retrievals. Understanding the surface micromechanics of UHMWPE is critical to determining the wear, deformation, and fracture at the surface of implants [187]. These properties have been inaccessible through traditional mechanical characterization techniques. Some researchers used small punch testing and micro-indentation (Table 17). Key research findings highlight the association between structural factors to mechanical properties [187], but importantly, the variations in mechanical properties can be variable and localized based on the testing scale.

Table 17 – A summary of researchers using small length scale characterization technique to assess retrievals.

Title (Reference)	Objective	Characterization Technique	Joint
On the assessment of oxidative and microstructure changes after <i>in vivo</i> degradation of historical UHMWPE knee components by means of vibrational spectroscopies and nanoindentation [36]	Suitability of different experimental techniques to evaluate chemical, microstructure and mechanical changes associated with <i>in vivo</i> oxidation	Micro-indenter FTIR Raman spectroscopy XP Nanoindenter	Knee
Micromechanics of shelf-aged and retrieved UHMWPE tibial inserts: Indentation testing, oxidative profiling, and thickness effects [188]	Determine the effect of <i>in vivo</i> conditions on the mechanical properties	Microindentation FTIR	Knee
The relationship between the clinical performance and large deformation mechanical behavior of retrieved UHMWPE tibial inserts [134]	Clinical performance of UHMWPE tibial inserts is related to the large-deformation mechanical behavior measured near the articulating surface	Small punch TEM	Knee
Mechanical behavior, wear surface morphology, and clinical performance of UHMWPE acetabular components after 10 years of implantation [189]	Mechanical behavior of UHMWPE is related to clinical performance	Small punch	Hip
Development and validation of the small punch test for UHMWPE used in TJR [190]	Identifying the relationship between clinical performance and large deformation mechanical behavior at the articulating surface	Small punch TEM	Hip and Knee
Validation of a small punch testing technique to characterize the mechanical behavior [191]	Develop a methodology to measure local tensile and static fracture of new and retrieved UHMWPE components.	Small punch	Knee
Degradation of mechanical behavior in UHMWPE after natural and accelerated aging [32]	Determine the mechanisms of mechanical degradation of UHMWPE and clinical performance	Small punch FTIR	Hip and Knee

5.3 Methods and Materials

This study characterized the nanomechanical properties of four Prolong Highly Crosslinked Polyethylene tibial inserts. The *in vivo* time of the implant vary between short and long term (Zimmer Biomet). The implants are of the same design, however, the varying parameter is the length of time it was in the patient. The implants were sectioned using a bandsaw; this allowed a TriboIndenter to reach and contact the implants.

Characterizing the Articulating Surface

A Ti-900 TriboIndenter (Hysitron, Minneapolis, MN) was used to perform indentations at ambient temperature using a Berkovich diamond tip with a 100 nm radius. The indentations were load-controlled with a rate of 30 $\mu\text{N/s}$. A trapezoidal loading-unloading function was used. Each indent was prescribed a maximum load of 400 μN . The modulus value was calculated according to the Oliver and Pharr method.

Characterizing the Cross Section

A Ti-900 TriboIndenter (Hysitron, Minneapolis, MN) was used to perform indentations at ambient temperature using a conospherical diamond tip with a 20 μm radius. The indentations were load-controlled with a rate of 30 $\mu\text{N/s}$. A trapezoidal loading-unloading function was used. Each indent was prescribed a maximum load of 400 μN . The modulus value was calculated according to the Oliver and Pharr method.

5.4 Results

The indentation reduced modulus for a short- and long- term implant are noted in Table 18. The average modulus for the long-term (Implant A) implanted tibial insert is 814.4 ± 164.3 MPa, while the short-term (Implant B) implanted tibial insert is 897.6 ± 175.3 MPa. These samples were characterized at the articulating surface using a Berkovich tip. The frequency distribution for the indentation reduced modulus are illustrated in Figure 29.

By contrast, the samples characterized using a conospherical tip and at the cross section of the implant are noted in Table 18, along with the frequency distribution in Figure 30. Noteworthy observations include a decrease of indentation modulus with increase implantation time for the tibial insert, both at the articulating and cross section of the implant.

Table 18 - Sample size, indentation reduced elastic modulus (mean \pm standard deviation), standard error of mean for E of Implant 18032742 and 1611143.

	Long-Term: Implant A (18032742)	Short-Term: Implant B (1611143)
Sample Size (N)	2727	1411
Mean \pm Std. Dev (MPa)	814.4 ± 164.3	897.6 ± 175.3
Standard Error of Mean	0.0033	0.0046

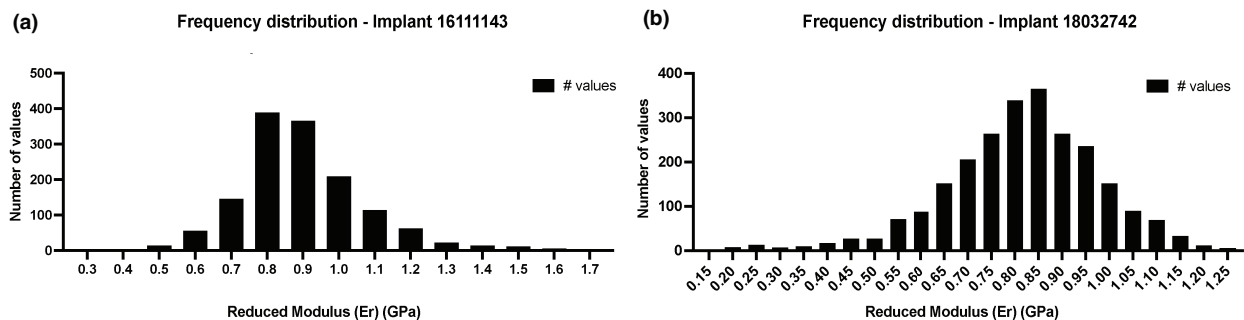


Figure 29 – Frequency distribution for the indentation reduced elastic modulus for (a) implant 1611143 and (b) Implant 18032742.

Table 19 – Sample size, indentation reduced elastic modulus (mean ± standard deviation), standard error of mean for E of Implant 20111844 and 18032544.

	Long-Term: Implant C (20111844)	Short-Term: Implant D (18032544)
Sample Size (N)	2727	1710
E: Mean ± Std. Dev (MPa)	502.7 ± 130.3	675.02 ± 157.5
Standard Error of Mean	0.0024	0.0038

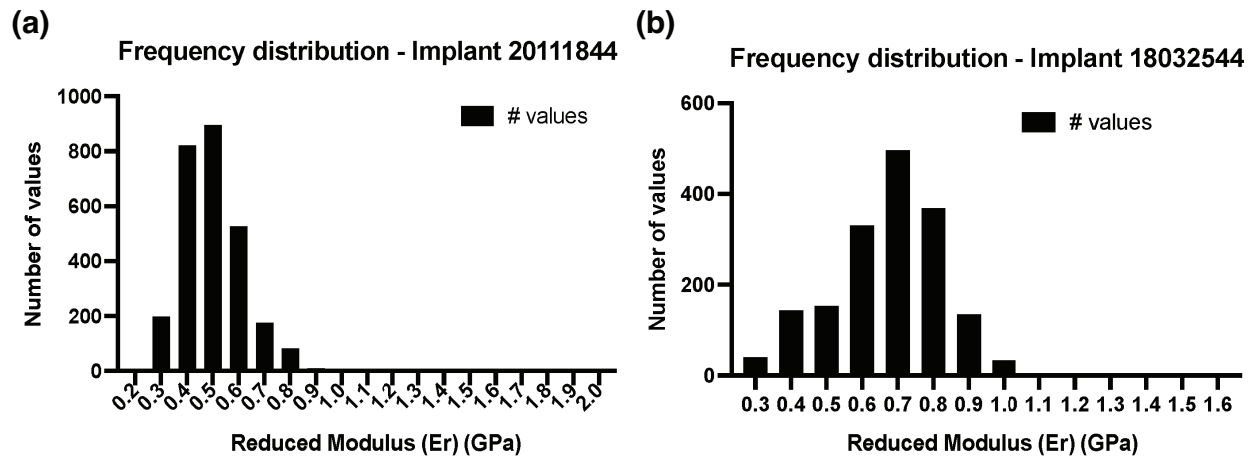


Figure 30 –Frequency distribution for the indentation reduced elastic modulus for (a) implant 20111844 and (b) Implant 18032544.

Welch’s t-test compares the mean indentation modulus between the short- and long-term implants. As illustrated in Figure 31a, the reduced modulus between Implant D and Implant C are statistically different ($P < 0.05$). Similarly, there is a statistical difference between implants Implant C and Implant D (Figure 31b). These results suggest that indentation can differentiate changes in mechanical properties resulting in varying *in vivo* times at the articulating surface and the cross-section.

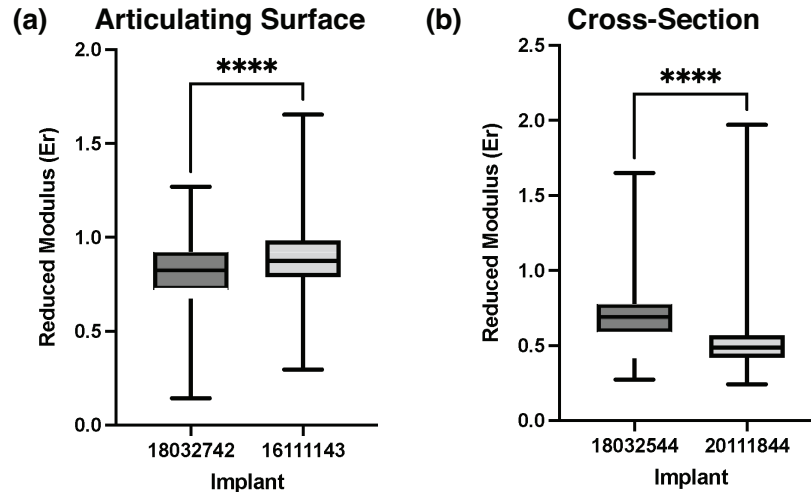


Figure 31- Welch test to compare the reduced modulus of implants at the (a) articulating surface (Implant A and B) and (b) cross-section (Implant C and D).

5.5 Discussion and Concluding Remarks

This study utilizes nanoindentation methods to examine the mechanical behavior at the articulating surface and cross-section of retrievals. Nanoindentation is a critical mechanical behavior characterization technique as it can provide quantitative measurements of the changes occurring *in vivo* on the implants without needing large samples. However, the complex shape of the implant challenges the nano-mechanical characterization of these implants. A limitation to testing at the articulating surface is the difficulty in obtaining a flat contact between implant and tip, owing to the implant's complex concavity. Xu and colleagues found that sample tilt increases indentation load, thereby increasing the contact area and subsequently contact stiffness at the same penetration depth [192]. Further, there was an observed variability in the loading slope, indicative of initial partial tip contact with the sample's surface [192]. In contrast, Kashani found, through FEA simulations, that the nano-mechanical behavior properties for materials exhibiting either sink-in or pile-up are overestimated [193]. In particular, Kashani and colleagues observed a 12% error in hardness with a 5-degree tilt. However, geometric corrections reduced the error to 2% [193]. Understanding and identifying how the properties are affected by indenting on a sample with tilt is of significant interest. Most importantly is identifying the error incurred when indenting on the articulating surface, for which the tilt angle can be greater than 5 degrees. While Kashani enforces correction factors to obtain more reliable data, most indentation instruments are not capable of indenting on a surface past 20-degrees. As such, an alternative to reducing the tilt angle is to section the implant into smaller coupons to reduce the tilt angle.

Nevertheless, the loss in mechanical properties with an increasing *in vivo* times is consistent with the softening in material from previous studies [180]. Edidin suggested that the accumulation of plastic strains resulted in a softening. Further, researchers believe that *in vivo* articulation leads to molecular chain alignment at the surface, resulting in localized anisotropy and strain softening in the direction transverse to the oriented molecular chains [180,194]. This phenomenon may better understand wear and its relation to surface mechanical properties.

Future studies will include the nano-modulus mapping of the articulating surface across a spectrum of *in vivo* times. Understanding modulus variation across the implant will enable a better understanding of the areas that exhibited more significant changes in modulus. We predict that nanoindentation can determine which areas have undergone the most articulation based on

the local modulus values. Furthermore, a nano-modulus mapping of the retrieval's cross-sections may assist in correlating the oxidative degradation to nano-mechanical properties. In summary, assessing the nano-scale properties of retrievals provides an opportunity to understand structure-property evolution owed to *in vivo* conditions.

Chapter 6 – Discussion and Future Direction

Issues of wear, fracture resistance, and oxidation are prevalent in UHMWPE implants. As such, researchers are tailoring the microstructure to optimize the mechanical behavior. However, with the ever-increasing formulations of UHMWPE, it becomes essential to understand how these microstructural changes affect the mechanical properties. These mechanical properties are commonly obtained from stress-strain relations and are necessary for simulating material deformation. However, with the advent of small-length scale testing, it is possible to characterize the mechanical behavior at the microstructural length scale.

In summary, chapter 2 focuses on developing a framework (illustrated in Figure 16-17) to be used for designing a nanoindentation experiment to accurately measure the nanomechanical properties of soft and hydrated materials. The framework provides guidance to novice users on probe selection, experimental set-up, data collection challenges and data analysis methods. This framework highlights the important factors for considering a probe and testing parameters. This body of work compiles the indentation research and summarizes experimental set-ups commonly used in a variety of research fields. An important part of this research is addressing common challenges encountered during indentation testing that may result in erroneous data. As nanoindentation continues to rise in utility for testing soft polymers, it becomes imperative to recognize the assumptions and limitations in the traditional methods for analyzing load-displacement curves, and consider other contact mechanics models for analyzing data. As nanoindentation continues to rise in utility and expand across many disciplines from medicine to materials science, it is imperative to understand and address the multifactorial parameters involved in nanoindentation of soft or hydrated materials. As a result, this decision framework can serve as a guide to facilitate determination and dissemination of reliable, accurate nanoindentation moduli when testing soft or hydrated materials.

As discussed in chapter 3, the motivation behind characterizing medical-grade polymers is to understand the mechanical behavior and identify any anisotropic behavior that may affect the clinical performance of the material in the body. Researchers observed an increase in wear resistance with preferential crystal alignment [137]. The basic behavior of these clinical formulations of UHMWPE can be obtained from stress-strain curves to simulate material deformation. However, to gain insight into the microstructural changes occurring from various tailoring of the implant, microstructural analysis becomes important. As demonstrated in chapter 3, the mechanical properties positively correlate with the microstructural properties. The impact of this research is the ample of mechanical (tensile, compressive and nanoindentation) and microstructural properties that can enable clinicians and designers develop improved devices.

In addition to characterizing the gold-standard polymer (UHMWPE), this research focused on characterizing medical grade PEEK and PEEK composites. As discussed in chapter 4, this body of work also evaluates the ability of nanoindentation to assess microstructural changes in PEEK systems. A notable result is the ability for nanoindentation to discern the influence of heat treatment and carbon fiber type on the mechanical behavior. In this research, two different tip diameter sizes were used. While both tips captured the local mechanical behavior in response to thermal treatments; The tip with a smaller radius improved the ability to capture the behavior of the constituents in CFR PEEK. This is the first body of work that aims to develop structure-property relationships on composites and correlate microindentation to nanoindentation values.

In summary, this dissertation shows that nanoindentation is an effective characterization tool for discerning fiber-matrix interactions and measuring the mechanical behavior in response to

thermal treatment and carbon fiber type in PEEK composites. As a result, nanoindentation is a viable tool for developing structure-property relationships and optimizing biomaterial properties for structural applications such as orthopedics.

Future direction for this work involves developing a detailed modulus map of the articulating surface of retrievals to better understand modulus variations resulting from *in vivo* conditions. Additional experiments to analyze the microstructure and oxidation levels are warranted to obtain a microstructural snapshot of changes occurring *in vivo*. The hypothesis is that nanoindentation is sensitive to microstructural changes and can correlate to microstructural properties (e.g. crystallinity, oxidation index, lamellar alignment). The impact of this research is to provide insight to the orthopedic community the pathways for surface degradation, thereby enabling improved material composition and designs.

REFERENCES

- [1] E. Pascual, V. Jovaní, Synovial fluid analysis, *Best Pract. Res. Clin. Rheumatol.* 19 (2005) 371–386. doi:10.1016/j.berh.2005.01.004.
- [2] B.M. Wroblewski, Professor Sir John Charnley (1911-1982), *Rheumatology.* 41 (2002) 824–825. doi:10.1093/rheumatology/41.7.824.
- [3] S. Kurtz, K. Ong, E. Lau, F. Mowat, M. Halpern, Projections of primary and revision hip and knee arthroplasty in the United States from 2005 to 2030, *J. Bone Jt. Surg.* 89 (2007) 780–785. doi:10.2106/JBJS.F.00222.
- [4] S.M. Kurtz, K.L. Ong, J. Schmier, F. Mowat, K. Saleh, E. Dybvik, J. Kärrholm, G. Garellick, L.I. Havelin, O. Furnes, H. Malchau, E. Lau, Future clinical and economic impact of revision total hip and knee arthroplasty, *J. Bone Jt. Surg.* 89 (2007) 144–151. doi:10.2106/JBJS.G.00587.
- [5] K.I. Bohsali, M.A. Wirth, C.A. Rockwood, Current concepts review: Complications of total shoulder arthroplasty, *J. Bone Jt. Surg. - Ser. A.* 88 (2006) 2279–2292. doi:10.2106/JBJS.F.00125.
- [6] G.M. ALBERTON, W.A. HIGH, B.F. MORREY, Dislocation After Revision Total Hip Arthroplasty, *J. Bone Jt. Surgery-American Vol.* 84 (2002) 1788–1792. doi:10.2106/00004623-200210000-00008.
- [7] K.J. Bozic, S.M. Kurtz, E. Lau, K. Ong, D.T.P. Vail, D.J. Berry, The epidemiology of revision total hip arthroplasty in the united states, *J. Bone Jt. Surg.* 91 (2009) 128–133. doi:10.2106/JBJS.H.00155.
- [8] S.M. Kurtz, M.S. Austin, K. Azzam, P.F. Sharkey, D.W. MacDonald, F.J. Medel, W.J. Hozack, Mechanical properties, oxidation, and clinical performance of retrieved highly cross-linked crossfire liners after intermediate-term implantation, *J. Arthroplasty.* 25 (2010) 614-623.e2. doi:10.1016/j.arth.2009.04.022.
- [9] D.A. Baker, R.S. Hastings, L. Pruitt, Compression and tension fatigue resistance of medical grade ultra high molecular weight polyethylene: The effect of morphology, sterilization, aging and temperature, *Polymer (Guildf).* (2000). doi:10.1016/S0032-3861(99)00199-8.
- [10] F.J. Medel, J. Furmanski, Chapter 30 – Fatigue and Fracture of UHMWPE, in: *UHMWPE Biomater. Handb.*, 2009: pp. 451–472. doi:10.1016/B978-0-12-374721-1.00030-4.
- [11] N. Shahemi, S. Liza, A.A. Abbas, A.M. Merican, Long-term wear failure analysis of uhmwpe acetabular cup in total hip replacement, *J. Mech. Behav. Biomed. Mater.* 87 (2018) 1–9. doi:10.1016/j.jmbbm.2018.07.017.
- [12] F.J. Medel, S.M. Kurtz, J. Parvizi, G.R. Klein, M.J. Kraay, C.M. Rimnac, In Vivo Oxidation Contributes to Delamination but not Pitting in Polyethylene Components for Total Knee Arthroplasty, *J. Arthroplasty.* 26 (2011) 802–810. doi:10.1016/j.arth.2010.07.010.
- [13] F. Ansari, B. Gludovatz, A. Kozak, R.O. Ritchie, L.A. Pruitt, Notch fatigue of ultrahigh molecular weight polyethylene (UHMWPE) used in total joint replacements, *J. Mech. Behav. Biomed. Mater.* (2016). doi:10.1016/j.jmbbm.2016.02.014.
- [14] A.M. Kandahari, X. Yang, K.A. Laroche, A.S. Dighe, D. Pan, Q. Cui, A review of UHMWPE wear-induced osteolysis: The role for early detection of the immune response, *Bone Res.* 4 (2016). doi:10.1038/boneres.2016.14.
- [15] E.M. Schwarz, T.W. Bauer, J. Bechtold, M. Bostrom, P.A. Campbell, V. Goldberg, S.B.

- Goodman, E.M. Greenfield, J.J. Jacobs, Y. Konttinen, R. O’Keefe, F.Y.I. Lee, A.S. Shanbhag, R.L. Smith, R.S. Tuan, J.M. Wilkinson, What potential biologic treatments are available for osteolysis?, *J. Am. Acad. Orthop. Surg.* 16 (2008) S72–S75. doi:10.5435/00124635-200800001-00015.
- [16] J.H. Dumbleton, M.T. Manley, A.A. Edidin, A literature review of the association between wear rate and osteolysis in total hip arthroplasty, *J. Arthroplasty.* 17 (2002) 649–661. doi:10.1054/arth.2002.33664.
- [17] S.A. Atwood, D.W. Van Citters, E.W. Patten, J. Furmanski, M.D. Ries, L.A. Pruitt, Tradeoffs amongst fatigue, wear, and oxidation resistance of cross-linked ultra-high molecular weight polyethylene, *J. Mech. Behav. Biomed. Mater.* (2011). doi:10.1016/j.jmbbm.2011.03.012.
- [18] M.D. Ries, L. Pruitt, Effect of Cross-linking on the Microstructure and Mechanical Properties of Ultra-High Molecular Weight Polyethylene, *Clin. Orthop. Relat. Res.* 440 (2005) 149–156. doi:10.1097/01.blo.0000185310.59202.e5.
- [19] L.A. Pruitt, Deformation, yielding, fracture and fatigue behavior of conventional and highly cross-linked ultra high molecular weight polyethylene, *Biomaterials.* 26 (2005) 905–915. doi:10.1016/j.biomaterials.2004.03.022.
- [20] S.M. Kurtz, A Primer on UHMWPE, (n.d.).
- [21] F. Ansari, M.D. Ries, L. Pruitt, Effect of processing, sterilization and crosslinking on UHMWPE fatigue fracture and fatigue wear mechanisms in joint arthroplasty, *J. Mech. Behav. Biomed. Mater.* 53 (2016) 329–340. doi:10.1016/j.jmbbm.2015.08.026.
- [22] H. Mckellop, F.-W. Shen, B. Lu, Patricia Campbell, R. Salovey, Development of an Extremely Wear-Resistant Ultra High Molecular Weight Polyethylene for Total Hip Replacements, *J. Orthopaedic Res. J. Bone Jt. Surg.* 17 (1999) 157–167.
- [23] L. Costa, P. Bracco, Mechanisms of Cross-Linking, Oxidative Degradation, and Stabilization of UHMWPE, in: *UHMWPE Biomater. Handb. Ultra High Mol. Weight Polyethyl. Total Jt. Replace. Med. Devices Third Ed.*, 2015. doi:10.1016/B978-0-323-35401-1.00026-0.
- [24] P. Bracco, V. Brunella, M. Zanetti, M.P. Luda, L. Costa, Stabilisation of ultra-high molecular weight polyethylene with Vitamin E, *Polym. Degrad. Stab.* (2007). doi:10.1016/j.polymdegradstab.2007.02.023.
- [25] L. Bradford, D. Baker, M.D. Ries, L.A. Pruitt, Fatigue Crack Propagation Resistance of Highly Crosslinked Polyethylene, (n.d.). doi:10.1097/01.blo.0000150124.34906.34.
- [26] K.S. Simis, A. Bistolfi, A. Bellare, L.A. Pruitt, The combined effects of crosslinking and high crystallinity on the microstructural and mechanical properties of ultra high molecular weight polyethylene, *Biomaterials.* 27 (2006) 1688–1694. doi:10.1016/j.biomaterials.2005.09.033.
- [27] G.B. Cornwall, C.M. Hansson, A.J. Bowe, J.T. Bryant, Surface degradation features and microstructural properties of ultra-high molecular weight polyethylene (UHMWPE), *J. Mater. Sci. Mater. Med.* 8 (1997) 303–309. doi:10.1023/A:1018564412753.
- [28] J. Furmanski, M. Anderson, S. Bal, A.S. Greenwald, D. Halley, B. Penenberg, M. Ries, L. Pruitt, Clinical fracture of cross-linked UHMWPE acetabular liners, *Biomaterials.* (2009). doi:10.1016/j.biomaterials.2009.07.013.
- [29] J. Furmanski, M.J. Kraay, C.M. Rimnac, Crack Initiation in Retrieved Cross-Linked Highly Cross-Linked Ultrahigh-Molecular-Weight Polyethylene Acetabular Liners. An Investigation of 9 Cases, *J. Arthroplasty.* 26 (2011) 796–801.

- doi:10.1016/j.arth.2010.07.016.
- [30] O.K. Muratoglu, Chapter 13 – Highly Crosslinked and Melted UHMWPE, in: UHMWPE Biomater. Handb., 2009: pp. 197–204. doi:10.1016/B978-0-12-374721-1.00013-4.
- [31] B. Currier, J. Collier, M. Mayor, D. Van Citters, In vivo oxidation of highly cross-linked UHMWPE bearings, *Annu. Meet. Orthop. Res. Soc.* (2010) 170.
- [32] A.A. Edidin, C.W. Jewett, A. Kalinowski, K. Kwarteng, S.M. Kurtz, Degradation of mechanical behavior in UHMWPE after natural and accelerated aging, *Biomaterials*. 21 (2000) 1451–1460. doi:10.1016/S0142-9612(00)00021-1.
- [33] B.M. Willie, L.J. Foot, M.W. Prall, R.D. Bloebaum, Examining the influence of short-term implantation on oxidative degradation in retrieved highly crosslinked polyethylene tibial components, *J. Biomed. Mater. Res. - Part B Appl. Biomater.* 85 (2008) 385–397. doi:10.1002/jbm.b.30957.
- [34] M. Goldman, M. Lee, R. Gronsky, L. Pruitt, Oxidation of ultrahigh molecular weight polyethylene characterized by Fourier Transform Infrared Spectrometry, (n.d.).
- [35] C.J. Bell, P.S. Walker, M.R. Abeysondera, J.M.H. Simmons, P.M. King, G.W. Blunn, Effect of oxidation on delamination of ultrahigh-molecular-weight polyethylene tibial components, *J. Arthroplasty*. 13 (1998) 280–290. doi:10.1016/S0883-5403(98)90173-5.
- [36] F.J. Medel, C.M. Rimnac, S.M. Kurtz, On the assessment of oxidative and microstructural changes after in vivo degradation of historical UHMWPE knee components by means of vibrational spectroscopies and nanoindentation, *J. Biomed. Mater. Res. - Part A*. 89 (2009) 530–538. doi:10.1002/jbm.a.31992.
- [37] V. Premnath, W.H. Harris, M. Jasty, E.W. Merrill, Gamma sterilization of UHMWPE articular implants: An analysis of the oxidation problem, *Biomaterials*. 17 (1996) 1741–1753. doi:10.1016/0142-9612(95)00349-5.
- [38] S.J. Gencur, C.M. Rimnac, S.M. Kurtz, Fatigue crack propagation resistance of virgin and highly crosslinked, thermally treated ultra-high molecular weight polyethylene, *Biomaterials*. (2006). doi:10.1016/j.biomaterials.2005.09.010.
- [39] J.A. Puértolas, F.J. Medel, J. Cegoñino, E. Gomez-Barrena, R. Ríos, Influence of the remelting process on the fatigue behavior of electron beam irradiated UHMWPE, *J. Biomed. Mater. Res. - Part B Appl. Biomater.* 76 (2006) 346–353. doi:10.1002/jbm.b.30378.
- [40] M.C. Sobieraj, C.M. Rimnac, Ultra high molecular weight polyethylene: Mechanics, morphology, and clinical behavior, *J. Mech. Behav. Biomed. Mater.* (2009). doi:10.1016/j.jmbsm.2008.12.006.
- [41] E. Oral, K.K. Wannomae, N. Hawkins, W.H. Harris, O.K. Muratoglu, α -Tocopherol-doped irradiated UHMWPE for high fatigue resistance and low wear, *Biomaterials*. 25 (2004) 5515–5522. doi:10.1016/j.biomaterials.2003.12.048.
- [42] L. Costa, P. Bracco, E. Brach Del Prever, M.P. Luda, L. Trossarelli, Analysis of products diffused into UHMWPE prosthetic components in vivo, *Biomaterials*. 22 (2001) 307–315. doi:10.1016/S0142-9612(00)00182-4.
- [43] S. Kurtz, P. Bracco, L. Costa, Chapter 16 – Vitamin-E-Blended UHMWPE Biomaterials, in: UHMWPE Biomater. Handb., 2009: pp. 237–247. doi:10.1016/B978-0-12-374721-1.00016-X.
- [44] E. Oral, O.K. Muratoglu, Vitamin E diffused, highly crosslinked UHMWPE: a review, *Int. Orthop.* 35 (2010) 215–223. doi:10.1007/s00264-010-1161-y.
- [45] E. Oral, C.A. Godleski Beckos, A.J. Lozynsky, A.S. Malhi, O.K. Muratoglu, Improved

- resistance to wear and fatigue fracture in high pressure crystallized vitamin E-containing ultra-high molecular weight polyethylene, *Biomaterials*. (2009). doi:10.1016/j.biomaterials.2008.12.029.
- [46] S.M. Kurtz, J. Nevelos, PEEK Bearing Materials for Total Joint Replacement, 2nd ed., Elsevier Inc., 2019. doi:10.1016/b978-0-12-812524-3.00024-7.
- [47] B. Berg-Johansen, S. Lovald, E. Altiok, S.M. Kurtz, Applications of Polyetheretherketone in Arthroscopy, 2nd ed., Elsevier Inc., 2019. doi:10.1016/b978-0-12-812524-3.00017-x.
- [48] M. Regis, A. Bellare, T. Pascolini, P. Bracco, Characterization of thermally annealed PEEK and CFR-PEEK composites: Structure-properties relationships, *Polym. Degrad. Stab.* 136 (2017) 121–130. doi:10.1016/j.polymdegradstab.2016.12.005.
- [49] D.J. Blundell, B.N. Osborn, The morphology of poly(aryl-ether-ether-ketone), *Polymer (Guildf)*. 24 (1983) 953–958. doi:10.1016/0032-3861(83)90144-1.
- [50] S.E. Arevalo, D.M. Ebenstein, L.A. Pruitt, A methodological framework for nanomechanical characterization of soft biomaterials and polymers, *J. Mech. Behav. Biomed. Mater.* (2022) 105384. doi:10.1016/j.jmbbm.2022.105384.
- [51] G.M. Pharr, W.C. Oliver, Measurement of Thin Film Mechanical Properties Using Nanoindentation, *MRS Bull.* 17 (1992) 28–33. doi:10.1557/S0883769400041634.
- [52] D.M. Ebenstein, L.A. Pruitt, Nanoindentation of biological materials, *Nano Today*. 1 (2006) 26–33. doi:10.1016/S1748-0132(06)70077-9.
- [53] M.L. Oyen, T.A.V. Shean, D.G.T. Strange, M. Galli, Size effects in indentation of hydrated biological tissues, *J. Mater. Res.* 27 (2012) 245–255. doi:10.1557/jmr.2011.322.
- [54] F. Carrillo, S. Gupta, M. Balooch, S.J. Marshall, G.W. Marshall, L. Pruitt, C.M. Puttlitz, Nanoindentation of polydimethylsiloxane elastomers: Effect of crosslinking, work of adhesion, and fluid environment on elastic modulus, *J. Mater. Res.* 20 (2005) 2820–2830. doi:10.1557/JMR.2005.0354.
- [55] M. Galli, K.S.C. Comley, T.A.V. Shean, M.L. Oyen, Viscoelastic and poroelastic mechanical characterization of hydrated gels, *J. Mater. Res.* 24 (2009) 973–979. doi:10.1557/jmr.2009.0129.
- [56] J.D. Kaufman, G.J. Miller, E.F. Morgan, C.M. Klapperich, Time-dependent mechanical characterization of poly(2-hydroxyethyl methacrylate) hydrogels using nanoindentation and unconfined compression, 23 (2008) 1472–1481. doi:10.1557/jmr.2008.0185.
- [57] J.C. Kohn, D.M. Ebenstein, Eliminating adhesion errors in nanoindentation of compliant polymers and hydrogels, *J. Mech. Behav. Biomed. Mater.* 20 (2013) 316–326. doi:10.1016/j.jmbbm.2013.02.002.
- [58] O. Franke, M. Göken, M.A. Meyers, K. Durst, A.M. Hodge, Dynamic nanoindentation of articular porcine cartilage, *Mater. Sci. Eng. C*. 31 (2011) 789–795. doi:10.1016/j.msec.2010.12.005.
- [59] N.K. Simha, H. Jin, M.L. Hall, S. Chiravambath, J.L. Lewis, Effect of indenter size on elastic modulus of cartilage measured by indentation, *J. Biomech. Eng.* 129 (2007) 767–775. doi:10.1115/1.2768110.
- [60] D.M. Ebenstein, L.A. Pruitt, Nanoindentation of soft hydrated materials for application to vascular tissues, *J. Biomed. Mater. Res. - Part A*. 69 (2004) 222–232. doi:10.1002/jbm.a.20096.
- [61] A.C. Fischer-Cripps, Critical review of analysis and interpretation of nanoindentation test data, *Surf. Coatings Technol.* 200 (2006) 4153–4165. doi:10.1016/j.surfcoat.2005.03.018.
- [62] M. Farine, Instrumented Indentation of Soft Materials and Biological Tissues, ETH

- Zurich, 2013. <https://doi.org/10.3929/ethz-a-010051403>.
- [63] N. V. Perepelkin, F.M. Borodich, A.E. Kovalev, S.N. Gorb, Depth-sensing indentation as a microand nanomechanical approach to characterisation of mechanical properties of soft, biological, and biomimetic materials, *Nanomaterials*. 10 (2020). doi:10.3390/nano10010015.
- [64] L. Qian, H. Zhao, Nanoindentation of soft biological materials, *Micromachines*. 9 (2018). doi:10.3390/mi9120654.
- [65] A.C. Chang, J. Der Liao, B.H. Liu, Practical assessment of nanoscale indentation techniques for the biomechanical properties of biological materials, *Mech. Mater.* 98 (2016) 11–21. doi:10.1016/j.mechmat.2016.03.005.
- [66] M.L. Oyen, Nanoindentation of hydrated materials and tissues, *Curr. Opin. Solid State Mater. Sci.* 19 (2015) 317–323. doi:10.1016/j.cossms.2015.03.001.
- [67] F. Haque, Application of Nanoindentation Development of Biomedical to Materials, *Surf. Eng.* (2003). doi:10.1179/026708403322499173.
- [68] M.L. Oyen, R.F. Cook, A practical guide for analysis of nanoindentation data, *J. Mech. Behav. Biomed. Mater.* 2 (2009) 396–407. doi:10.1016/j.jmbbm.2008.10.002.
- [69] G.M. Oliver, W.C. Pharr, Measurement of Thin Film Mechanical Properties Using Nanoindentation, *MRS Bull.* 17 (1992) 28–33.
- [70] F. Haque, Application of nanoindentation to development of biomedical materials, *Surf. Eng.* 19 (2003) 255–268. doi:10.1179/026708403322499173.
- [71] R. Lakes, Materials with structural hierarchy, *Nature*. 361:511–15 (1993) 511–515. <https://www.nature.com/articles/361511a0.pdf>.
- [72] R.K. Korhonen, M.S. Laasanen, J. Töyräs, H.J. Helminen, Jurvelin, Superficial Collagen Network Modifies Differently Equilibrium Response of Articular Cartilage in Unconfined Compression and Indentation, *Trans. Orthop. Res. Soc.* 27 (2002) 903–909. <http://luotain.uef.fi/content/abstracts/ORS/0079.pdf>.
- [73] C.M. Buffinton, K.J. Tong, R.A. Blaho, E.M. Buffinton, D.M. Ebenstein, Comparison of mechanical testing methods for biomaterials: Pipette aspiration, nanoindentation, and macroscale testing, *J. Mech. Behav. Biomed. Mater.* 51 (2015) 367–379. doi:10.1016/j.jmbbm.2015.07.022.
- [74] S.E. Arevalo, L.A. Pruitt, Nanomechanical analysis of medical grade PEEK and carbon fiber-reinforced PEEK composites, *J. Mech. Behav. Biomed. Mater.* 111 (2020). doi:10.1016/j.jmbbm.2020.104008.
- [75] J.L. Cuy, A.B. Mann, K.J. Livi, M.F. Teaford, T.P. Weihs, Nanoindentation mapping of the mechanical properties of human molar tooth enamel, *Arch. Oral Biol.* 47 (2002) 281–291. doi:10.1016/S0003-9969(02)00006-7.
- [76] J. il Jang, G.M. Pharr, Influence of indenter angle on cracking in Si and Ge during nanoindentation, *Acta Mater.* 56 (2008) 4458–4469. doi:10.1016/j.actamat.2008.05.005.
- [77] A. Hodzic, Z.. Stachurski, J. Kim, Nano-indentation of polymer-glass interfaces PartI. Experimental and mechanical Analysis, *Polymer (Guildf)*. (1999) 6895–6905.
- [78] A. Dey, R. Chakraborty, A.K. Mukhopadhyay, Nanoindentation of Soda Lime-Silica Glass: Effect of Loading Rate, *Int. J. Appl. Glas. Sci.* 2 (2011) 144–155. doi:10.1111/j.2041-1294.2011.00046.x.
- [79] P. Zysset, X. Guo, C. Hoffler, K. Moore, Elastic modulus and hardness of cortical and trabecular bone lamellae measured by nanoindentation in the human femur, *J. Biomech.* 32 (1999) 1005–1012.

- [80] J.C. Grunlan, X. Xia, D. Rowenhorst, W.W. Gerberich, Preparation and evaluation of tungsten tips relative to diamond for nanoindentation of soft materials, *Rev. Sci. Instrum.* 72 (2001) 2804–2810. doi:10.1063/1.1370564.
- [81] D.M. Ebenstein, J.M. Chapman, C. Li, D. Saloner, J. Rapp, L.A. Pruitt, Assessing structure-property relations of diseased tissues using nanoindentation and FTIR, *Mater. Res. Soc. Symp. - Proc.* 711 (2002) 47–52. doi:10.1557/proc-711-ff4.2.1.
- [82] K.J. Tong, D.M. Ebenstein, Comparison of Spherical and Flat Tips for Indentation of Hydrogels, *Jom.* 67 (2015) 713–719. doi:10.1007/s11837-015-1332-9.
- [83] J.D. Kaufman, C.M. Klapperich, Surface detection errors cause overestimation of the modulus in nanoindentation on soft materials, *J. Mech. Behav. Biomed. Mater.* (2009). doi:10.1016/j.jmbbm.2008.08.004.
- [84] C. Klapperich, K. Komvopoulos, L. Pruitt, Nanomechanical Properties of Polymers Determined From Nanoindentation Experiments, *J. Tribol.* (2001). doi:10.1115/1.1330736.
- [85] K.S. Katti, B. Mohanty, D.R. Katti, Nanomechanical properties of nacre, *J. Mater. Res.* 21 (2006) 1237–1242. doi:10.1557/jmr.2006.0147.
- [86] W.G. Mao, Y.G. Shen, C. Lu, Nanoscale elastic-plastic deformation and stress distributions of the C plane of sapphire single crystal during nanoindentation, *J. Eur. Ceram. Soc.* 31 (2011) 1865–1871. doi:10.1016/j.jeurceramsoc.2011.04.012.
- [87] A. Barnoush, M.T. Welsch, H. Vehoff, Correlation between dislocation density and pop-in phenomena in aluminum studied by nanoindentation and electron channeling contrast imaging, *Scr. Mater.* 63 (2010) 465–468. doi:10.1016/j.scriptamat.2010.04.048.
- [88] M.L. Oyen, *Handbook of nanoindentation with biological applications*, 1st ed., Taylor & Francis, n.d.
- [89] C. Edward Hoffler, X. Edward Guo, P.K. Zysset, S.A. Goldstein, An application of nanoindentation technique to measure bone tissue lamellae properties, *J. Biomech. Eng.* 127 (2005) 1046–1053. doi:10.1115/1.2073671.
- [90] Z. Wang, A.A. Volinsky, N.D. Gallant, Nanoindentation study of polydimethylsiloxane elastic modulus using berkovich and flat punch tips, *J. Appl. Polym. Sci.* 132 (2015). doi:10.1002/app.41384.
- [91] K. Liu, M.R. VanLandingham, T.C. Ovaert, Mechanical characterization of soft viscoelastic gels via indentation and optimization-based inverse finite element analysis, *J. Mech. Behav. Biomed. Mater.* 2 (2009) 355–363. doi:10.1016/j.jmbbm.2008.12.001.
- [92] J. Deuschle, S. Enders, E. Arzt, Surface detection in nanoindentation of soft polymers, (2017). doi:10.1557/JMR.2007.0394.
- [93] D.M. Ebenstein, D. Coughlin, J. Chapman, C. Li, L.A. Pruitt, Nanomechanical properties of calcification, fibrous tissue, and hematoma from atherosclerotic plaques, *J. Biomed. Mater. Res. - Part A.* 91 (2009) 1028–1037. doi:10.1002/jbm.a.32321.
- [94] S. Gupta, J. Lin, P. Ashby, L. Pruitt, A fiber reinforced poroelastic model of nanoindentation of porcine costal cartilage: A combined experimental and finite element approach, *J. Mech. Behav. Biomed. Mater.* 2 (2009) 326–338. doi:10.1016/j.jmbbm.2008.09.003.
- [95] Y. Cao, D. Yang, W. Soboyejoy, Nanoindentation method for determining the initial contact and adhesion characteristics of soft polydimethylsiloxane, *J. Mater. Res.* 20 (2005) 2004–2011. doi:10.1557/JMR.2005.0256.
- [96] J.D. Kaufman, G.J. Miller, E.F. Morgan, C.M. Klapperich, Time-dependent mechanical

- characterization of poly(2-hydroxyethyl methacrylate) hydrogels using nanoindentation and unconfined compression, (n.d.). doi:10.1557/JMR.2008.0185.
- [97] D.M. Ebenstein, Nano-JKR force curve method overcomes challenges of surface detection and adhesion for nanoindentation of a compliant polymer in air and water, *J. Mater. Res.* (2011). doi:10.1557/jmr.2011.42.
- [98] C.M. Buffinton, K.J. Tong, R.A. Blaho, E.M. Buffinton, D.M. Ebenstein, Comparison of mechanical testing methods for biomaterials: Pipette aspiration, nanoindentation, and macroscale testing, *J. Mech. Behav. Biomed. Mater.* 51 (2015) 367–379. doi:10.1016/j.jmbbm.2015.07.022.
- [99] O.E. Armitage, M.L. Oyen, Indentation across interfaces between stiff and compliant tissues, *Acta Biomater.* 56 (2017) 36–43. doi:10.1016/j.actbio.2016.12.036.
- [100] C.L. Slaboch, M.S. Alber, E.D. Rosen, T.C. Ovaert, Mechano-rheological properties of the murine thrombus determined via nanoindentation and finite element modeling, *J. Mech. Behav. Biomed. Mater.* 10 (2012) 75–86. doi:10.1016/j.jmbbm.2012.02.012.
- [101] B.J. Briscoe, L. Fiori, E. Pelillo, Nano-indentation of polymeric surfaces, *J. Phys. D. Appl. Phys.* 31 (1998) 2395–2405. doi:10.1088/0022-3727/31/19/006.
- [102] D.M. Ebenstein, Nano-JKR force curve method overcomes challenges of surface detection and adhesion for nanoindentation of a compliant polymer in air and water, *J. Mater. Res.* 26 (2011) 1026–1035. doi:10.1557/jmr.2011.42.
- [103] J.D. Kaufman, J. Song, C.M. Klapperich, Nanomechanical analysis of bone tissue engineering scaffolds, *J. Biomed. Mater. Res. Part A.* 81A (2007) 611–623. doi:10.1002/jbm.a.30976.
- [104] W.C. Oliver, G.M. Pharr, Nanoindentation in materials research: Past, present, and future, *MRS Bull.* 35 (2010) 897–907. doi:10.1557/mrs2010.717.
- [105] W.C. Oliver, F.R. Brotzen, On the generality of the relationship among contact stiffness, contact area, and elastic modulus during indentation, *J. Mater. Res.* 7 (1992) 613–617. doi:10.1557/JMR.1992.0613.
- [106] L.G. Malito, S. Arevalo, A. Kozak, S. Spiegelberg, A. Bellare, L. Pruitt, Material properties of ultra-high molecular weight polyethylene: Comparison of tension, compression, nanomechanics and microstructure across clinical formulations, *J. Mech. Behav. Biomed. Mater.* (2018). doi:10.1016/j.jmbbm.2018.03.029.
- [107] K.L. Johnson, K. Kendall, A.D. Roberts, Surface energy and the contact of elastic solids, *Proc. R. Soc. A.* (1971) 301–313. doi:10.1088/0022-3727/6/9/304.
- [108] I.N. Sneddon, The relation between load and penetration in the axisymmetric boussinesq problem for a punch of arbitrary profile, *Int. J. Eng. Sci.* 3 (1965) 47–57. doi:10.1016/0020-7225(65)90019-4.
- [109] J.C. Hay, A. Bolshakov, G. Pharr, A critical examination of the fundamental relations used in the analysis of nanoindentation data, *J. Mater. Res.* 14 (1999) 2296–2305.
- [110] W.C. Oliver, G.M. Pharr, An improved technique for determining hardness and elastic modulus using load and displacement sensing indentation experiments, *J. Mater. Res.* 7 (1992) 1564–1583.
- [111] B.J. Briscoe, L. Fiori, E. Pelillo, Nano-indentation of polymeric surfaces, *J. Phys. D. Appl. Phys.* 31 (1998) 2395–2405. doi:10.1088/0022-3727/31/19/006.
- [112] C. Klapperich, L. Pruitt, K. Komvopoulos, Nanomechanical properties of energetically treated polyethylene surfaces, *J. Mater. Res.* (2002). doi:10.1557/JMR.2002.0059.
- [113] A.C. Fischer-Cripps, *Nanoindentation*, 3rd ed., Springer-Verlag New York, New York,

2011. doi:10.1007/978-1-4419-9872-9.
- [114] D. Tabor, Surface forces and surface interactions, *J. Colloid Interface Sci.* 58 (1977) 2–13. doi:10.1016/0021-9797(77)90366-6.
- [115] D.M. Ebenstein, K.J. Wahl, A comparison of JKR-based methods to analyze quasi-static and dynamic indentation force curves, *J. Colloid Interface Sci.* 298 (2006) 652–662. doi:10.1016/j.jcis.2005.12.062.
- [116] C. Jin, Z. Wang, A.A. Volinsky, A. Sharfeddin, N.D. Gallant, Mechanical characterization of crosslinking effect in polydimethylsiloxane using nanoindentation, *Polym. Test.* 56 (2016) 329–336. <https://www.sciencedirect.com/science/article/pii/S0142941816309680>.
- [117] M. Ciavarella, J. Joe, A. Papangelo, J.R. Barber, The role of adhesion in contact mechanics, *J. R. Soc. Interface.* 16 (2019). doi:10.1098/rsif.2018.0738.
- [118] S. Gupta, F. Carrillo, C. Li, L. Pruitt, C. Puttlitz, Adhesive forces significantly affect elastic modulus determination of soft polymeric materials in nanoindentation, *Mater. Lett.* 61 (2007) 448–451. doi:10.1016/j.matlet.2006.04.078.
- [119] C. Jin, D.M. Ebenstein, Nanoindentation of compliant materials using Berkovich tips and flat tips, *J. Mater. Res.* 32 (2017) 435–450. doi:10.1557/jmr.2016.483.
- [120] Q. Liao, J. Huang, T. Zhu, C. Xiong, J. Fang, A hybrid model to determine mechanical properties of soft polymers by nanoindentation, *Mech. Mater.* (2010). doi:10.1016/j.mechmat.2010.09.005.
- [121] L. Chen, A. Ahadi, J. Zhou, J.E. Ståhl, Modeling effect of surface roughness on nanoindentation tests, *Procedia CIRP.* 8 (2013) 334–339. doi:10.1016/j.procir.2013.06.112.
- [122] J.Y. Rho, G.M. Pharr, Effects of drying on the mechanical properties of bovine femur measured by nanoindentation, *J. Mater. Sci. Mater. Med.* 10 (1999) 485–488. doi:10.1023/A:1008901109705.
- [123] Z. Kalcioğlu, M. Qu, K.J. Van Vliet, K.E. Strawhecker, M.R. VanLandingham, Multiscale characterization of relaxation times of tissue surrogate gels and soft tissues, 27th Army Conf. (2010) 1–7. http://vvgroup.scripts.mit.edu/WP/wp-content/uploads/2010/06/27thArmyScienceConferenceManuscript_FP001.pdf.
- [124] A.B. Mann, J.B. Pethica, Nanoindentation studies in a liquid environment, *Langmuir.* 12 (1996) 4583–4586. doi:10.1021/la950901z.
- [125] B. Tang, A.H.W. Ngan, Nanoindentation measurement of mechanical properties of soft solid covered by a thin liquid film, *Soft Mater.* 5 (2007) 169–181. doi:10.1080/15394450701538919.
- [126] R. Saha, W.D. Nix, Effects of the substrate on the determination of thin film mechanical properties by nanoindentation, *Acta Mater.* 50 (2002) 23–38. doi:10.1016/S1359-6454(01)00328-7.
- [127] J. Deuschle, S. Enders, E. Arzt, Surface detection in nanoindentation of soft polymers, *J. Mater. Res.* 22 (2007) 3107–3119. doi:10.1557/jmr.2007.0394.
- [128] A.. Fischer-Cripps, A review of analysis methods for sub-micron indentation testing, *Vacuum.* 58 (2000) 569–585. doi:10.1016/S0042-207X(00)00377-8.
- [129] M.R. VanLandingham, J.S. Villarrubia, W.F. Guthrie, G.F. Meyers, Nanoindentation of polymers: an overview, *Macromol. Symp.* 167 (2001) 15–44. doi:10.1002/1521-3900(200103)167:1<15::AID-MASY15>3.0.CO;2-T.
- [130] L.G. Malito, S. Arevalo, A. Kozak, S. Spiegelberg, A. Bellare, L. Pruitt, Material properties of ultra-high molecular weight polyethylene: Comparison of tension,

- compression, nanomechanics and microstructure across clinical formulations, *J. Mech. Behav. Biomed. Mater.* 83 (2018). doi:10.1016/j.jmbbm.2018.03.029.
- [131] P. Bracco, E. Oral, Vitamin E-stabilized UHMWPE for total joint implants: A review, *Clin. Orthop. Relat. Res.* 469 (2011) 2286–2293. doi:10.1007/s11999-010-1717-6.
- [132] E. Oral, O.K. Muratoglu, Vitamin E diffused, highly crosslinked UHMWPE: A review, *Int. Orthop.* 35 (2011) 215–223. doi:10.1007/s00264-010-1161-y.
- [133] J.H. Dumbleton, A. Wang, K. Sutton, M.T. Manley, Chapter 14 – Highly Crosslinked and Annealed UHMWPE, in: *UHMWPE Biomater. Handb.*, 2009: pp. 205–219. doi:10.1016/B978-0-12-374721-1.00014-6.
- [134] S.M. Kurtz, C.M. Rimnac, L. Pruitt, C.W. Jewett, V. Goldberg, A.A. Edidin, The relationship between the clinical performance and large deformation mechanical behavior of retrieved UHMWPE tibial inserts, *Biomaterials.* 21 (2000) 283–291. doi:10.1016/S0142-9612(99)00178-7.
- [135] L. Pruitt, D. Rondinone, The effect of specimen thickness and stress ratio on the fatigue behavior of polycarbonate, *Polym. Eng. Sci.* (1996). doi:10.1002/pen.10524.
- [136] S.A. Atwood, D.W. Van Citters, E.W. Patten, J. Furmanski, M.D. Ries, L.A. Pruitt, Tradeoffs amongst fatigue, wear, and oxidation resistance of cross-linked ultra-high molecular weight polyethylene, *J. Mech. Behav. Biomed. Mater.* 4 (2011) 1033–1045. doi:10.1016/j.jmbbm.2011.03.012.
- [137] M. Ohta, S.H. Hyon, S. Tsutumi, Control of crystalline orientation to enhance the wear resistance of ultra-high molecular weight polyethylene crystallization cups for artificial joints, *Wear.* 255 (2003) 1045–1050. doi:10.1016/S0043-1648(03)00284-9.
- [138] S.M. Kurtz, *Applications of Polyaryletheretherketone in Spinal Implants: Fusion and Motion Preservation.* Fusion and Motion Preservation., Elsevier Inc., 2012. doi:10.1016/B978-0-323-22805-3.00010-4.
- [139] S.M. Kurtz, J.N. Devine, PEEK biomaterials in trauma, orthopedic, and spinal implants, *Biomaterials.* (2007). doi:10.1016/j.biomaterials.2007.07.013.
- [140] H.B. Skinner, Composite technology for total hip arthroplasty, *Clin. Orthop. Relat. Res.* (1988) 224–236. doi:10.1097/00003086-198810000-00022.
- [141] H.K. Uthoff, P. Poitras, D.S. Backman, Internal plate fixation of fractures: Short history and recent developments, *J. Orthop. Sci.* 11 (2006) 118–126. doi:10.1007/s00776-005-0984-7.
- [142] J. Day, S.M. Kurtz, K. Ong, *Isoelastic PEEK Implants for Total Joint Replacement*, 2nd ed., Elsevier Inc., 2019. doi:10.1016/b978-0-12-812524-3.00021-1.
- [143] S.C. Scholes, A. Unsworth, Wear studies on the likely performance of CFR-PEEK/CoCrMo for use as artificial joint bearing materials, *J. Mater. Sci. Mater. Med.* 20 (2009) 163–170. doi:10.1007/s10856-008-3558-3.
- [144] M. Regis, A. Lanzutti, P. Bracco, L. Fedrizzi, Wear behavior of medical grade PEEK and CFR PEEK under dry and bovine serum conditions, *Wear.* (2018). doi:10.1016/j.wear.2018.05.005.
- [145] C.L. Brockett, S. Carbone, J. Fisher, L.M. Jennings, PEEK and CFR-PEEK as alternative bearing materials to UHMWPE in a fixed bearing total knee replacement: An experimental wear study, *Wear.* 374–375 (2017) 86–91. doi:10.1016/j.wear.2016.12.010.
- [146] S.C. Scholes, I.A. Inman, A. Unsworth, E. Jones, Tribological assessment of a flexible carbon-fibre-reinforced poly(ether-ether-ketone) acetabular cup articulating against an alumina femoral head, *Proc. Inst. Mech. Eng. Part H J. Eng. Med.* 222 (2008) 273–283.

- doi:10.1243/09544119JEIM334.
- [147] Q.Q. Wang, J.J. Wu, A. Unsworth, A. Briscoe, M. Jarman-Smith, C. Lowry, D. Simpson, S. Collins, Biotribological study of large diameter ceramic-on-CFR-PEEK hip joint including fluid uptake, wear and frictional heating, *J. Mater. Sci. Mater. Med.* 23 (2012) 1533–1542. doi:10.1007/s10856-012-4617-3.
- [148] A.A. Corvelli, J.C. Roberts, P.J. Biermann, J.H. Cranmer, Characterization of a peek composite segmental bone replacement implant, *J. Mater. Sci.* 34 (1999) 2421–2431. doi:10.1023/A:1004562732460.
- [149] E. Altiok, B. Berg-Johansen, S. Lovald, S.M. Kurtz, *Applications of Polyetheretherketone in Craniomaxillofacial Surgical Reconstruction*, 2nd ed., Elsevier Inc., 2019. doi:10.1016/b978-0-12-812524-3.00019-3.
- [150] S. Lovald, B. Berg-Johansen, E. Altiok, S.M. Kurtz, *Polyetheretherketone in Trauma*, 2nd ed., Elsevier Inc., 2019. doi:10.1016/b978-0-12-812524-3.00018-1.
- [151] A.D. Schwitalla, T. Spintig, I. Kallage, W.D. Müller, Flexural behavior of PEEK materials for dental application, *Dent. Mater.* 31 (2015) 1377–1384. doi:10.1016/j.dental.2015.08.151.
- [152] A. Schwitalla, W.D. Müller, PEEK dental implants: A review of the literature, *J. Oral Implantol.* 39 (2013) 743–749. doi:10.1563/AAID-JOI-D-11-00002.
- [153] N. Bonnheim, F. Ansari, M. Regis, P. Bracco, L. Pruitt, Effect of carbon fiber type on monotonic and fatigue properties of orthopedic grade PEEK, *J. Mech. Behav. Biomed. Mater.* 90 (2019) 484–492. doi:10.1016/j.jmbbm.2018.10.033.
- [154] A. Godara, D. Raabe, S. Green, The influence of sterilization processes on the micromechanical properties of carbon fiber-reinforced PEEK composites for bone implant applications, *Acta Biomater.* 3 (2007) 209–220. doi:10.1016/j.actbio.2006.11.005.
- [155] A.A. Stratton-Powell, K.M. Pasko, C.L. Brockett, J.L. Tipper, The Biologic Response to Polyetheretherketone (PEEK) Wear Particles in Total Joint Replacement: A Systematic Review, *Clin. Orthop. Relat. Res.* 474 (2016) 2394–2404. doi:10.1007/s11999-016-4976-z.
- [156] S. Utschneider, F. Becker, T.M. Grupp, B. Sievers, A. Paulus, O. Gottschalk, V. Jansson, Inflammatory response against different carbon fiber-reinforced PEEK wear particles compared with UHMWPE in vivo, *Acta Biomater.* 6 (2010) 4296–4304. doi:10.1016/j.actbio.2010.06.002.
- [157] W.C. Oliver, G.M. Pharr, G.M. Pharr, W.C. Oliver, *Nanoindentation in materials research : Past , present , and future The original nanoindenter*, (2018).
- [158] Q. Yuan, S.A. Bateman, K. Friedrich, Thermal and mechanical properties of PAN- and pitch-based carbon fiber reinforced PEEK composites, *J. Thermoplast. Compos. Mater.* 21 (2008) 323–336. doi:10.1177/0892705708089478.
- [159] G.Z. Voyiadjis, A. Samadi-Dooki, L. Malekmoie, Nanoindentation of high performance semicrystalline polymers: A case study on PEEK, *Polym. Test.* (2017). doi:10.1016/j.polymertesting.2017.05.005.
- [160] B. Chen, P.C. Tai, R. Harrison, Y. Pan, Novel hybrid hierarchical-K-means clustering method (H-K-means) for microarray analysis, 2005 IEEE Comput. Syst. Bioinforma. Conf. Work. Poster Abstr. (2005) 105–108. doi:10.1109/CSBW.2005.98.
- [161] M.L. Oyen, Y.A. Toivola, R.F. Cook, Load Dispersion behavior during sharp indentation of Viscous elastic plastic materials, *Mat.Res. Soc. Symp.* 649 (2001) 1–6.
- [162] A. D’Amore, A. Pompo, L. Nicolais, Viscoelastic effects in poly(ether ether ketone)

- (PEEK) and PEEK-based composites, *Compos. Sci. Technol.* 41 (1991) 303–325. doi:10.1016/0266-3538(91)90005-A.
- [163] J.D.D. Melo, D.W. Radford, Viscoelastic properties of PEEK-IM7 related to temperature, *J. Reinf. Plast. Compos.* 24 (2005) 545–556. doi:10.1177/0731684405045019.
- [164] Z. Jiang, P. Liu, H.J. Sue, T. Bremner, Effect of annealing on the viscoelastic behavior of poly(ether-ether-ketone), *Polymer (Guildf)*. 160 (2019) 231–237. doi:10.1016/j.polymer.2018.11.052.
- [165] J. Chen, M.A. Birch, S.J. Bull, Nanomechanical characterization of tissue engineered bone grown on titanium alloy in vitro, *J. Mater. Sci. Mater. Med.* 21 (2010) 277–282. doi:10.1007/s10856-009-3843-9.
- [166] A.A. Khan, A.A. Al-Kheraif, A.M. Al-Shehri, E. Säilynoja, P.K. Vallittu, Polymer matrix of fiber-reinforced composites: Changes in the semi-interpenetrating polymer network during the shelf life, *J. Mech. Behav. Biomed. Mater.* 78 (2018) 414–419. doi:10.1016/j.jmbbm.2017.11.038.
- [167] V. Gountsidou, H.M. Polatoglou, Modeling of the Indentation of Fiber Reinforced Materials Using Spherical Indenters Modeling of the Indentation of Fiber Reinforced Materials Using Spherical Indenters, 312 (2010) 1–7.
- [168] P. Duan, Y. Xia, S. Bull, J. Chen, Finite element modeling of nanoindentation response of elastic fiber-matrix composites, *J. Mater. Res.* 33 (2018) 2494–2503. doi:10.1557/jmr.2018.243.
- [169] E. Koumoulos, G. Konstantopoulos, C. Charitidis, Applying machine learning to nanoindentation data of (nano-) enhanced composites, *Fibers.* 8 (2020) 1–13. doi:10.3390/fib8010003.
- [170] G. Konstantopoulos, E.P. Koumoulos, C.A. Charitidis, Classification of mechanism of reinforcement in the fiber-matrix interface: Application of Machine Learning on nanoindentation data, *Mater. Des.* 192 (2020) 108705. doi:10.1016/j.matdes.2020.108705.
- [171] S. Kurtz, *UHMWPE Biomaterials Handbook*, 2016.
- [172] W. Świąszkowski, P. Bednarz, P.J. Prendergast, Contact stresses in the glenoid component in total shoulder arthroplasty, *Proc. Inst. Mech. Eng. Part H J. Eng. Med.* 217 (2003) 49–57. doi:10.1243/095441103762597737.
- [173] T.M. McGloughlin, A.G. Kavanagh, Wear of ultra-high molecular weight polyethylene (UHMWPE) in total knee prostheses: A review of key influences, *Proc. Inst. Mech. Eng. Part H J. Eng. Med.* 214 (2000) 349–359. doi:10.1243/0954411001535390.
- [174] D.L. Bartel, A.H. Burstein, M.D. Toda, D.L. Edwards, The effect of conformity and plastic thickness on contact stresses in metal-backed plastic implants, *J. Biomech. Eng.* 107 (1985) 193–199. doi:10.1115/1.3138543.
- [175] P.S. Walker, M. Ben-Dov, M.J. Askew, J. Pugh, The deformation and wear of plastic components in artificial knee joints; an experimental study, *Eng. Med.* 10 (1981) 33–38. doi:10.1243/EMED_JOUR_1981_010_010_02.
- [176] F.J. Medel, C.M. Rimnac, S.M. Kurtz, On the assessment of oxidative and microstructural changes after in vivo degradation of historical UHMWPE knee components by means of vibrational spectroscopies and nanoindentation, *J. Biomed. Mater. Res. - Part A.* (2009). doi:10.1002/jbm.a.31992.
- [177] S.M. Kurtz, W. Hozack, M. Marcolongo, J. Turner, C. Rimnac, A. Edidin, Degradation of mechanical properties of UHMWPE acetabular liners following long-term implantation, in: *J. Arthroplasty*, 2003. doi:10.1016/S0883-5403(03)00292-4.

- [178] J.D. Wernlé, J.L. Gilbert, Micromechanics of shelf-aged and retrieved UHMWPE tibial inserts: Indentation testing, oxidative profiling, and thickness effects, *J. Biomed. Mater. Res. - Part B Appl. Biomater.* (2005). doi:10.1002/jbm.b.30285.
- [179] S.M. Kurtz, W. Hozack, M. Marcolongo, J. Turner, C. Rimnac, A. Edidin, Degradation of mechanical properties of UHMWPE acetabular liners following long-term implantation, *J. Arthroplasty.* 18 (2003) 68–78. doi:10.1016/S0883-5403(03)00292-4.
- [180] A. Edidin, L. Pruitt, C.W. Jewett, D.J. Crane, D. Roberts, S.M. Kurtz, Plasticity-Induced Damage Layer Is a Precursor to Wear in Radiation-Cross-Linked UHMWPE Acetabular Components for Total Hip Replacements, *J. Arthroplasty.* 14 (1999).
- [181] S.M. Kurtz, C.M. Rimnac, W.J. Hozack, J. Turner, M. Marcolongo, V.M. Goldberg, M.J. Kraay, A.A. Edidin, In vivo degradation of polyethylene liners after gamma sterilization in air, *J. Bone Jt. Surg. - Ser. A.* 87 (2005) 815–823. doi:10.2106/JBJS.D.02111.
- [182] G. Blunn, E.M.B. Preva, L. Costa, J. Fisher, M.A.R. Freeman, ULTRA HIGH MOLECULAR-WEIGHT POLYETHYLENE (UHMWPE) IN TOTAL KNEE REPLACEMENT: FABRICATION, STERILISATION AND WEAR G. Blunn, E. M. Brach del Preva, L. Costa, J. Fisher, M. A. R. Freeman, (2002) 946–949.
- [183] H. McKellop, I.C. Clarke, K.L. Markolf, H.C. Amstutz, Wear characteristics of UHMW polyethylene: A method for accurately measuring extremely low wear rates, *J. Biomed. Mater. Res.* 12 (1978) 895–927. doi:10.1002/jbm.820120611.
- [184] D.L. Bartel, J.J. Rawlinson, A.H. Burstein, C.S. Ranawat, W.F.J. Flynn, Stresses in polyethylene components of contemporary total knee replacements., *Clin. Orthop. Relat. Res.* (1995) 76–82.
- [185] F.F. Buechel, M.J. Pappas, G. Makris, Evaluation of contact stress in metal-backed patellar replacements. A predictor of survivorship., *Clin. Orthop. Relat. Res.* (1991) 190–197.
- [186] J.N. Argenson, J.J. O'Connor, Polyethylene wear in meniscal knee replacement: A one to nine-year retrieval analysis of the Oxford knee, *J. Bone Jt. Surg. - Ser. B.* 74 (1992) 228–232. doi:10.1302/0301-620x.74b2.1544958.
- [187] J.L. Gilbert, I. Merkhani, Rate effects on the microindentation-based mechanical properties of oxidized, crosslinked, and highly crystalline ultrahigh-molecular-weight polyethylene, *J. Biomed. Mater. Res. - Part A.* 71 (2004) 549–558. doi:10.1002/jbm.a.30196.
- [188] J.D. Wernlé, J.L. Gilbert, Micromechanics of shelf-aged and retrieved UHMWPE tibial inserts: Indentation testing, oxidative profiling, and thickness effects, *J. Biomed. Mater. Res. - Part B Appl. Biomater.* 75 (2005) 113–121. doi:10.1002/jbm.b.30285.
- [189] A.A. Edidin, C.M. Rimnac, V.M. Goldberg, S.M. Kurtz, Mechanical behavior, wear surface morphology, and clinical performance of UHMWPE acetabular components after 10 years of implantation, *Wear.* (2001). doi:10.1016/S0043-1648(01)00616-0.
- [190] A.A. Edidin, S.M. Kurtz, Development and validation of the small punch test for UHMWPE used in total joint replacements, *Key Eng. Mater.* (2001) 1–40. doi:10.4028/www.scientific.net/kem.198-199.1.
- [191] S.M. Kurtz, J.R. Foulds, C.W. Jewett, S. Srivastav, A.A. Edidin, Validation of a small punch testing technique to characterize the mechanical behaviour of ultra-high-molecular-weight polyethylene, *Biomaterials.* (1997). doi:10.1016/S0142-9612(97)00124-5.
- [192] Z.H. Xu, X. Li, Effect of sample tilt on nanoindentation behaviour of materials, *Philos. Mag.* 87 (2007) 2299–2312. doi:10.1080/14786430601175516.
- [193] M.S. Kashani, V. Madhavan, Analysis and correction of the effect of sample tilt on results

- of nanoindentation, *Acta Mater.* 59 (2011) 883–895. doi:10.1016/j.actamat.2010.09.051.
- [194] A. Wang, D.C. Sun, S. Yau, B. Edwards, M. Sokol, A. Essner, V.K. Polineni, C. Stark, J.H. Dumbleton, Orientation softening in the deformation and wear of ultra high molecular weight polyethylene, *Wear.* 204 (1997) 230–241.
- [195] B. Poon, D. Rittel, G. Ravichandran, An analysis of nanoindentation in linearly elastic solids, *Int. J. Solids Struct.* (2008). doi:10.1016/j.ijsolstr.2008.07.021.
- [196] M.F. Doerner, W.D. Nix, A method for interpreting the data from depth-sensing indentation instruments, *J. Mater. Res.* 1 (1986).
- [197] J.L. Loubet, J.M. Georges, O. Marchesini, G. Meille, VICKERS INDENTATION CURVES OF MAGNESIUM OXIDE (MgO), *J. Tribol. Trans. ASME.* 106 (1984) 43–48.
- [198] A.E.H. Love, Boussinesq’s problem for a rigid cone, *Q. J. Math.* os-10 (1939) 161–175. doi:10.1093/qmath/os-10.1.161.
- [199] N.A. Stilwell, D. Tabor, Elastic recovery of conical indentations, *Proc. Phys. Soc.* 78 (1961) 169–179. doi:10.1088/0370-1328/78/2/302.
- [200] G.M. Pharr, A. Bolshakov, Understanding nanoindentation unloading curves, *J. Mater. Res.* 17 (2002) 2660–2671. doi:10.1557/JMR.2002.0386.
- [201] T.Y. Tsui, W.C. Oliver, G.M. Pharr, Indenter geometry effects on the measurement of mechanical properties by nanoindentation with sharp indenters, *Mater. Res. Soc. Symp. - Proc.* 436 (1996) 147–152. doi:10.1557/proc-436-147.
- [202] B. V. Derjaguin, V.M. Muller, Y.P. Toporov, Effect of contact deformation on the adhesion of elastic solids, *J. Colloid Interface Sci.* 53 (1975) 314–326.
[http://linkinghub.elsevier.com/retrieve/pii/0021979775900181%0Apapers3://publication/doi/10.1016/0021-9797\(75\)90018-1](http://linkinghub.elsevier.com/retrieve/pii/0021979775900181%0Apapers3://publication/doi/10.1016/0021-9797(75)90018-1).
- [203] D. TABOR, *Surface Forces and Surface Interactions*, ACADEMIC PRESS, INC., 1977. doi:10.1016/b978-0-12-404501-9.50009-2.
- [204] D. Maugis, Adhesion of spheres: The JKR-DMT transition using a dugdale model, *J. Colloid Interface Sci.* (1992). doi:10.1016/0021-9797(92)90285-T.

APPENDIX A – Seminal papers providing the basis for utilizing the main equations for analysis of load-displacement curves

Reference	Summary
I.N. Sneddon, 1986 [195]	The relation between load and penetration in the axisymmetric boussinesq problem for a punch of arbitrary profile Derives a solution of the axisymmetric Boussinesq problem that deduces simple formulae for the depth of penetration of the probe for a punch of arbitrary profile and the the total applied load to achieve this penetration.
M.F. Doerner, W.D. Nix, 1986 [196]	A method for interpreting the data from depth-sensing indentation instruments Describes an early method for determining the hardness and young’s modulus from depth-sensing indentation data. The initial one-third of the unloading region is used to calculate the stiffness of the material.
J.L Loubet, J.M Georges, O. Marchesini, G. Meille, 1984 [197]	Vickers Indentation Curves of Magnesium Oxide Investigation of the load-displacement curve to understand the role of plasticity and elasticity, and determining the physical meaning of Vickers hardness by using residual indentation measurements
A.E.H. Love, 1939 [198]	Boussinesq’s problem for a rigid cone Using Boussinesq’s equations to find a solution for the cases when the surface of the rigid body is a surface of revolution
N.A. Stillwell, D. Tabor, 1961 [199]	Elastic recovery of conical indentations This paper discusses the formation of plastic indentation when a hard conical indenter is pressed into a metal. Further, an analytical expression in terms of material’s elastic constants shows an agreement between the theoretical and observed depth changes. The calculated energy released when the indenter is withdrawn is shown to account for the elastic rebound, which is observed when a conical probe indents an elasto-plastic metal.

APPENDIX B – Seminal papers for the development and advancement of the Oliver and Pharr indentation theory

Reference	Summary
G.M Pharr, A. Bolkashov [200]	Understanding Nanoindentation unloading curves Developing a conceptual framework to explain the mathematical form of experimental nanoindentation unloading curves obtained using a sharp, geometrically self-similar indenter (pyramids and cones)
G.M Pharr, W.C Oliver [69]	Measurement of thin film mechanical properties using nanoindentation Discusses the method for analyzing and procuring mechanical properties of thin-films
JC. Hay, A. Bolshakov, GM. Pharr [109]	A critical examination of the fundamental relations used in the analysis of nanoindentation data An examination of Sneddon’s solution for indentation by a rigid cone to address the largely ignored features that affect nanoindentation properties. A Finite element and analytical results are presented to show correction to Sneddon’s equations.

<p>GM. Pharr, WC. Oliver, FR. Brotzen [105]</p>	<p>On the generality of the relationship among contact stiffness, contact area, and elastic modulus during indentation Using the result of sneddon’s analysis, this paper shows a relationship between contact stiffness, contact area and the elastic modulus that is independent on the geometry of the punch.</p>
<p>TY. Tsui, WC. Oliver, GM. Pharr [201]</p>	<p>Indenter geometry effects on the measurement of mechanical properties by nanoindentation with sharp indenters Discussion on the application of sharp indenters in the measurement of hardness and elastic modulus using nanoindentation methods and addresses some of the challenges</p>

APPENDIX C– Seminal papers for the development and advancement of the adhesion based nanoindentation theory

Reference	Summary
K.L Johnson, K. Kendall, A.D. Roberts, 1971 [107]	<p>Surface energy and the contact of elastic solids A discussion on the influence of surface energy on the contact between elastic solids. This paper derives the equations to determine the effect of contact size and the force of adhesion between two spherical solid surfaces. Experiments on rubber and gelatine spheres were performed to support theoretical findings.</p>
B.V. Derjaguin, V.M. Muller, Y.P.Toporov, 1975 [202]	<p>Effect of contact deformations on the adhesion of particles Develops a theory that identifies the influence of the contact deformation and molecular attraction of a ball and a plane. The theory shows that forces required to overcome the molecular forces when the contact is broken does not increase, regardless of the van der Waals forces being capable of increasing the elastic contact area. Rather, it remains equal to the attraction force value between the point contact of a non-deformed ball with a plane.</p>
D. Tabor. J., 1977 [203]	<p>Surface forces and surface interactions A discussion on the theoretical problems relating to surface problems, particularly the calculation of interaction energies between condensed phases in atomic contact. The paper provides an experiment on the adhesion between soft elastic solids, and highlights the importance of implementing concepts from surface energies with principles of contact mechanics.</p>
D. Maugis, 1992 [204]	<p>Adhesion of spheres: The JKR-DMT transition using a Dugdale model A brief overview of the development and derivation of the adhesion based contact mechanics that are essential to the analysis of nanoindentation data.</p>